THE IMPACT OF FROZEN GROUND DEGRADATION ON SURFACE-ATMOSPHERE INTERACTIONS

A Dissertation

by

DANIEL JOSEPH VECELLIO

Submitted to the Graduate and Professional School of
Texas A&M University
in partial fulfillment of the requirements for the degree of

DOCTOR OF PHILOSOPHY

Chair of Committee,	Oliver Frauenfeld
Committee Members,	Brendan Roark
	David Cairns
	Huilin Gao
Head of Department,	David Cairns

August 2021

Major Subject: Geography

ABSTRACT

Climate change is having a significant impact on the Arctic and will continue to do so in the future. Much of the previous literature has focused on heat and moisture exchange associated with diminished sea ice and increased amounts of open Arctic waters, but overlooked the impact of land areas. Permafrost regions of Eurasia have experienced an increase in active layer thickness over the past century due to this warming climate, according to previous studies. As a result, these soils have been able to absorb and retain more heat during the warm season, leading to a delayed freeze-up and a seasonally redistributed surface energy budget. This has also led to changes in surface hydrology in the region. These factors can play a role in energy transfer into the boundary layer and, on extended time scales, synoptic circulation patterns. However, most previous research on permafrost's impact on climate change has been centered on biogeochemical cycles and carbon feedbacks. A geophysical narrative is important to fully describe the role of frozen ground on the climate, but it can be difficult to separate the influence on atmospheric variables only due to permafrost degradation. In this dissertation, an idealized modeling study was completed to quantify the differences across scales given different permafrost conditions as well as synoptic setups. Moister active layers in continuous permafrost led to decreased surface air temperatures but increased atmospheric instability on short time scales. With confirmation that permafrost degradation does impact land-atmosphere interactions, analysis of a large ensemble of the Community Earth System Model and use of the dynamical adjustment methodology

indicated that permafrost influences on the evolution of surface air temperatures were restricted to the autumn as dynamics and internal variability dominated in the spring. Autumn surface-based influence was due to a shift in the partitioning of turbulent surface fluxes in the summer and autumn over the 21st century and subsequent hydrothermal responses at the surface and sub-surface in continuous and discontinuous permafrost, including increased spring snow, soil moisture, and convective precipitation. This novel dissertation shows that permafrost degradation has geophysical implications in climate change which must be considered.

ACKNOWLEDGEMENTS

I would like to thank my committee chair, Dr. Oliver Frauenfeld, for his guidance and support, both academically and personally, throughout the course of this research. Without his encouragement, I would not have finished this dissertation, let alone be graduating with a doctorate. I am lucky to have had him as an advisor and am even luckier to continue to have him as a mentor and a friend.

I would also like to thank my other committee members, Dr. Brendan Roark, Dr. David Cairns, and Dr. Huilin Gao for their constructive feedback throughout the dissertation process.

There are many other Geography faculty that have helped in numerous ways. Specifically, I would like to thank Drs. Rodrigo Bombardi, Inci Guneralp, Vatche Tchakerian, George Allen, John Casellas Connors, Wendy Jepson, Courtney Thompson, Andrew Klein, and Erik Prout for their sharing of knowledge that has made me a better geographer, counsel on navigating the ups and downs of graduate school, and general willingness to listen and discuss issues with me and the rest of the graduate student body.

I would also like to thank Dr. Christopher Nowotarski from Atmospheric Sciences who provided immense guidance on the first results chapter of this dissertation as well as a much nicer spot for watching Penn State football in the fall than my recycled furniture and 20” television.

The front office staff in the Department of Geography have taken care of more administrative issues than I can count on both hands over the last six years and I cannot thank them enough. Thank you Carria, Jessica, Sandra, Debbie, Fernanda, and Donna for all your help. Hopefully my baked goods over the years were at least a fraction of an acceptable repayment. And to our department academic advisor, Kristi Wolff, who has done the job of three or four people as one person, thank you for all the last-minute course assignments for GEOG 213, for reminding me how many credits I had to take in each semester every semester, and the candy and pep talks when I would just pop in for a break.

I would not have made it through six years without the comradery of my fellow graduate students within the department. This goes double for everyone in the Climate Science Lab. Thank you, all.

On more personal notes, I would like to thank Dr. Jennifer Vanos, my PI from my Masters, who took me in as her first student when I was ready to leave graduate school behind. I would not still be on this journey if it weren't for you. I'm honored to have been deemed worthy and competent enough to now be a colleague and a friend. I'd also like to thank Dr. Michael Allen for the beer-aided brainstorming sessions at conferences, workshops, or on Zoom to discuss research or the highs and lows of academia and what I'm getting myself into.

Thanks to the PSU Twitter Slack and all the characters in there for talking about at least one ridiculous topic a day that provided respite for the research-riddled mind.

Cheers, fellas, and thanks for a distraction from the absolute grueller that has been the last 6+ years.

This document and all the time it took to get to this point of writing it, defending it, and earning my doctorate would not have been possible without my parents. They supported my thirst for knowledge from a young age, always ensuring, along with Grandma and Grandpa Vecellio, that there was a TV Guide around so that I had reading material at the age of 2. They always encouraged me to take the enrichment classes in elementary schools, the advanced math classes in middle school, and the Advanced Placement courses in high school. But they also were there for the Little League games, the indoor soccer Saturdays, and the district championships and state playoff games in gyms across Pennsylvania in high school. Mom and Dad, you've supported me in every single thing I've done for over 30 years now and I can never begin to tell you how thankful I am for that.

And while it hasn't been 30+ years, I must also thank my future in-laws for all the support they have given over the past 4 years. Your support of me from nearly the beginning of my relationship with Victoria has been an important part of my life and your encouragement has helped me reach this finish line.

Finally, I need to thank my partner in life, my fiancé, Victoria. Being able to have someone on this same journey as me to come home to everyday and discuss our accomplishments, our struggles, our achievements, and our stumbles has been a saving grace for both of us. We've supported each other academically, emotionally, mentally, and kept each other sane during COVID isolation, ensuring that we'll be able to tackle

whatever the rest of our lives throw at us. You will get to the top of the dissertation mountain soon enough and I'll be there to help you as you finish up just like you were there for me. I love you so much.

Oh, and my furry research assistants Frederick T. Cat and Montgomery T. Fluff-face, of course.

CONTRIBUTORS AND FUNDING SOURCES

Contributors

This work was supervised by a dissertation committee consisting of Professor Oliver Frauenfeld [advisor], Professors Brendan Roark and David Cairns of the Department of Geography and Professor Huilin Gao of the Department of Civil Engineering.

All work conducted for this dissertation was completed by the student independently.

Funding Sources

Graduate study was supported by a dissertation research fellowship from the Office of Graduate and Professional Studies at Texas A&M University.

This work was also made possible in part by the ATMO-GEOG Endowed Chair Fund Collaboration in the College of Geosciences at Texas A&M University. Its contents are solely the responsibility of the authors and do not necessarily represent the official views of the College of Geosciences or Texas A&M University.

NOMENCLATURE

CAPE	Convective available potential energy
CESM-LE	Community Earth System Model Large Ensemble
CMIP5	Coupled Model Intercomparison Project, Phase 5
ContDis	Continuous-discontinuous combined permafrost zone
EM	Ensemble member
HI_{low}	Low-level humidity index
IF	Information flow
IPCC	Intergovernmental Panel on Climate Change
LCL	Lifting condensation level
NonPF	Non-permafrost zone
PZI	Permafrost Zonation Index
RCP	Representative Concentration Pathway
SAT	Surface air temperature
SporIso	Sporadic-isolated combined permafrost zone
VWC	Volumetric water capacity
WRF	Weather, Research, and Forecasting Model

TABLE OF CONTENTS

Page

LIST OF FIGURES

Page

LIST OF TABLES

Page

1. INTRODUCTION AND LITERATURE REVIEW

1.1. Introduction

Climate change is having a significant impact on the Arctic and will continue to do so in the future. The Arctic is warming at a faster pace than any other region on the globe with temperatures increasing at double the rate than its mid-latitude and tropical counterparts (IPCC, 2013, Winton, 2006). Arctic amplification is the term given to the anomalous warming of the high latitudes of the Northern Hemisphere due to the reduction of sea ice and the ice-albedo feedback (Serreze and Francis, 2006). The effects of this high-latitude warming, however, are not restricted to the Arctic. Bekryaev et al. (2010) note that effects are on both the local scale as well as the synoptic scale. The modeled thinning of sea ice and degradation of permafrost regions in the Arctic in Lawrence et al. (2008) led to a warming that reached 1,500 kilometers inland from the Arctic, affecting the circulation and weather patterns of the mid-latitudes. Both atmospheric and oceanic circulations are affected in their poleward transfer of heat due to the decreasing temperature gradient between the pole and the tropics (Ting et al., 2009, Yang et al., 2010a, Wood and Overland, 2010). Therefore, evidence shows that a warming Arctic will play a role in the changing of physical processes and weather patterns well outside the confines of the Arctic.

Much of the previous literature has focused on heat and moisture exchange associated with diminished sea ice and increased amount of open Arctic waters (Holland and Bitz, 2003, Serreze and Barry, 2011) but has overlooked the importance of land

areas that are staying unfrozen longer into the cold season and increasing the period for potentially exchanging more energy with the atmosphere, possibly affecting regional- and global-scale circulations. This leads to three research questions that will be the focus of this dissertation:

1. What are the effects of Arctic permafrost degradation on the surface energy budget, boundary layer, and atmospheric circulation?
2. What is the surface-based, thermodynamic influence of permafrost degradation on local surface air temperatures over Eurasia?
3. What are the mechanisms whereby permafrost degradation influences past and future surface air temperatures?

The results of this research will enhance our understanding of Arctic land-atmosphere interactions, detailing the under-studied, high-latitude terrestrial impacts on Arctic amplification and global climate change.

1.2. Literature Review

Permafrost underlies nearly one-quarter of the Northern Hemispheric land areas (Dobinski, 2011, Zhang et al., 2008). It is defined as ground that remains at or below 0°C for at least two consecutive years (Subcommittee, 1988). Areas that contain permafrost are characterized by the extent of permafrost with designations of continuous (90-100%), discontinuous (50-90%), sporadic (10-50%), and isolated (<10%) (Permafrost Subcommittee, 1988) or by the more recently developed Permafrost Zonation Index (Gruber, 2012). Due to its importance to the cryospheric state, observing networks like the Circumpolar Active Layer Monitoring (Shiklomanov et al., 2008) and

Global Terrestrial Network for Permafrost (Biskaborn et al., 2015) have been developed to maintain active layer and soil temperature records. Seasonally frozen ground, classified as land that freezes and thaws annually (Permafrost Subcommittee, 1988), can also be considered in land-based cryospheric studies. The latest Intergovernmental Panel on Climate Change (IPCC) report (Vaughan et al., 2014) concluded that permafrost temperatures in cold permafrost (primarily continuous permafrost) have risen more than their warm (primarily discontinuous permafrost) counterparts. Frauenfeld et al. (2004) looked at changes in the thickness of the active layer, the maximum layer of permafrost thaw during the warm season, as well as the freezing depths of seasonally frozen ground on interannual time scales over several decades at stations over Russia. They concluded that these soil changes will become more apparent as the Arctic continues to warm due to the effects of climate change, resulting in thawed ground to retain more heat throughout the warm season, increasing the amount of time for it to refreeze in the next cold season. In an update to Frauenfeld et al. (2004), Frauenfeld and Zhang (2011) found that between 1930 and 2000, seasonal freeze depths decreased 4.5 cm per decade and that most of the trend was linked to a large negative trend between 1970 and 1990. Freezing index, the sum of below-freezing temperatures during the freezing season, was determined to account for most of the variability and a link between the North Atlantic Oscillation (NAO) and the rapid decrease in freeze depth over the 20-year period was discovered. Other studies have also shown a linkage between teleconnection indices, such as the NAO, and the warming high-latitude regions (Panagiotopoulos et al., 2005). A number of other studies focusing on soil temperature trends in Eurasia have confirmed

the active layer deepening and/or soil temperature increases (Zhang et al., 2005, Streletskiy et al., 2015, Chen et al., 2021). These temperature increases are also projected to continue into the future based on climate model simulations (Soong et al., 2020). Using a fingerprint analysis technique, Guo et al. (2020) confirmed that observed permafrost thaw trends and variability in the Northern Hemisphere were attributed to greenhouse gas forcing on the climate and not natural forcing or aerosol effects, denoting anthropogenic climate change's impact on frozen ground. These changes were especially significant on the southern edge of permafrost in Eurasia. While permafrost warming is widespread throughout the Northern Hemisphere, through an analysis of air and soil temperature trends, Chudinova et al. (2006) highlighted the Central Siberian Plateau as a projected future focus for maximum effects on permafrost degradation.

Climate projections show continued increases in soil temperatures (Soong et al., 2020) and continued decreases in permafrost extent. Lawrence and Slater (2005), using the Community Climate System Model 3, found a drastic decrease in permafrost extent using a high emission scenario where less than one million km^2 of near-surface frozen ground would remain in 2100. While the shallow soil model (~3.5 m) and poor representation of hydrology were limiting factors of the study, it did provide a worst-case scenario for permafrost degradation by climate change. Using the updated suite of Coupled Model Intercomparison Project Phase 5 models, Slater and Lawrence (2013) returned a conservative value of 3.5 million km^2 of permafrost under the Representative Concentration Pathway 8.5 (RCP 8.5) scenario in 2100, which assumes an 8.5 W/m^2 increase in radiative forcing in 2100 as compared to pre-industrial levels. Guo and

Wang (2016) found similar reductions in permafrost extent as only 3.5 million km^2 of frozen ground remained in 2100 under the RCP 8.5 scenario, much of which remained around central Siberia. In a follow-up study, significant soil temperature increases and permafrost extent decreases persisted when accounting for 2°C of future warming (Guo and Wang, 2017). Chadburn et al. (2017) also used the 2°C global warming benchmark to find a 6.6 million km^2 reduction in permafrost extent relative to present-day. A 1.5°C stabilization would save nearly 2 million km^2 of permafrost extent according to Chadburn et al. (2017), though permafrost extent could still recede by 1-3.5°of latitude, affecting southern Siberia, according to Kong and Wang (2017). Overall, the Fifth Assessment Report of the IPCC concludes that it was "virtually certain" that surface permafrost will decrease as the climate continues to warm (Collins et al., 2013).

Not only does the climate have an effect on the degradation of permafrost, but degraded permafrost also feeds back onto the climate system itself. Much of the permafrost feedback literature has been framed in terms of how carbon released from thawed soils affects future climatic warming (Schuur et al., 2015, Wieder et al., 2019, Miller et al., 2010) given its characterization as a climate change "tipping point" (Lenton, 2012, Lenton et al., 2008). In total, there is about 1700 Pg of carbon stored within northern hemispheric permafrost soils (Tarnocai et al., 2009) which is expelled into the atmosphere in the form of carbon dioxide (CO_2) or methane (CH_4) via aerobic and anaerobic processes, respectively. In a recent observational study, Masyagina and Menyailo (2020) found increasing trends in CO_2 flux across central and eastern Siberia associated with increased soil temperatures, though the CO_2 flux trends were not

statistically significant. However, in the same region, they did find significant increasing trends in CH_4 fluxes in the region associated with increased soil temperatures and soil water content (Masyagina and Menyailo, 2020), likely a result of melting soil ice (Grosse et al., 2011). Even peatlands, which historically have been a carbon sink in cold regions, are expected to become carbon sources due to climatic warming and permafrost thaw in the future (Hugelius et al., 2020). Abrupt thaw is expected to occur in limited sections of regions of permafrost but could play a much larger role in carbon release (Turetsky et al., 2020). Coupling biogeochemical with land and atmosphere components in earth system models allow for estimations of carbon feedbacks' impact on surface temperature. Schaefer et al. (2014)'s simulations, forced by RCP 8.5, found as much as a 0.5°C increase in global temperatures due to carbon release alone by 2100, while a study by MacDougall et al. (2012) found a possible 1.69°C carbon-related increase by 2300.

However, due to the changing physical nature of permafrost soils that will accompany degradation, geophysical impacts such as changing land-atmosphere interactions are also occurring and relevant to the climate system given transitioning energy transfer pathways between the ground and surface atmospheric layer. Current hotspots of land-atmosphere interactions are found in places such as the Great Plains region of the United States and sub-Saharan Africa (Koster et al., 2004). Projections indicate that climate change will allow the interior of Russia, namely areas near the Central Siberian Plateau, to become an emerging region for increased surface-atmosphere coupling (Dirmeyer et al., 2013). This coincides with the area also identified in Chudinova et al. (2006)'s area of substantial permafrost degradation as discussed

above. In an intercomparison between land models, Andresen et al. (2020) found that permafrost regions will experience increased hydrologic cycles in the future, yet a decrease in soil moisture, likely due to increases in active layer depth and subsequent infiltration into the groundwater system. Most models, especially the Community Land Model, however, show increased soil moisture in far northern continuous permafrost regions. This may be due to the very deep permafrost table and subsequent waterlogging of near-surface soils. Increasing soil temperatures can lead to soil ice melt, leading to a concurrent increase in soil water content, most prevalent during the warm season when increased shortwave radiation heats the surface at higher latitudes. In addition to the soil ice melt, warm season precipitation maxima (Serreze and Etringer, 2003) may also exacerbate water-logging of active layer soils. This increase in soil moisture is a positive feedback on the degradation process (Loranty et al., 2018) as the higher thermal conductivity of water allows for more heat to be transferred deeper into the soil column. However, once all soil ice is melted and the permafrost table is lowered enough to where soil water can percolate into the groundwater system (Woo et al., 2008, Taylor et al., 2013), vertical degradation slows and most heat is retained in soils near the surface. This transitional process can be seen at the same time in areas where drainage occurs in permafrost regions (Göckede et al., 2017). Soil moisture differences over this transition is a distinct control on land-atmosphere interactions and energy transfer into the lower atmosphere (Dirmeyer, 2011, Seneviratne et al., 2010). This precipitates a shift from a latent heat flux-dominated surface-atmosphere interaction regime to one that favors the sensible heat flux. However, unlike the studies described above detailing the permafrost-

carbon feedback, impacts on near-surface climate due to the geophysical feedbacks that occur as a result of changes to the surface energy budget have not been as closely examined.

Impacts of surface changes are not confined to the near-surface atmospheric layer, but can also lead to energy transfers which affect larger atmospheric processes. (Teufel and Sushama, 2019) found that a change in the soil hydrothermal regime of permafrost regions led to not only a modification of the surface energy budget, but also local atmospheric stability and convective processes. Analogously, there is a breadth of literature on how irrigation (de Vrese and Hagemann, 2018, Puma and Cook, 2010, Qian et al., 2013) and land use and land cover change (Chen and Dirmeyer, 2016, Mahmood et al., 2010, Quesada et al., 2017, Swann et al., 2012) can alter the surface energy budget, boundary layer processes, and synoptic circulation itself. As high-latitude terrestrial regions begin to evolve in their connections with the atmosphere, new ways to examining other important climate phenomena might emerge. For example, much work has been done on the atmospheric circulation linkages between the Arctic and the mid-latitudes, with varying conclusions on the existence or strength of the connection. Francis and Vavrus (2012) introduced the concept of Arctic-mid latitude linkages nearly a decade ago, though recent work by others, including Barnes (2013) and Blackport and Screen (2020) have cast doubt on the robustness of the physical mechanisms causing this connection. Most, if not all, of these studies have used Arctic Ocean sea ice extent as the main cryospheric driver of this relationship. However, around 23 million km^2 of land underlain by permafrost sit between the Arctic Ocean and the mid-latitudes, much of that

in Eurasia. As discussed above, this terrestrial link between the Arctic and mid-latitudes has been and will continue to change as more permafrost continues to thaw and degrade, leading to evolving surface-energy exchanges. Permafrost should be considered an important factor to provide more clarity and either prove or disprove the hypothesis of Arctic and mid-latitude climatic connections.

While not considered in this dissertation, there are a number of other variables and processes that affect land-atmosphere interactions in permafrost regions. These include shifts in vegetation regimes that develop as permafrost thaws and root systems have more area to anchor themselves in newly unfrozen soil. This, in turn, affects the surface energy balance through changes in albedo, longwave radiation, and evapotranspiration (Eugster et al., 2000). Greening of most of the North Eurasian tundra has been observed in recent decades (Goetz et al., 2007, Mao et al., 2016) and future warming is expected to cause a northward shift of boreal forest into the tundra (Sitch et al., 2008). However, recent studies on the Tibetan Plateau showed that warming and subsequent permafrost thaw have actually helped the growth of old larch trees in the region (Zhang et al., 2019). Current Eurasian boreal forest is already succumbing to increased heat and drought (Buermann et al., 2014). This effect could continue as the biome shifts north, bringing with it increased fire risk and subsequent increased permafrost degradation. Depending on topography, different ecosystem shifts can develop in response to permafrost thaw, especially in regions of initially ice-rich permafrost. This landscape heterogeneity can create highly complex patterns of plant productivity which may not actually be resolved through remotely sensed analyses

(Myers-Smith et al., 2020). While areas with elevation gradients may dry out easier due to increased drainage and support shrubs and other drought-tolerant species, flatter regions that will retain increased soil moisture will begin to take on wetland characteristics (Yang et al., 2010b).

1.3. Research Objectives

The underlying premise of this dissertation is that the continued thaw of high latitude permafrost areas, specifically continuous permafrost areas, will result in a rise in near-surface soil temperatures. Thawing will also enhance spring and summer soil moisture availability due to earlier spring snowmelt and ground ice melt. These factors will be the impetus for an increase in land-atmosphere interactions due to a conversion of energy into sensible and latent heat flux rather than ground heat flux, and will play a role in micro-, meso-, and synoptic-scale weather and climatic changes. Furthermore, as permafrost thaws to a point where taliks develop on the path to complete degradation, the nature of the land-atmosphere interactions will change. As soil water has the ability to infiltrate into the groundwater system and soils dry out, this may lead to a transition between wet and dry soil regimes (Seneviratne et al., 2010). Therefore, the purpose of this dissertation is to quantify the geophysical impacts of permafrost degradation on the overlying, near-surface atmosphere.

To determine the impacts of permafrost thaw on the surface energy budget, a modeling approach will be used to simulate the response of sensible and latent fluxes, the near-surface atmosphere, and synoptic circulation changes to transitioning ground

conditions. Once the extent of these changes has been determined, the role of frozen ground will be investigated over longer time scales using an earth system model by examining surface impacts on surface air temperatures via thermodynamic influence. Lastly, frozen ground effects on near-surface temperature will be quantified to determine how the surface energy balance and the transfer of heat and moisture from the ground to the atmosphere might change due to permafrost degradation. Therefore, the three specific objectives of this study are:

1. Quantify the effects of Arctic permafrost degradation on the surface energy budget, boundary layer, and atmospheric circulation.

   Using the Weather Research and Forecasting (WRF) model to simulate the physical processes between the land and atmosphere as permafrost degrades, sets of idealized experiments serve as a proof of concept to motivate the rest of the dissertation. A pair of idealized soil conditions (permafrost vs. non-permafrost) in addition to a pair of idealized atmospheric conditions (active vs. quiescent patterns) will provide the basis for four experiments to ascertain ground-based and dynamic influences on land-atmosphere interactions, boundary layer growth, and 500-hPa atmospheric flow patterns.

2. Determine the surface-based, thermodynamic influence of permafrost degradation on local surface air temperatures over Eurasia.

Based on the subsequent geophysical impacts of permafrost degradation on other parts of the climate system as found in Objective 1, the CESM Large Ensemble, in conjunction with a dynamical adjustment methodology (Deser et al., 2016), are used to explore the impacts of internal variability and external forcing on surface air temperature changes over Eurasia. By using dynamical adjustment, dynamic and thermodynamic influences can be separated and analyzed over different permafrost regions of Eurasia to determine the influence of degradation on the climate over a longer time period.

3. Establish the mechanisms whereby permafrost degradation influences past and future surface air temperatures.

This objective builds on the results from Objective 2 and specifically attempts to pinpoint the geophysical, ground-based mechanism for thermodynamically influenced surface air temperature increase and how it changes over permafrost type and over time. To quantify the interaction between temperature and a suite of ground-based variables, an information flow technique (San Liang, 2014, Xiao et al., 2020) is used for a time series analysis to statistically describe the connection between the variables. This will clarify why and how permafrost degradation has a geophysical impact on the climate system.

1.4. References

ANDRESEN, C. G., LAWRENCE, D. M., WILSON, C. J., MCGUIRE, A. D., KOVEN, C., SCHAEFER, K., JAFAROV, E., PENG, S., CHEN, X., GOUTTEVIN, I., BURKE, E., CHADBURN, S., JI, D., CHEN, G., HAYES, D. & ZHANG, W. 2020. Soil moisture and hydrology projections of the permafrost region – a model intercomparison. *The Cryosphere,* 14**,** 445-459.

BARNES, E. A. 2013. Revisiting the evidence linking Arctic amplification to extreme weather in midlatitudes. *Geophysical Research Letters,* 40**,** 4734-4739.

BEKRYAEV, R. V., POLYAKOV, I. V. & ALEXEEV, V. A. 2010. Role of Polar Amplification in Long-Term Surface Air Temperature Variations and Modern Arctic Warming. *Journal of Climate,* 23**,** 3888-3906.

BISKABORN, B. K., LANCKMAN, J. P., LANTUIT, H., ELGER, K., STRELETSKIY, D. A., CABLE, W. L. & ROMANOVSKY, V. E. 2015. The new database of the Global Terrestrial Network for Permafrost (GTN-P). *Earth Syst. Sci. Data,* 7**,** 245-259.

BLACKPORT, R. & SCREEN, J. A. 2020. Weakened evidence for mid-latitude impacts of Arctic warming. *Nature Climate Change,* 10**,** 1065-1066.

BUERMANN, W., PARIDA, B., JUNG, M., MACDONALD, G. M., TUCKER, C. J. & REICHSTEIN, M. 2014. Recent shift in Eurasian boreal forest greening response may be associated with warmer and drier summers. *Geophysical Research Letters,* 41**,** 1995-2002.

CHADBURN, S. E., BURKE, E. J., COX, P. M., FRIEDLINGSTEIN, P., HUGELIUS, G. & WESTERMANN, S. 2017. An observation-based constraint on permafrost loss as a function of global warming. *Nature Climate Change,* 7**,** 340-344.

CHEN, L., AALTO, J. & LUOTO, M. 2021. Significant shallow–depth soil warming over Russia during the past 40 years. *Global and Planetary Change,* 197**,** 103394.

CHEN, L. & DIRMEYER, P. A. 2016. Adapting observationally based metrics of biogeophysical feedbacks from land cover/land use change to climate modeling. *Environmental Research Letters,* 11**,** 034002.

CHUDINOVA, S. M., FRAUENFELD, O. W., BARRY, R. G., ZHANG, T. & SOROKOVIKOV, V. A. 2006. Relationship between air and soil temperature trends and periodicities in the permafrost regions of Russia. *Journal of Geophysical Research: Earth Surface,* 111.

COLLINS, M., KNUTTI, R., ARBLASTER, J., DUFRESNE, J.-L., FICHEFET, T., FRIEDLINGSTEIN, P., GAO, X., GUTOWSKI, W. J., JOHNS, T. & KRINNER, G. 2013. Long-term climate change: projections, commitments and irreversibility. *Climate Change 2013-The Physical Science Basis: Contribution of Working Group I to the Fifth Assessment Report of the Intergovernmental Panel on Climate Change.* Cambridge University Press.

DE VRESE, P. & HAGEMANN, S. 2018. Uncertainties in modelling the climate impact of irrigation. *Climate Dynamics,* 51**,** 2023-2038.

DESER, C., TERRAY, L. & PHILLIPS, A. S. 2016. Forced and internal components of winter air temperature trends over North America during the past 50 years: Mechanisms and implications. *Journal of Climate,* 29**,** 2237-2258.

DIRMEYER, P. A. 2011. The terrestrial segment of soil moisture–climate coupling. *Geophysical Research Letters,* 38.

DIRMEYER, P. A., JIN, Y., SINGH, B. & YAN, X. 2013. Trends in Land–Atmosphere Interactions from CMIP5 Simulations. *Journal of Hydrometeorology,* 14**,** 829-849.

DOBINSKI, W. 2011. Permafrost. *Earth-Science Reviews,* 108**,** 158-169.

EUGSTER, W., ROUSE, W. R., PIELKE, R. A., MCFADDEN, J. P., BALDOCCHI, D. D., KITTEL, T. G. F., CHAPIN, F. S., LISTON, G. E., VIDALE, P. L., VAGANOV, E. & CHAMBERS, S. 2000. Land-atmosphere energy exchange in Arctic tundra and boreal forest: available data and feedbacks to climate. *Global Change Biology,* 6**,** 84-115.

FRANCIS, J. A. & VAVRUS, S. J. 2012. Evidence linking Arctic amplification to extreme weather in mid-latitudes. *Geophysical Research Letters,* 39.

FRAUENFELD, O. W. & ZHANG, T. J. 2011. An observational 71-year history of seasonally frozen ground changes in the Eurasian high latitudes. *Environmental Research Letters,* 6.

FRAUENFELD, O. W., ZHANG, T. J., BARRY, R. G. & GILICHINSKY, D. 2004. Interdecadal changes in seasonal freeze and thaw depths in Russia. *Journal of Geophysical Research-Atmospheres,* 109.

GÖCKEDE, M., KITTLER, F., KWON, M. J., BURJACK, I., HEIMANN, M., KOLLE, O., ZIMOV, N. & ZIMOV, S. 2017. Shifted energy fluxes, increased Bowen ratios, and reduced thaw depths linked with drainage-induced changes in permafrost ecosystem structure. *The Cryosphere,* 11**,** 2975-2996.

GOETZ, S. J., MACK, M. C., GURNEY, K. R., RANDERSON, J. T. & HOUGHTON, R. A. 2007. Ecosystem responses to recent climate change and fire disturbance at northern high latitudes: observations and model results contrasting northern Eurasia and North America. *Environmental Research Letters,* 2**,** 045031.

GROSSE, G., ROMANOVSKY, V., JORGENSON, T., ANTHONY, K. W., BROWN, J. & OVERDUIN, P. P. 2011. Vulnerability and Feedbacks of Permafrost to Climate Change. *Eos, Transactions American Geophysical Union,* 92**,** 73-74.

GRUBER, S. 2012. Derivation and analysis of a high-resolution estimate of global permafrost zonation. *Cryosphere,* 6**,** 221-233.

GUO, D., SUN, J., LI, H., ZHANG, T. & ROMANOVSKY, V. E. 2020. Attribution of historical near-surface permafrost degradation to anthropogenic greenhouse gas warming. *Environmental Research Letters,* 15**,** 084040.

GUO, D. & WANG, H. 2017. Permafrost degradation and associated ground settlement estimation under 2 °C global warming. *Climate Dynamics,* 49**,** 2569-2583.

GUO, D. L. & WANG, H. J. 2016. CMIP5 permafrost degradation projection: A comparison among different regions. *Journal of Geophysical Research-Atmospheres,* 121**,** 4499-4517.

HOLLAND, M. M. & BITZ, C. M. 2003. Polar amplification of climate change in coupled models. *Climate Dynamics,* 21**,** 221-232.

HUGELIUS, G., LOISEL, J., CHADBURN, S., JACKSON, R. B., JONES, M., MACDONALD, G., MARUSHCHAK, M., OLEFELDT, D., PACKALEN, M., SIEWERT, M. B., TREAT, C., TURETSKY, M., VOIGT, C. & YU, Z. 2020. Large stocks of peatland carbon and nitrogen are vulnerable to permafrost thaw. *Proceedings of the National Academy of Sciences,* 117**,** 20438-20446.

IPCC 2013. Climate Change 2013: The Physical Science Basis. Contribution of Working Group I to the Fifth Assessment Report of the Intergovernmental Panel on Climate Change. *In:* STOCKER, T. F., D. QIN, G.-K. PLATTNER, M. TIGNOR, S.K. ALLEN, J. BOSCHUNG, A. NAUELS, Y. XIA, V. BEX AND P.M. MIDGLEY (ed.). Cambridge, United Kingdom and New York, NY, USA.

KONG, Y. & WANG, C.-H. 2017. Responses and changes in the permafrost and snow water equivalent in the Northern Hemisphere under a scenario of 1.5 °C warming. *Advances in Climate Change Research,* 8**,** 235-244.

KOSTER, R. D., DIRMEYER, P. A., GUO, Z., BONAN, G., CHAN, E., COX, P., GORDON, C. T., KANAE, S., KOWALCZYK, E., LAWRENCE, D., LIU, P., LU, C.-H., MALYSHEV, S., MCAVANEY, B., MITCHELL, K., MOCKO, D., OKI, T., OLESON, K., PITMAN, A., SUD, Y. C., TAYLOR, C. M., VERSEGHY, D., VASIC, R., XUE, Y. & YAMADA, T. 2004. Regions of Strong Coupling Between Soil Moisture and Precipitation. *Science,* 305**,** 1138-1140.

LAWRENCE, D. M. & SLATER, A. G. 2005. A projection of severe near-surface permafrost degradation during the 21st century. *Geophysical Research Letters,* 32.

LAWRENCE, D. M., SLATER, A. G., TOMAS, R. A., HOLLAND, M. M. & DESER, C. 2008. Accelerated Arctic land warming and permafrost degradation during rapid sea ice loss. *Geophysical Research Letters,* 35.

LENTON, T. M. 2012. Arctic Climate Tipping Points. *AMBIO,* 41**,** 10-22.

LENTON, T. M., HELD, H., KRIEGLER, E., HALL, J. W., LUCHT, W., RAHMSTORF, S. & SCHELLNHUBER, H. J. 2008. Tipping elements in the Earth's climate system. *Proceedings of the National Academy of Sciences,* 105**,** 1786-1793.

LORANTY, M. M., ABBOTT, B. W., BLOK, D., DOUGLAS, T. A., EPSTEIN, H. E., FORBES, B. C., JONES, B. M., KHOLODOV, A. L., KROPP, H., MALHOTRA, A., MAMET, S. D., MYERS-SMITH, I. H., NATALI, S. M., O'DONNELL, J. A., PHOENIX, G. K., ROCHA, A. V., SONNENTAG, O., TAPE, K. D. & WALKER, D. A. 2018. Reviews and syntheses: Changing ecosystem influences on soil thermal regimes in northern high-latitude permafrost regions. *Biogeosciences,* 15**,** 5287-5313.

MACDOUGALL, A. H., AVIS, C. A. & WEAVER, A. J. 2012. Significant contribution to climate warming from the permafrost carbon feedback. *Nature Geoscience,* 5**,** 719-721.

MAHMOOD, R., PIELKE, R. A., HUBBARD, K. G., NIYOGI, D., BONAN, G., LAWRENCE, P., MCNIDER, R., MCALPINE, C., ETTER, A., GAMEDA, S., QIAN, B., CARLETON, A., BELTRAN-PRZEKURAT, A., CHASE, T., QUINTANAR, A. I., ADEGOKE, J. O., VEZHAPPARAMBU, S., CONNER, G., ASEFI, S., SERTEL, E., LEGATES, D. R., WU, Y., HALE, R., FRAUENFELD, O. W., WATTS, A., SHEPHERD, M., MITRA, C., ANANTHARAJ, V. G., FALL, S., LUND, R., TREVIÑO, A., BLANKEN, P., DU, J., CHANG, H.-I., LEEPER, R., NAIR, U. S., DOBLER, S., DEO, R. & SYKTUS, J. 2010. Impacts of Land Use/Land Cover Change on Climate and Future Research Priorities. *Bulletin of the American Meteorological Society,* 91**,** 37-46.

MAO, J., RIBES, A., YAN, B., SHI, X., THORNTON, P. E., SÉFÉRIAN, R., CIAIS, P., MYNENI, R. B., DOUVILLE, H., PIAO, S., ZHU, Z., DICKINSON, R. E., DAI, Y., RICCIUTO, D. M., JIN, M., HOFFMAN, F. M., WANG, B., HUANG, M. & LIAN, X. 2016. Human-induced greening of the northern extratropical land surface. *Nature Climate Change,* 6**,** 959-963.

MASYAGINA, O. V. & MENYAILO, O. V. 2020. The impact of permafrost on carbon dioxide and methane fluxes in Siberia: A meta-analysis. *Environmental Research,* 182**,** 109096.

MILLER, G. H., ALLEY, R. B., BRIGHAM-GRETTE, J., FITZPATRICK, J. J., POLYAK, L., SERREZE, M. C. & WHITE, J. W. C. 2010. Arctic amplification: can the past constrain the future? *Quaternary Science Reviews,* 29**,** 1779-1790.

MYERS-SMITH, I. H., KERBY, J. T., PHOENIX, G. K., BJERKE, J. W., EPSTEIN, H. E., ASSMANN, J. J., JOHN, C., ANDREU-HAYLES, L., ANGERS-BLONDIN, S., BECK, P. S. A., BERNER, L. T., BHATT, U. S., BJORKMAN, A. D., BLOK, D., BRYN, A., CHRISTIANSEN, C. T., CORNELISSEN, J. H. C., CUNLIFFE, A. M., ELMENDORF, S. C., FORBES, B. C., GOETZ, S. J., HOLLISTER, R. D., DE JONG, R., LORANTY, M. M., MACIAS-FAURIA, M., MASEYK, K., NORMAND, S., OLOFSSON, J., PARKER, T. C., PARMENTIER, F.-J. W., POST, E., SCHAEPMAN-STRUB, G., STORDAL, F., SULLIVAN, P. F., THOMAS, H. J. D., TØMMERVIK, H., TREHARNE, R., TWEEDIE, C. E., WALKER, D. A., WILMKING, M. & WIPF, S. 2020. Complexity revealed in the greening of the Arctic. *Nature Climate Change,* 10**,** 106-117.

PANAGIOTOPOULOS, F., SHAHGEDANOVA, M., HANNACHI, A. & STEPHENSON, D. B. 2005. Observed Trends and Teleconnections of the Siberian High: A Recently Declining Center of Action. *Journal of Climate,* 18**,** 1411-1422.

PUMA, M. J. & COOK, B. I. 2010. Effects of irrigation on global climate during the 20th century. *Journal of Geophysical Research: Atmospheres,* 115.

QIAN, Y., HUANG, M., YANG, B. & BERG, L. K. 2013. A Modeling Study of Irrigation Effects on Surface Fluxes and Land–Air–Cloud Interactions in the Southern Great Plains. *Journal of Hydrometeorology,* 14**,** 700-721.

QUESADA, B., ARNETH, A. & DE NOBLET-DUCOUDRÉ, N. 2017. Atmospheric, radiative, and hydrologic effects of future land use and land cover changes: A global and multimodel climate picture. *Journal of Geophysical Research: Atmospheres,* 122**,** 5113-5131.

SAN LIANG, X. 2014. Unraveling the cause-effect relation between time series. *Physical Review E,* 90**,** 052150.

SCHAEFER, K., LANTUIT, H., ROMANOVSKY, V. E., SCHUUR, E. A. G. & WITT, R. 2014. The impact of the permafrost carbon feedback on global climate. *Environmental Research Letters,* 9.

SCHUUR, E. A. G., MCGUIRE, A. D., SCHADEL, C., GROSSE, G., HARDEN, J. W., HAYES, D. J., HUGELIUS, G., KOVEN, C. D., KUHRY, P., LAWRENCE, D. M., NATALI, S. M., OLEFELDT, D., ROMANOVSKY, V. E., SCHAEFER, K., TURETSKY, M. R., TREAT, C. C. & VONK, J. E. 2015. Climate change and the permafrost carbon feedback. *Nature,* 520**,** 171-179.

SENEVIRATNE, S. I., CORTI, T., DAVIN, E. L., HIRSCHI, M., JAEGER, E. B., LEHNER, I., ORLOWSKY, B. & TEULING, A. J. 2010. Investigating soil moisture–climate interactions in a changing climate: A review. *Earth-Science Reviews,* 99**,** 125-161.

SERREZE, M. C. & BARRY, R. G. 2011. Processes and impacts of Arctic amplification: A research synthesis. *Global and Planetary Change,* 77**,** 85-96.

SERREZE, M. C. & ETRINGER, A. J. 2003. Precipitation characteristics of the Eurasian Arctic drainage system. *International Journal of Climatology,* 23**,** 1267-1291.

SERREZE, M. C. & FRANCIS, J. A. 2006. The Arctic Amplification Debate. *Climatic Change,* 76**,** 241-264.

SHIKLOMANOV, N., NELSON, F., STRELETSKIY, D., HINKEL, K. & BROWN, J. The circumpolar active layer monitoring (CALM) program: data collection, management, and dissemination strategies. Proceedings of the Ninth International Conference on Permafrost, 2008 Fairbanks, Alaska.

SITCH, S., HUNTINGFORD, C., GEDNEY, N., LEVY, P. E., LOMAS, M., PIAO, S. L., BETTS, R., CIAIS, P., COX, P., FRIEDLINGSTEIN, P., JONES, C. D., PRENTICE, I. C. & WOODWARD, F. I. 2008. Evaluation of the terrestrial carbon cycle, future plant geography and climate-carbon cycle feedbacks using five Dynamic Global Vegetation Models (DGVMs). *Global Change Biology,* 14**,** 2015-2039.

SLATER, A. G. & LAWRENCE, D. M. 2013. Diagnosing present and future permafrost from climate models. *Journal of Climate,* 26**,** 5608-5623.

SOONG, J. L., PHILLIPS, C. L., LEDNA, C., KOVEN, C. D. & TORN, M. S. 2020. CMIP5 Models Predict Rapid and Deep Soil Warming Over the 21st Century. *Journal of Geophysical Research: Biogeosciences,* 125**,** e2019JG005266.

STRELETSKIY, D. A., SHERSTIUKOV, A. B., FRAUENFELD, O. W. & NELSON, F. E. 2015. Changes in the 1963-2013 shallow ground thermal regime in Russian permafrost regions. *Environmental Research Letters,* 10.

SUBCOMMITTEE, P. 1988. Glossary of permafrost and related ground-ice terms. *Associate Committee on Geotechnical Research, National Research Council of Canada, Ottawa,* 156.

SWANN, A. L. S., FUNG, I. Y. & CHIANG, J. C. H. 2012. Mid-latitude afforestation shifts general circulation and tropical precipitation. *Proceedings of the National Academy of Sciences,* 109**,** 712-716.

TARNOCAI, C., CANADELL, J. G., SCHUUR, E. A. G., KUHRY, P., MAZHITOVA, G. & ZIMOV, S. 2009. Soil organic carbon pools in the northern circumpolar permafrost region. *Global Biogeochemical Cycles,* 23.

TAYLOR, R. G., SCANLON, B., DÖLL, P., RODELL, M., VAN BEEK, R., WADA, Y., LONGUEVERGNE, L., LEBLANC, M., FAMIGLIETTI, J. S., EDMUNDS, M., KONIKOW, L., GREEN, T. R., CHEN, J., TANIGUCHI, M., BIERKENS, M. F. P., MACDONALD, A., FAN, Y., MAXWELL, R. M., YECHIELI, Y., GURDAK, J. J., ALLEN, D. M., SHAMSUDDUHA, M., HISCOCK, K., YEH, P. J. F., HOLMAN, I. & TREIDEL, H. 2013. Ground water and climate change. *Nature Climate Change,* 3**,** 322-329.

TEUFEL, B. & SUSHAMA, L. 2019. Abrupt changes across the Arctic permafrost region endanger northern development. *Nature Climate Change,* 9**,** 858-862.

TING, M., KUSHNIR, Y., SEAGER, R. & LI, C. 2009. Forced and Internal Twentieth-Century SST Trends in the North Atlantic. *Journal of Climate,* 22**,** 1469-1481.

TURETSKY, M. R., ABBOTT, B. W., JONES, M. C., ANTHONY, K. W., OLEFELDT, D., SCHUUR, E. A., GROSSE, G., KUHRY, P., HUGELIUS, G. & KOVEN, C. 2020. Carbon release through abrupt permafrost thaw. *Nature Geoscience,* 13**,** 138-143.

VAUGHAN, D. G., COMISO, J., ALLISON, I., CARRASCO, J., KASER, G., KWOK, R., MOTE, P., MURRAY, T., PAUL, F. & REN, J. 2014. Observations: Cryosphere. *Climate Change 2013-The Physical Science Basis: Contribution of Working Group I to the Fifth Assessment Report of the Intergovernmental Panel on Climate Change.* Cambridge University Press.

WIEDER, W. R., SULMAN, B. N., HARTMAN, M. D., KOVEN, C. D. & BRADFORD, M. A. 2019. Arctic Soil Governs Whether Climate Change Drives Global Losses or Gains in Soil Carbon. *Geophysical Research Letters,* 46**,** 14486-14495.

WINTON, M. 2006. Amplified Arctic climate change: What does surface albedo feedback have to do with it? *Geophysical Research Letters,* 33.

WOO, M.-K., KANE, D. L., CAREY, S. K. & YANG, D. 2008. Progress in permafrost hydrology in the new millennium. *Permafrost and Periglacial Processes,* 19**,** 237-254.

WOOD, K. R. & OVERLAND, J. E. 2010. Early 20th century Arctic warming in retrospect. *International Journal of Climatology,* 30**,** 1269-1279.

XIAO, H., ZHANG, F., MIAO, L., SAN LIANG, X., WU, K. & LIU, R. 2020. Long-term trends in Arctic surface temperature and potential causality over the last 100 years. *Climate Dynamics,* 55**,** 1443-1456.

YANG, X.-Y., FYFE, J. C. & FLATO, G. M. 2010a. The role of poleward energy transport in Arctic temperature evolution. *Geophysical Research Letters,* 37.

YANG, Z.-P., OU, Y. H., XU, X.-L., ZHAO, L., SONG, M.-H. & ZHOU, C.-P. 2010b. Effects of permafrost degradation on ecosystems. *Acta Ecologica Sinica,* 30**,** 33-39.

ZHANG, T., BARRY, R. G., KNOWLES, K., HEGINBOTTOM, J. A. & BROWN, J. 2008. Statistics and characteristics of permafrost and ground-ice distribution in the Northern Hemisphere. *Polar Geography,* 31**,** 47-68.

ZHANG, T., FRAUENFELD, O. W., SERREZE, M. C., ETRINGER, A., OELKE, C., MCCREIGHT, J., BARRY, R. G., GILICHINSKY, D., YANG, D., YE, H., LING, F. & CHUDINOVA, S. 2005. Spatial and temporal variability in active layer thickness over the Russian Arctic drainage basin. *Journal of Geophysical Research: Atmospheres,* 110.

ZHANG, X., BAI, X., HOU, M., CHEN, Z. & MANZANEDO, R. D. 2019. Warmer Winter Ground Temperatures Trigger Rapid Growth of Dahurian Larch in the Permafrost Forests of Northeast China. *Journal of Geophysical Research: Biogeosciences,* 124**,** 1088-1097.

2. THE ROLE OF PERMAFROST IN EURASIAN LAND-ATMOSPHERE INTERACTIONS*

2.1. Introduction

The potential impacts of recent and future changes in permafrost extent on regional climate through atmospheric surface and boundary layer feedback effects remain largely unknown. Permafrost, defined as ground that has been continuously frozen for at least two consecutive years (Subcommittee, 1988), underlies nearly a quarter of the land area in the Northern Hemisphere (Zhang et al., 1999). Permafrost plays an important role in climate change, the carbon balance, surface and subsurface hydrology, ecosystems, infrastructure, and human activities in cold regions (Anisimov et al., 2010, Romanovsky et al., 2010, Streletskiy et al., 2012, Streletskiy et al., 2015b). Each warm season, the upper layer of permafrost thaws to some depth, referred to as the active layer. Across Eurasia, soil temperatures and active layer depths have significantly increased since the middle of the 20th century in association with surface temperature increases (Frauenfeld et al., 2004, Romanovsky et al., 2007, Streletskiy et al., 2015a). The upper layers of these warmer and deeper unfrozen soils more readily retain water (Fedorov et al., 2014) during the summer months, which are characterized by snowmelt and increased precipitation relative to the cold season. Past studies have shown that permafrost thaw-

* This section is reprinted with permission from "The Role of Permafrost in Eurasian Land-Atmosphere Interactions" by Vecellio et al., 2019, Journal of Geophysical Research - Atmospheres, 124(22), 11,644–11,660, Copyright [2019] by the American Geophysical Union.

induced changes to local water storage have caused complete shifts in local vegetation structures (Walvoord and Kurylyk, 2016). Because the underlying permafrost layer reduces drainage, elevated soil moisture and temperature increase the moisture (i.e., latent heat) flux between the surface and the atmosphere in continuous permafrost regions (Gu et al., 2015, Serreze et al., 2002). Moreover, the ground stays thawed longer into autumn, delaying refreezing of the active layer in the cold season. While the impacts of permafrost degradation on carbon release from the ground has been studied in-depth (Koven et al., 2011, Schuur et al., 2013, Schuur et al., 2015), the potential energy and moisture feedbacks on the overlying atmosphere have not been evaluated.

Increases in low-level atmospheric temperature and moisture in the Arctic region during the spring and summer are the basis for subsequent land-atmosphere interactions, as the semi-permanent inversion is eroded and convective available potential energy increases (Cullather and Lynch, 2003). This has been shown to increase evaporative fraction, the ratio of latent heating to total energy at the surface, and the probability of precipitation over the continuous permafrost areas of central Eurasia during the summertime (Ford and Frauenfeld, 2016) and may play a part in modifications to storm tracks (Iijima et al., 2016) and atmospheric circulation patterns (Hiyama et al., 2016) across the continent. Similar results showing the importance of summertime soil moisture over continuous permafrost have been seen in modeling studies (Matsumura et al., 2010). These results are expected to differ when applied to zones of discontinuous, sporadic, or isolated permafrost, as surface water has an increased ability to percolate

into the ground, drying out the upper active layer, and increasing the sensible heat flux between the ground and atmosphere while, in turn, reducing the latent heat flux.

In addition to surface impacts, changing, complex interactions between the surface and the atmosphere likely take place as permafrost degrades (i.e., decreases in areal extent and/or thickness in response to a natural or artificial cause). Larger sensible heat fluxes are associated with a deeper planetary boundary layer as more energy is available to be transferred from the surface to the atmosphere through conduction and convection (Pan and Mahrt, 1987). Hence, areas over discontinuous permafrost are expected to have a deeper boundary layer than their continuous counterparts. Also, a deeper boundary layer is expected to persist later into the year in permafrost regions because positive heat flux anomalies are redistributed later into the season as the ground stays thawed longer. However, a deeper boundary layer does not necessarily translate into more clouds or increased precipitation, as low-level moisture is needed (Segal et al., 1998). Continuous permafrost regions, when the active layer is saturated due to spring snowmelt and early-season precipitation, can be an abundant source of low-level moisture. While the boundary layer may not grow as high, this moistening of the surface layer and lower levels of the troposphere due to increased latent heat fluxes may provide a more suitable thermodynamic environment for cloud development. This uncertainty in permafrost effects on the ratio of sensible to latent heating and low-level cloud cover is a key motivation for this study.

Past modeling studies have not explicitly investigated land-atmosphere interactions over different permafrost classifications. Ling and Zhang (2004) employed a

simple one-dimensional surface energy balance model to simulate the annual cycle of surface fluxes at a permafrost site with unfrozen water in Barrow, Alaska. However, permafrost modeling continues to be primarily focused on how processes at the surface affect subsurface properties such as permafrost area and extent, soil temperature, active layer thickness, and biogeochemical processes (Riseborough et al., 2008). This is true for coupled general circulation and earth system models (Koven et al., 2013, Lawrence and Slater, 2005, Lawrence et al., 2012) as well as land surface models (Chen et al., 2015, Guo et al., 2012, McGuire et al., 2016, McGuire et al., 2018). The potential for increased land-atmosphere interactions in these areas may play an important role in weather and climate patterns, much like other areas already determined to be feedback hotspots, such as the United States Great Plains and sub-Saharan Africa (Dirmeyer et al., 2012, Koster et al., 2004). In anticipation of a continued increasing trend in temperatures and decreasing trend in permafrost area extent, it is imperative to dissect the role that changing land conditions will have on weather and climate across spatial scales, from the surface to the general circulation of the atmosphere. Thus, land-atmosphere interactions in the context of varying permafrost conditions are the primary motivation of this modeling study. Impacts of a moisture-limited (representative of discontinuous permafrost) vs. moisture-rich (representative of continuous permafrost) land surface on boundary layer processes and synoptic-scale atmospheric variables will be investigated in two weather regimes: an environment relatively free of synoptic forcing (synoptically quiescent conditions dominated by surface high pressure) and in an environment with

relatively strong synoptic forcing (synoptically active conditions with a passing surface low-pressure system).

This study seeks to model the coupled land-atmosphere processes that take place over continuous and discontinuous permafrost during the summer using high-resolution, cloud-resolving regional Weather Research and Forecasting model (WRF) simulations. These simulations are "real" in that historical cases are used for initial and boundary conditions, yet the land surface conditions (temperature and moisture) have been prescribed to represent those typical of discontinuous and continuous permafrost environments so as to capture their differing effects on land-atmosphere interactions. Thus, despite no explicit inclusion of long-term permafrost degradation in the model, the effects of varying permafrost conditions are represented in the soil model. Four experiments, combining each of the synoptic (active vs. quiescent) and soil (continuous vs. discontinuous permafrost) scenarios, are performed to achieve this study's objectives. Specifically, this study will 1) investigate the impact of idealized surface soil conditions consistent with differing permafrost categories on the surface energy balance, boundary layer characteristics, and synoptic circulation and 2) determine whether ambient synoptic conditions are amplified or diminished over varying permafrost types.

2.2. Data and Methods

2.2.1. Model Setup

The Advanced Research WRF (WRF-ARW) model, version 3.7.1 (Skamarock et al., 2008) is used for all simulations in this study. Experiments are run over a parent domain (d01) centered over the Central Siberian Plateau in Russia with a horizontal grid spacing

of 9 km with three nested domains (3 km, 1 km, and 333.33 m horizontal grid spacing, which are considered domains d02, d03, and d04, respectively) within the parent as shown in Figure 1. This nested approach is necessary to achieve the final, high-resolution simulation that allows us to resolve atmospheric surface and boundary layer processes. All domains contain 39 vertical levels from the surface up to 100 hPa with decreased vertical grid spacing in the closest 200 hPa to the ground to provide enhanced resolution of the boundary layer. Table 2.1 lists the dimensions of each domain, while Figure 2.1 shows nest placement within the parent domain. A one-way nesting technique is employed for this study. Each nest's parent domain serves as the boundary conditions for the nest after being smoothed and interpolated. The nest is then simulated at its native resolution. The sub-grid scale parameterization choices (Table 2.2) were based on previous high-latitude studies (Hines and Bromwich, 2008, Hines et al., 2011). The cumulus parameterization is turned off for d03 and d04, as clouds can be reasonably resolved with grid spacing below 3 km. No planetary boundary layer scheme is used in d04 as grid spacing is adequate to resolve the largest boundary layer eddies. In the next section, synoptic-scale analysis will concentrate on d02, while surface and boundary layer analysis will focus on d04. Domain 3 is not used in analysis, but was required as an intermediate nest for model stability in order to provide the high resolution of d04. The first 12 hours of the model runs represent the spin-up time for the atmospheric dynamics, allowing the coupling between the atmospheric and land surface models to equilibrate. Analyses and interpretation are focused on model output after t=12 hours.

Table 2.1 WRF Model Domain Grid Sizes and Spatial Resolution

Domain	Grid size	Horizontal Grid Spacing
d01	432 × 376	9 km
d02	904 × 976	3 km
d03	300 × 300	1 km
d04	300 × 300	0.333 km

Table 2.2 WRF Model Parameterization Choices with Active Domains

	Model Parameterization Choices		
Shortwave radiation	Goddard	Chou and Suarez (1994)	d01, d02, d03, d04
Longwave radiation	Rapid Radiative Transfer Model (RRTM)	Mlawer et al. (1997)	d01, d02, d03, d04
Cloud physics	Morrison bulk microphysics	Morrison et al. (2005)	d01, d02, d03, d04
Land surface	Noah LSM	Tewari et al. (2004)	d01, d02, d03, d04
Planetary boundary layer	Mellor – Yamada – Janjic (MYJ)	Janjić (1994)	d01, d02, d03
Sub-grid scale cumulus	Grell	Grell and Dévényi (2002)	d01, d02

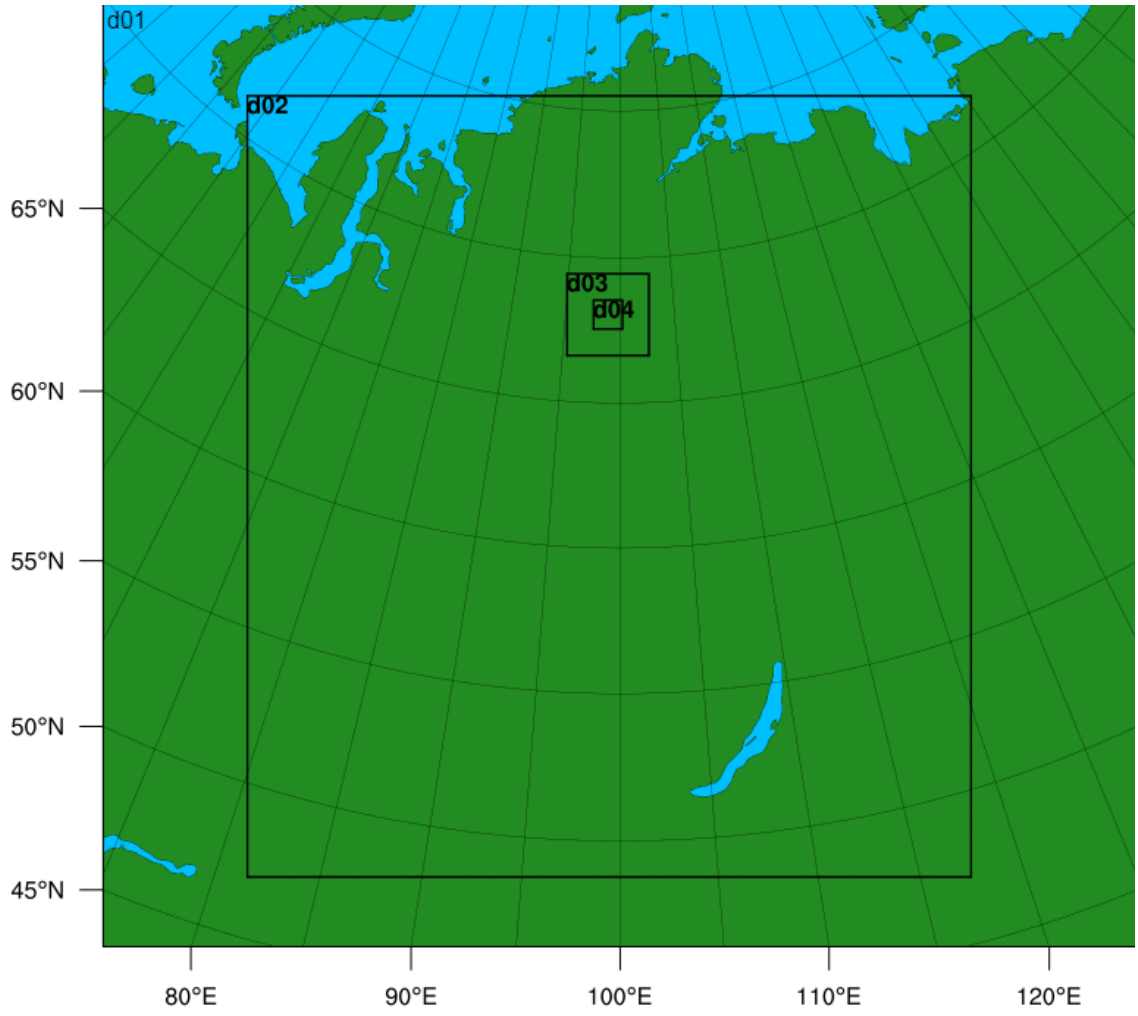

Figure 2.1 WRF parent domain (d01) with three associated nests (d02, d03, and d04).

The Noah land surface model has been the standard land surface model for coupled simulations in the WRF-ARW for nearly 20 years (Chen and Dudhia, 2001). The purpose of the soil model is to provide realistic surface roughness, skin temperature, and soil moisture availability so that surface fluxes of heat, moisture, and momentum may be calculated by WRF's atmospheric surface layer parameterization. As such, information from WRF (cloud cover, radiation tendencies, precipitation, etc.) is

communicated to the soil model, which, coupled with deep soil layer conditions within the soil model, is used to drive physically realistic changes to the surface condition at each model timestep. It contains four soil layers (0-10 cm, 10-40 cm, 40-100 cm, and 100-200 cm) and contains prognostic equations for soil temperature and moisture with model physics that account for processes in both thawed and frozen soils. Soil temperature and moisture profiles characterizing continuous and discontinuous permafrost areas were derived from observations at representative sites (see Section 2.2.3). These profiles were applied homogeneously to the nested domains, but allowed to vary after model initialization. Based on the dominant characteristics of the region, the land surface and soil type were set to a constant wooded tundra and loam across the entire domain, respectively. WRF initial and boundary conditions are set using the National Centers for Environmental Prediction Global Forecasting System's Analysis product. This dataset is provided on a 0.5° horizontal grid with 28 vertical levels. In total, four experiments are conducted in the study, incorporating combinations of two different synoptic weather patterns (active and quiescent) and two different soil conditions (continuous and discontinuous permafrost), as described below.

2.2.2. Synoptic regimes

To determine the role of ambient synoptic weather patterns in modulating the effect of different permafrost conditions, two historic three-day weather events are used to force the atmospheric component of the model. An active synoptic pattern occurred over the experimental domain between June 28th and July 1st, 2014. A low-pressure system entered from the west and traversed the domain over the 72-hour period (Figures

2.2a-d). The second scenario is characterized by a generally quiescent synoptic pattern taking place between July 2nd and July 5th, 2013, where the region's weather was dominated by a ridge of high surface pressure, leading to little organized, large-scale atmospheric forcing for clouds or precipitation over the experimental area (Figure 2e-h). A low-pressure system skirts the southeastern corner of the quiescent run's d02 during day 3 of the simulated period but does not affect d04 where the higher-resolution boundary layer analysis will be conducted.

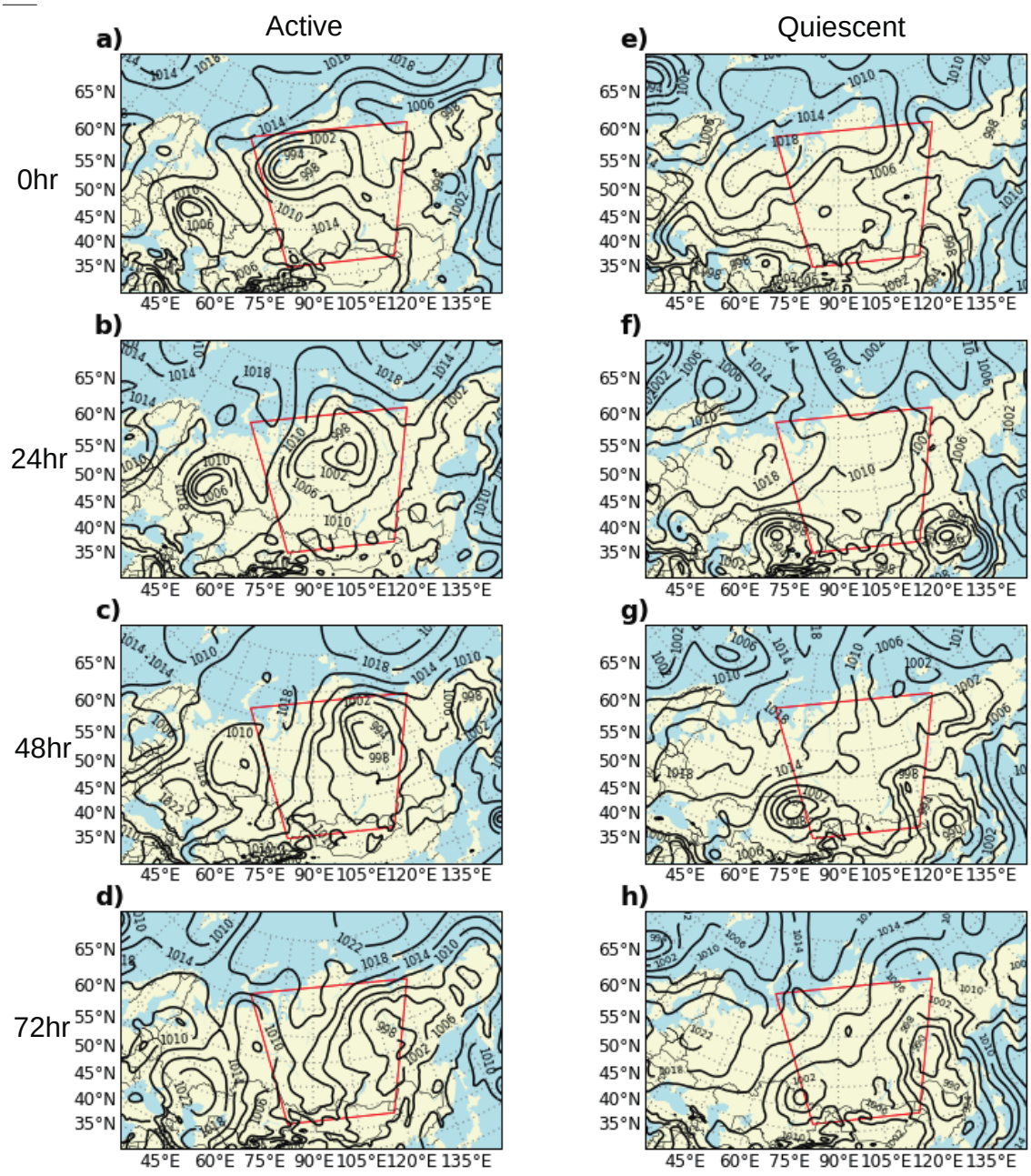

Figure 2.2: Synoptically active (left) and quiescent (right) events with mean sea-level pressure shown in black contours at 4-hPa increments at model hours a/e) 0; b/f) 24; c/g) 48; and d/h) 72; d02 is outlined in red.

2.2.3. Soil conditions

For both continuous and discontinuous permafrost, soil temperature values (Table 2.3) were calculated as an average of July 1st observations from 2000 – 2008 at representative stations from the All-Russia Research Institute of Hydrometeorological Information - World Data Centre database (obtained from http://meteo.ru/english/climate/soil.php). These observations were linearly interpolated to the midpoints of the four soil layers defined by the Noah land surface model, as described in Section 2.2.1. The soil temperature profile for the idealized discontinuous permafrost remains above freezing down to soil layer 4. This indicates an active layer that is deeper than 200 cm, however, the discontinuous experiment could therefore also be considered to apply to seasonally frozen ground regions. Soil moisture values (Table 3) were based on a percentage of the maximum volumetric water capacity (VWC) of loam. In the continuous permafrost experiments, the top three unfrozen layers are assumed to be completely saturated, so VWC values are 100% of the maximum value. The fourth layer (100 – 200 cm) is frozen, zero percolation of water from the top three layers into this layer is assumed, and the VWC is set to zero. This is meant to simulate surface and suprapermafrost water conditions at their most extreme after spring snowmelt with very little runoff (Michel and Van Everdingen, 1994). In the discontinuous permafrost experiments, VWC increases from the surface to the lowest layer, much like the observations of a discontinuous permafrost site in Zhang et al. (2003). Our idealized continuous and discontinuous permafrost conditions constitute the opposite ends of the spectrum in terms of permafrost degradation: a soil column with an

active layer that is saturated with water (from spring snowmelt and/or precipitation) that is unable to infiltrate the permafrost table, and a soil column that has a much deeper active layer (or no permafrost), better allowing any moisture to drain into the soil and potentially the groundwater system.

Table 2.3 Soil Temperature and Moisture Values for Idealized Continuous and Discontinuous Permafrost Ground Conditions

		Continuous		Discontinuous	
Soil layer		Temperature (K)	Soil moisture (m^3/m^3)	Temperature (K)	Soil moisture (m^3/m^3)
1	0–10 cm	283.31	0.439	288.20	0.120
2	10–40 cm	279.37	0.439	285.50	0.250
3	40–100 cm	273.79	0.439	282.80	0.250
4	100–200 cm	271.67	0.000	281.89	0.400

2.2.4. Calculation of boundary layer and lifted condensation level heights over d04

Due to the boundary layer parameterization being turned off for d04, WRF does not produce a boundary layer height variable that can be used for analysis in that domain. To compare the daytime boundary layer height with other variables in that domain, we calculated daytime boundary layer height according to Bryan and Fritsch (2002). This algorithm defines the boundary layer height as the height at which the virtual potential temperature first exceeds the value of the virtual potential temperature at the lowest model level. The height of the lifting condensation level (LCL) was calculated at each grid point in d04 by multiplying the surface dew point depression by the dry adiabatic lapse rate and adding the terrain elevation to the result to obtain the height of the LCL above mean sea level.

2.3. Results

2.3.1. Large-scale feature analysis

To examine the impact of permafrost ground conditions on surface and atmospheric variables, synoptic-scale features from d02 are analyzed first, before analyzing the underlying physical processes on the finer nested domains in later subsections, where boundary layer parameterizations are not required.

Qualitative differences are apparent in cloudiness within the lowest two kilometers in both the active and quiescent regimes as continuous permafrost experiences more cloudiness in the lower levels when compared to discontinuous permafrost (Figure 2.3). Differences in the low-level cloud fraction when comparing continuous and discontinuous permafrost with both an active and quiescent atmosphere (Figure 2.3a vs. 2.3b; Figure 2.3c vs. 2.3d) begin near model hours 0, 24, and 48 (~7:00 a.m. LST) near the surface and then expand vertically as the boundary layer grows throughout the day. When comparing the quiescent continuous and discontinuous cases (Figure 2.3c vs. 2.3d), clouds consistently extend below 2,000 m over the continuous permafrost whereas the cloud base remains at the 2,000 m mark over discontinuous permafrost. The low-level cloud fraction is greater in the quiescent continuous experiment (Figure 2.3c) when compared to the active continuous experiment (Figure 3a) by approximately 5%. Similar qualitative results in cloud fraction exist on d04 (shown later), where cumulus and boundary layer parameterizations are turned off, suggesting the cloud fraction results are directly related to the modified permafrost

conditions regardless of whether shallow convection and the boundary layer are parameterized or resolved by the model.

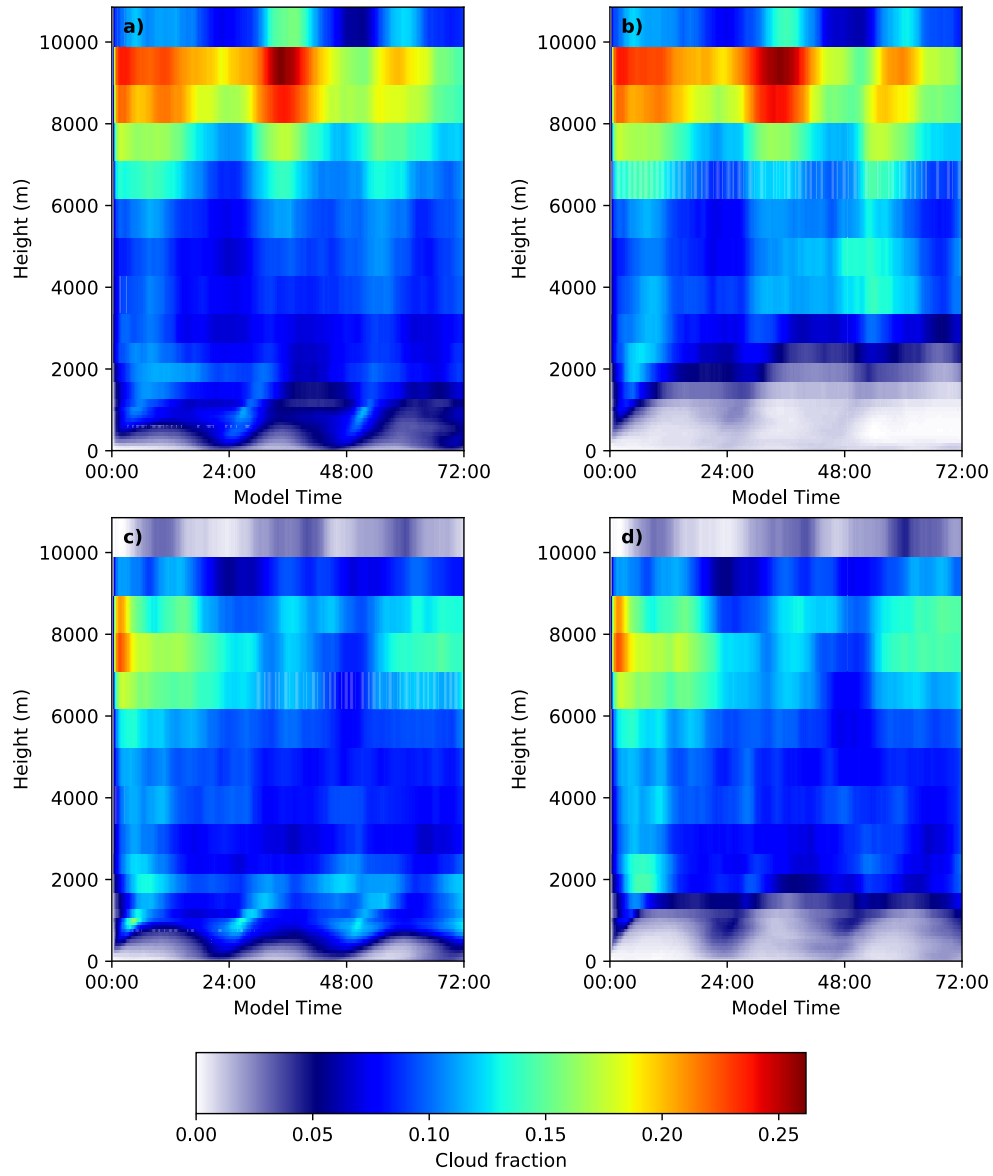

Figure 2.3: Time-height plots of horizontally averaged cloud fraction over d02 for a) active continuous, b) active discontinuous, c) quiescent continuous, and d) quiescent discontinuous experiments.

Continuous permafrost with both an active and quiescent atmosphere also exhibits greater total 72-hour accumulated precipitation (both in terms of spatial extent and maximum values) when compared to discontinuous permafrost (Figure 2.4). In addition to increased rainfall around the track of the center of the low pressure system which swept across the northern part of the domain (Figure 2.5), the active continuous case also has larger precipitation accumulation south of the low, below 60°N (Figure 2.4a), while the active discontinuous simulation's greatest precipitation is concentrated in the area around the low pressure center (Figure 2.4b). In the quiescent cases, there is a small spatial increase in the scattered precipitation accumulation across the southern portion of the domain in the continuous permafrost case (Figure 2.4c) when compared to discontinuous permafrost (Figure 2.4d). A low pressure system skirts the southeast portion of the domain in each of the quiescent cases late in the period, causing the observed maxima in accumulated precipitation. However, once again, continuous permafrost (Figure 2.4c) experiences larger maxima of accumulated precipitation.

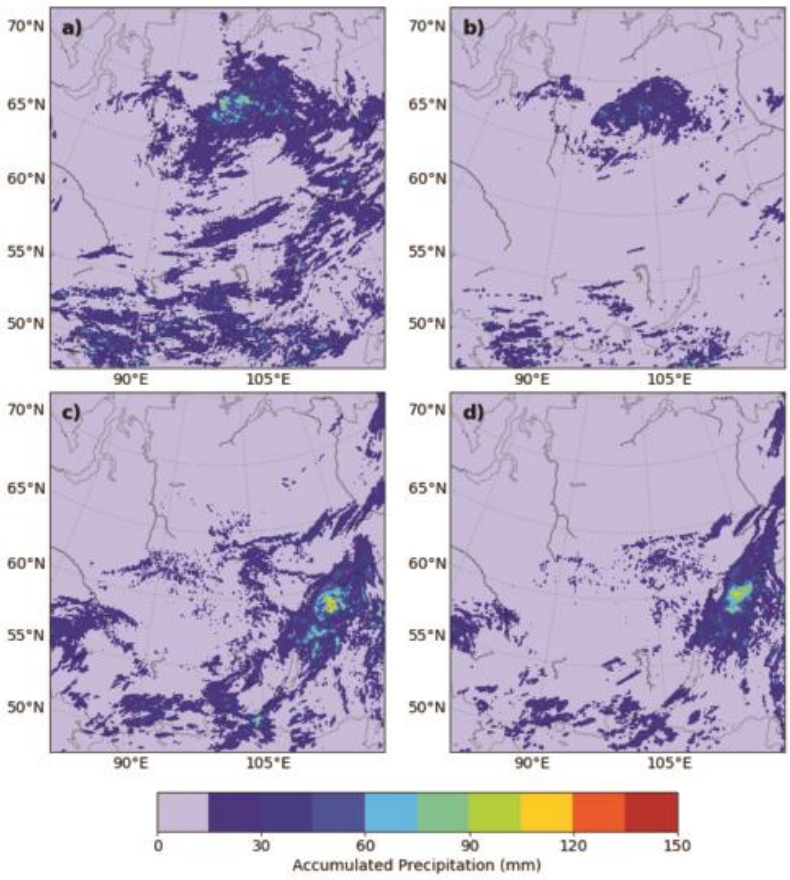

Figure 2.4: Time-height plots of accumulated precipitation over d02 for a) active continuous, b) active discontinuous, c) quiescent continuous, and d) quiescent discontinuous experiments.

Broad synoptic forcing patterns at the surface and upper levels (i.e., the 500 hPa pressure surface) were also analyzed to determine the influence of the soil conditions on the upper-level height fields and surface storm track in the synoptically active experiment. Figure 2.5 depicts the position and magnitude of the minimum surface pressure over the domain over the model period. Over the first 24 hours of the model run, both the continuous and discontinuous runs show no major differences in the minimum pressure value of the surface low. However, over the last 48 hours of the run,

there is a slight drift to the south for the center of low pressure in the discontinuous case, as it becomes deeper than the more northerly low in the continuous case. The low over discontinuous permafrost is stronger by 2-3 hPa and has a faster forward speed when compared to continuous permafrost, moving out of the model domain before the end of the 72-hour run.

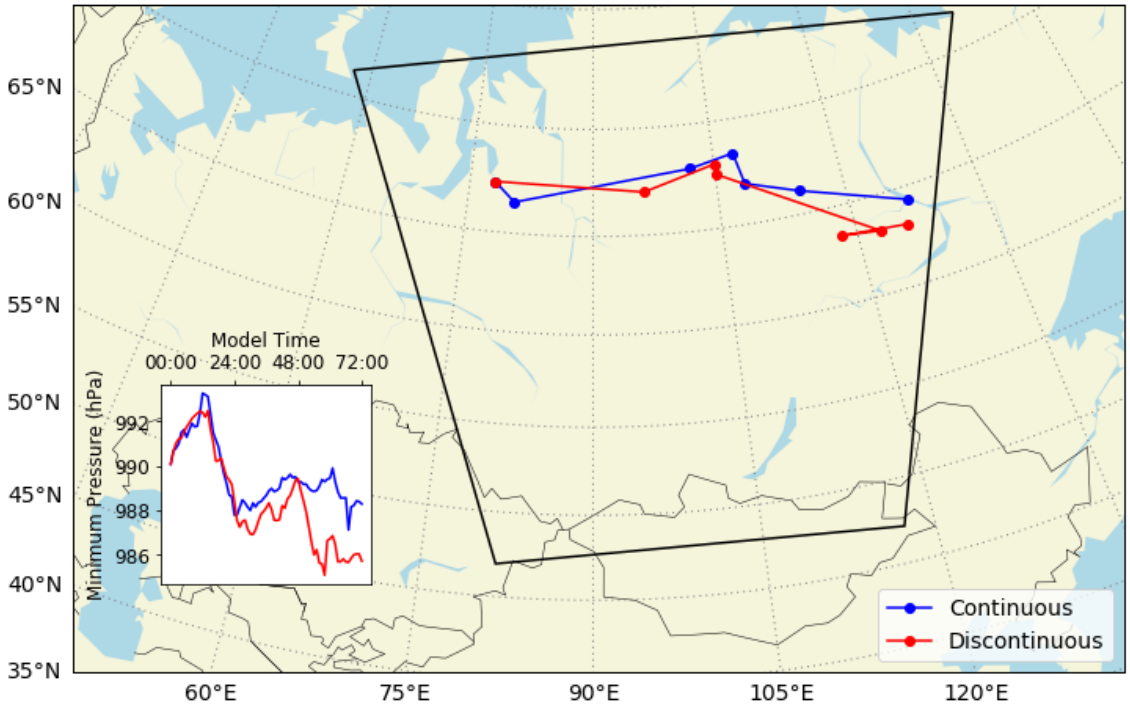

Figure 2.5: Map: Track of position of center of low pressure every 12 hours in the active model runs, with d02 outlined. Inset: Time series of the magnitudes of the minimum pressure in the domain for each of the active simulations.

The relative strengths of these large-scale features are quite the opposite when the 500 hPa height pattern at model hour 72 is analyzed (Figure 2.6). Over continuous permafrost, a stronger 500 hPa short-wave trough is evident with minimum heights below 544 dam in the center of a closed upper-level low (Figure 2.6a), compared with

the weaker 548 dam closed low over discontinuous permafrost (Figure 2.6b). The continuous experiment's 500 hPa short-wave trough also tracks farther south by ~3 degrees of latitude. In addition to the magnitude of the upper-level low, there is a wider swath of maximum winds around the feature over continuous permafrost when compared to discontinuous permafrost. This is in stark contrast with the 500 hPa patterns of the continuous and discontinuous cases in the quiescent experiments (not shown) which are largely indistinguishable from one another.

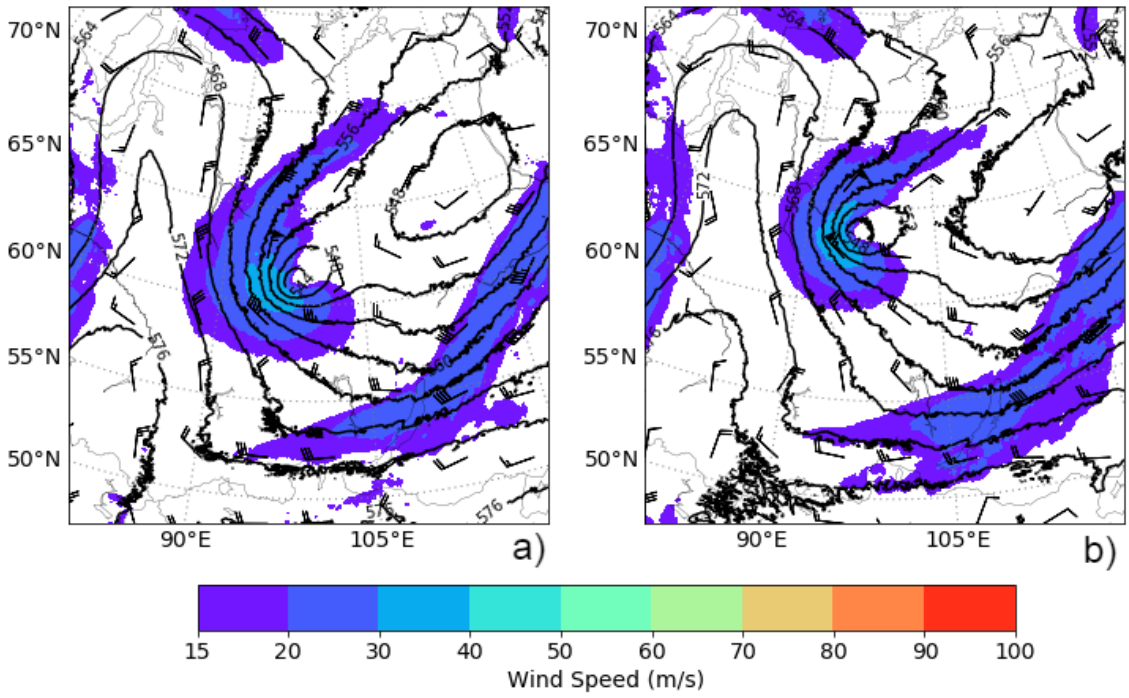

Figure 2.6: 500 hPa heights (dam) and winds at model hour 72 for the active a) continuous and b) discontinuous simulations.

2.3.2. Surface flux and boundary layer analysis

To elucidate the smaller-scale boundary layer processes that are associated with the larger-scale changes discussed above, we analyze the higher resolution d04. The fine

spatial resolution of this nest allows (at least coarse) resolution of convection and boundary layer turbulence, removing the need for cumulus or boundary layer parameterizations.

Discontinuous permafrost generally exhibits larger sensible heat fluxes (Figure 2.7a) compared to continuous permafrost because of the lack of soil moisture and consequently less evaporation. Given an active atmosphere, differences in sensible heat flux are smaller between continuous and discontinuous permafrost, likely due to the influence of stronger near-surface winds and widespread precipitation in d04 in the active regime. The cold front passes through d04 around t = 24 hours, after which the sensible heat fluxes are very similar. This is likely due to increased soil moisture in the discontinuous case due to precipitation, stronger advection, and vertical mixing as surface winds increase behind the front. Latent heat fluxes (Figure 2.7b) in the active experiments also show smaller differences after the cold front passage and its associated precipitation in the domain (Figure 2.7c). However, that relationship subsides and differences increase once again by the middle of day 3, which leads to that simulation's second period of precipitation accumulation starting around t = 60 hours. The quiescent atmosphere over discontinuous permafrost exhibits relatively weak latent heat fluxes over the entire 72-hour simulation period, while the initial saturated soil causes a stronger latent heat flux over continuous permafrost. In each of the continuous runs, the lower troposphere is much closer to saturation than over discontinuous permafrost (Figure 2.8) due to the increased latent heat flux moistening the boundary layer.

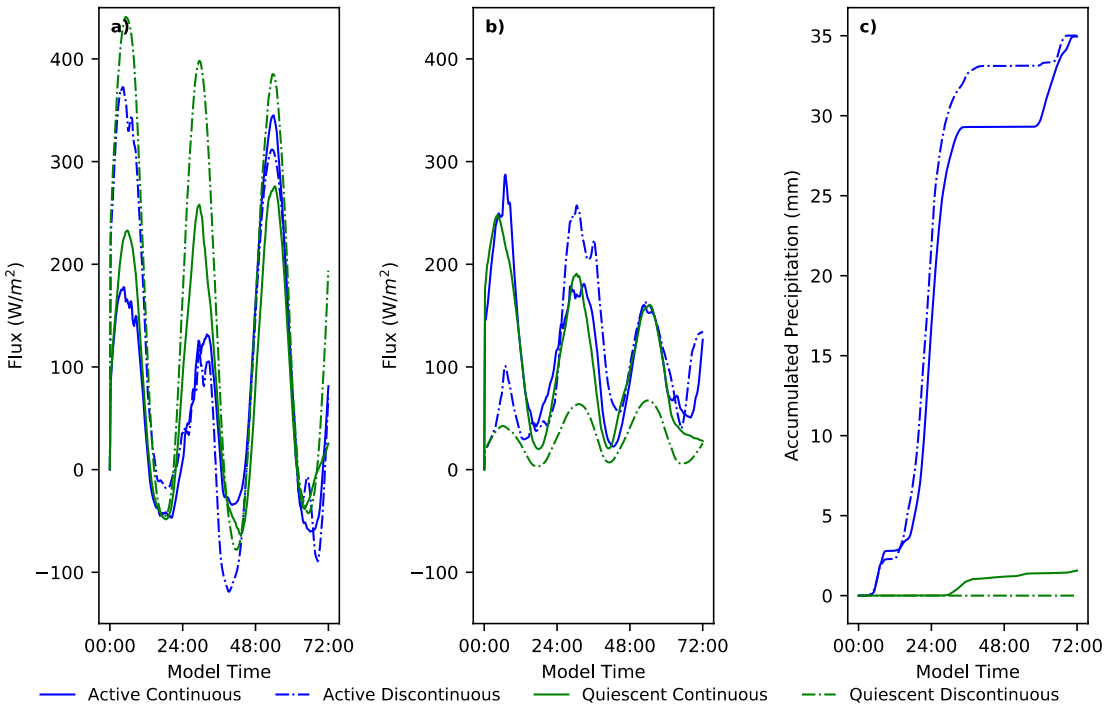

Figure 2.7: Time series of horizontally averaged a) sensible heat flux, b) latent heat flux, and c) accumulated precipitation over d04 for the four model experiments.

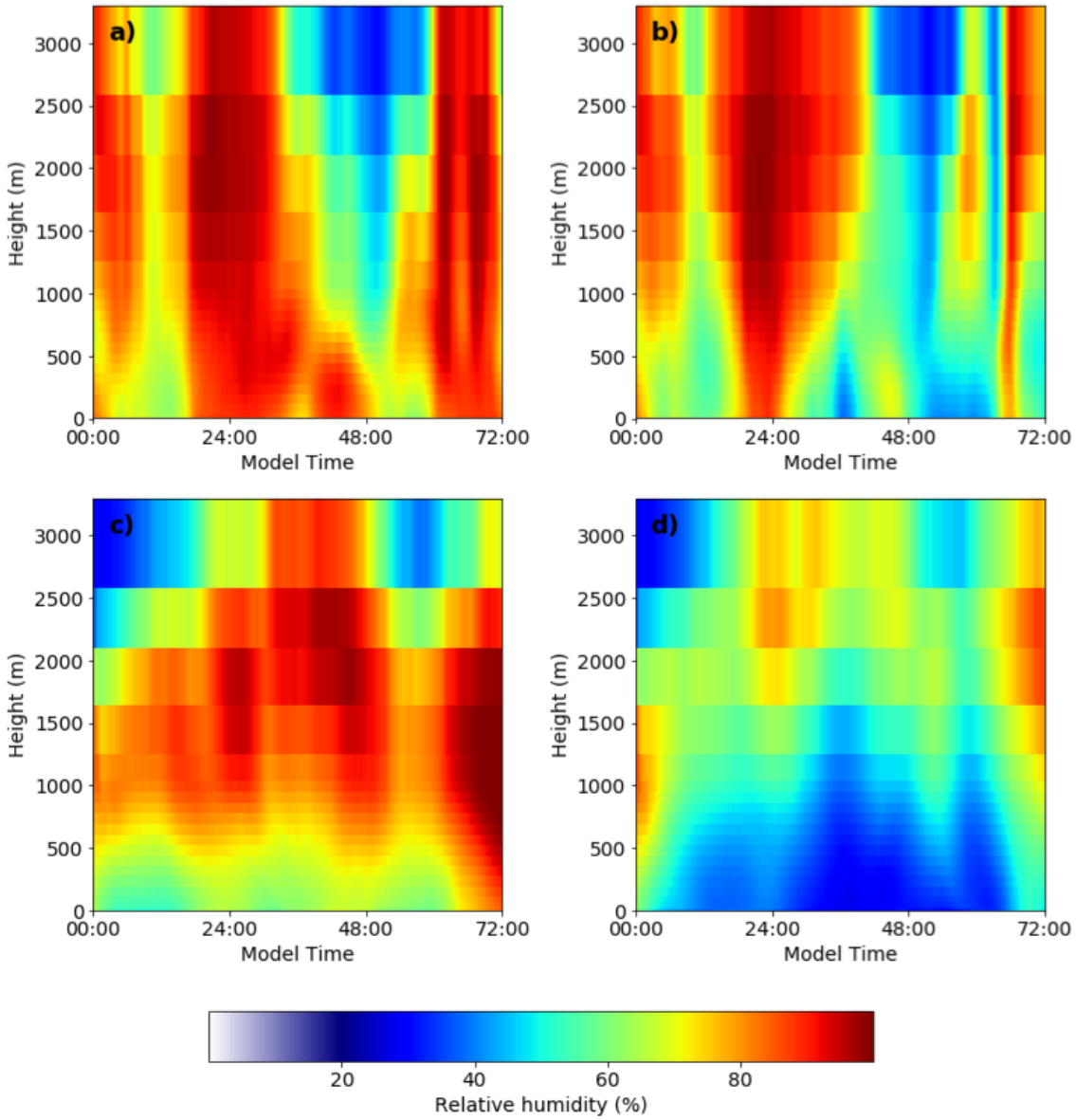

Figure 2.8: Time-height plots of horizontally-averaged d04 relative humidity for a) active continuous, b) active discontinuous, c) quiescent continuous, and d) quiescent discontinuous model experiments.

This soil moisture-cloud-precipitation feedback can partly be explained by the relationship between the boundary layer height and LCL. In the active case, the height of the boundary layer exceeds the LCL throughout the entire model run over continuous

permafrost (Figure 2.9a), consistent with the relatively high low-level relative humidity over that period, especially during the first 48 hours (Figure 2.8a). In contrast, there are only certain times throughout the simulation when the boundary layer grows above the LCL over discontinuous permafrost, most notably, directly preceding and during the precipitation event around hour 24. When the boundary layer does fall below the LCL, differences are not large (Figure 2.9a). The relatively comparable latent heat fluxes in the active continuous and discontinuous cases (Figure 2.7b) due to increased moisture advection and precipitation/soil moisture from the synoptic system likely allow for the lower-level saturation in both of the active scenarios.

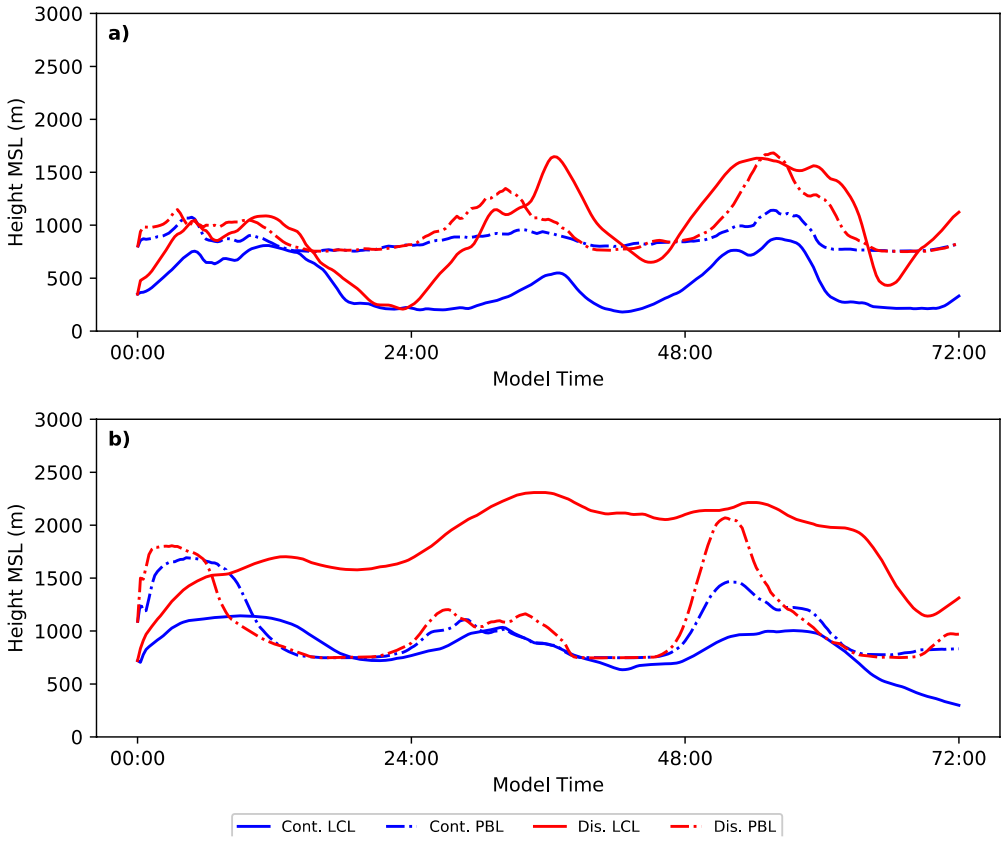

Figure 2.9: Comparisons between boundary layer height and lifting condensation level (LCL) for a) active and b) quiescent cases.

When synoptic forcing is absent, large differences in the height of the LCL between the quiescent continuous and discontinuous experiments become apparent (Figure 2.9b). The boundary layers develop fairly similarly over both continuous and discontinuous permafrost, with the largest difference occurring during the morning and early afternoon of Day 3 when the average boundary layer height over discontinuous permafrost reaches 2,000 m while over continuous permafrost it is limited to ~1,500 m. However, aided by large latent heat fluxes and a moistening of the lower atmosphere (Figure 2.8c), the LCL over continuous permafrost is consistently near or below 1,000 m for the entire 72-hour period. From the middle of Day 1 until the end of the 72-hour simulation, boundary layer heights exceed the LCL in the continuous permafrost simulation and lead to subsequent low-level cloud development throughout the period (Figure 2.10c). Over discontinuous permafrost, without a significant moisture input from the surface or horizontal advection, LCL heights increase throughout most of the period, starting around 750 m at the beginning of the model run and rising to over 2,000 m for most of days 2 and 3 before decreasing again toward the end of the 72-hour period. However, outside of the first few hours of the simulation, the boundary layer remains below the height of the LCL and the scant ambient moisture prohibits the development of any large-scale low-level clouds throughout the duration of the simulation (Figure 2.10d). Soil conditions do not play a large role in the cloud pattern aloft (which is more influenced by the large-scale flow), therefore Figure 2.10 focuses on the lower troposphere near the boundary layer top.

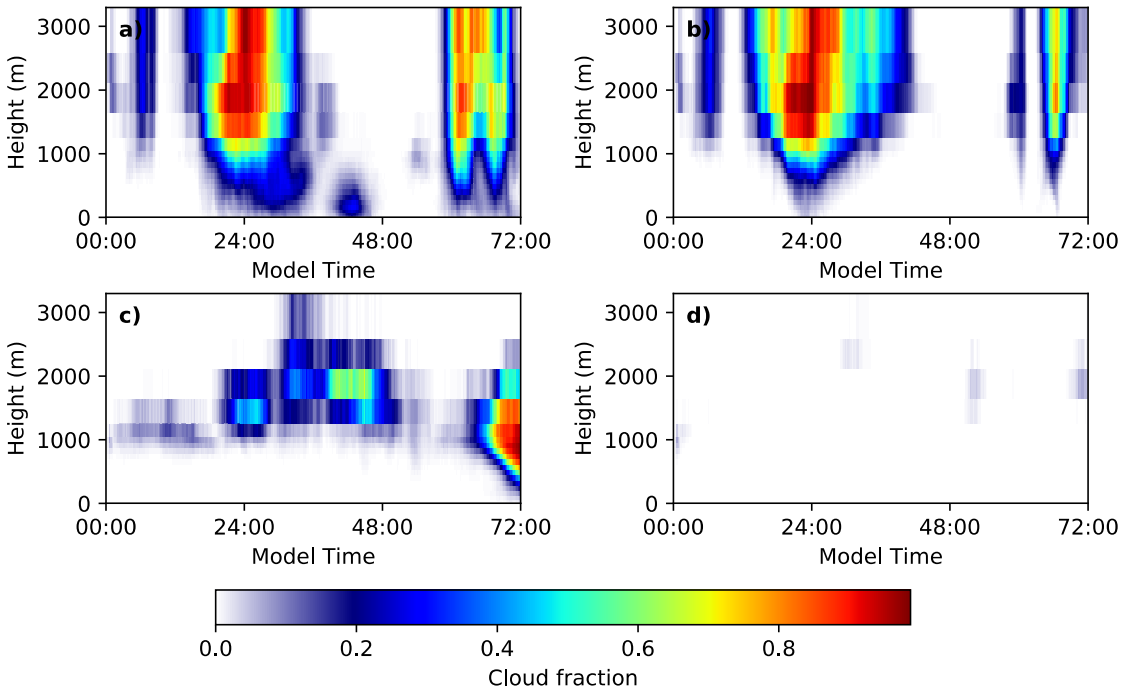

Figure 2.10: Time-height plots of horizontally averaged cloud fraction over d04 for a) active continuous, b) active discontinuous, c) quiescent continuous, and d) quiescent discontinuous experiments.

To provide context to the differences in the storm tracks and 500 hPa heights in the active cases described in Section 2.3.1, d04 is examined because it is near the storm track throughout the simulation. The storm track shift follows the results of Pal and Eltahir (2003, their Figure 8) who observed a southward displacement and eastward extension of a 500 hPa anomalous low associated with increased soil moisture in the southwestern United States. Temperatures in the boundary layer over continuous permafrost were lower than over discontinuous permafrost, as more of the energy was used for evaporation rather than heating the ground (Figure 2.11a, b). This corresponded with increased low-level clouds, which likely decreased the amount of low-level

radiative heating and sensible heat flux over continuous permafrost. Consequently, geopotential heights lowered over continuous permafrost (Figure 2.6) as described in Section 2.3.1, potentially leading to a southward position of the upper level short-wave trough.

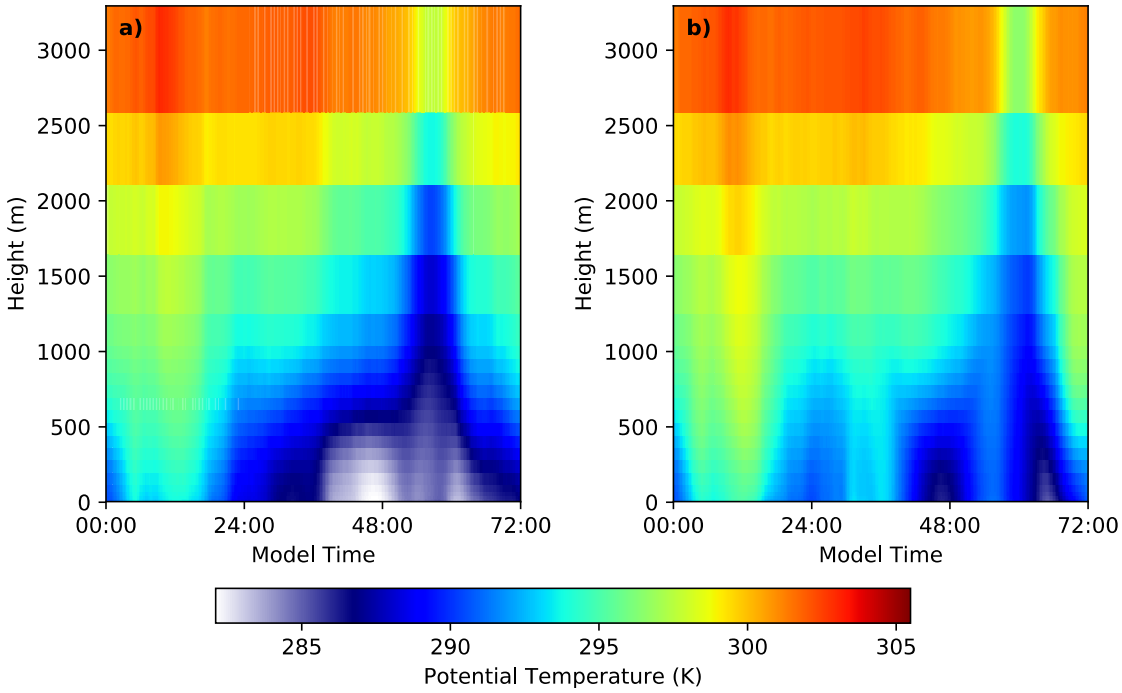

Figure 2.11: Time-height plots of horizontally averaged potential temperature over d04 for active a) continuous and b) discontinuous conditions.

2.4. Discussion

Soil conditions associated with continuous versus discontinuous permafrost are found to result in different boundary layer and large-scale weather processes. In both a synoptically active and quiescent atmosphere, low-level cloudiness is enhanced over continuous permafrost, where additional moisture retained in a saturated active layer evaporates into the boundary layer. This effect is most pronounced when comparing

continuous and discontinuous permafrost in the quiescent case, as the strong dynamic forcing in the active regime dominates the effect that the ground and boundary layer conditions have on the environment. While this study explores land-atmosphere interactions specific to summertime permafrost temperature and moisture characteristics, these findings are consistent with soil moisture-atmosphere feedbacks in other environments.

It is important to note that the idealized ground conditions presented here do not represent the fixed current and future states of permafrost. For example, areas of continuous permafrost can have taliks that allow water to reach the subpermafrost layer, and water can drain due to terrain features (Jafarov et al., 2018). Similarly, near-surface soils in discontinuous permafrost are able to retain water that can be evaporated into the lower atmosphere (Hayashi et al., 2004). Nevertheless, our approach of prescribing idealized wet and dry soil scenarios follows that of similar land-atmosphere interactions studies outside the Arctic (Findell and Eltahir, 2003, Margulis and Entekhabi, 2001, Schär et al., 1999). Margulis and Entekhabi (2001) noted the importance of boundary layer moisture as a conduit for surface-atmosphere energy exchanges. The results of this study support Schär et al. (1999)'s conclusion that increased precipitation over wet soils can be attributed to the enhancement of the low-level moisture profile in the wake of atmospheric advection. This is evident in our increased area extent of precipitation in the synoptically active continuous case versus the discontinuous experiment, whereas the effect was subdued when comparing the quiescent continuous and discontinuous experiments. While there were major differences in the partitioning of sensible and latent

heat fluxes between continuous and discontinuous permafrost in both the active and quiescent experiments, for each of the four scenarios, in sum, the cumulative fluxes were nearly identical. Lower boundary layer heights over continuous permafrost, due to higher contributions of latent heat flux at the expense of sensible heat flux, allow for an increased combined energy per unit depth of the boundary layer. Schär et al. (1999) noted that, as in previous studies, the higher moist entropy within the boundary layer is an acceptable indicator of convection, especially when synoptically forced events (e.g., active case) can support enhanced uplift of this air to the level of free convection.

When there is no large-scale forcing, the consequence of low-level humidity from evaporation over wet soils (i.e., continuous permafrost in our idealized case) is apparent in the formation of clouds near the top of the boundary layer. Findell and Eltahir (2003) created a low-level humidity index (HI_{low}) as one part of their framework for soil moisture-boundary layer interactions. HI_{low} is defined as the dewpoint depression difference between 50 and 150 hPa above the surface. Based on models and observations, they deduced that an atmosphere with early morning HI_{low} values of 5°C or lower will develop shallow clouds regardless of the soil conditions. Figure 2.12 shows the HI_{low} values for the four experimental runs in our study. Ignoring the active runs because synoptic forcing aids convective processes, minimal values of the index are present in the early mornings (~t = 0, 24, 48 hours) over continuous permafrost, which also exhibited low-level cloudiness throughout a majority of the model period. Conversely, quiescent HI_{low} index values for discontinuous permafrost are consistently above 10°C, a low-level environment far too dry to produce low-level clouds on its own.

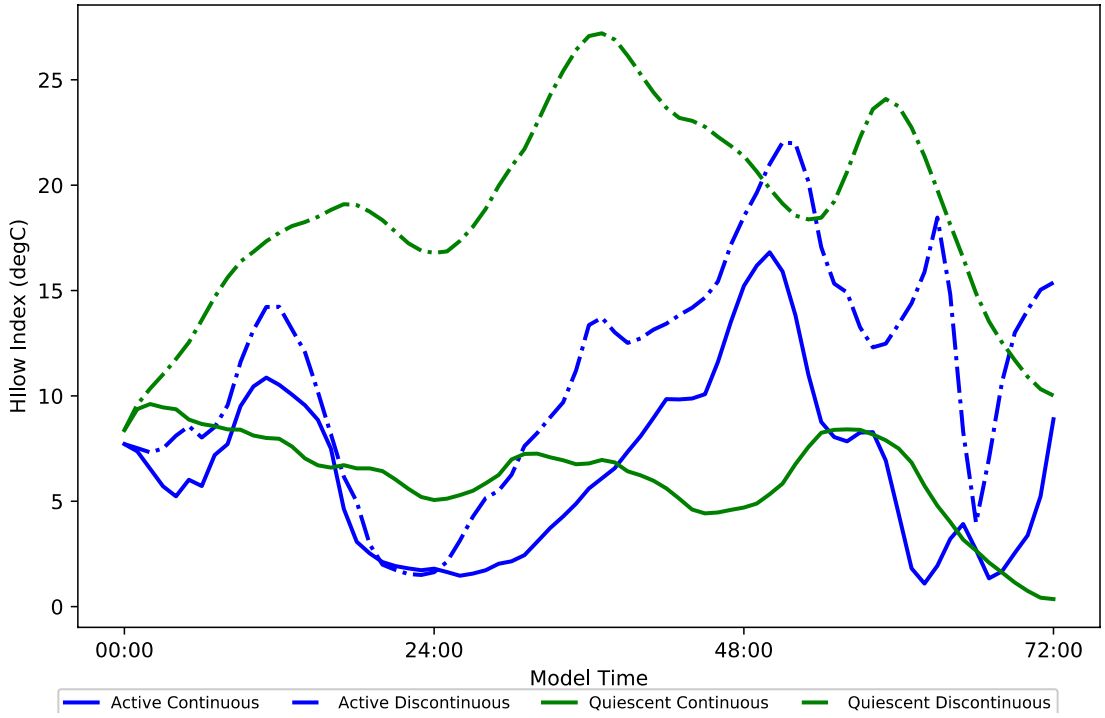

Figure 2.12: Time series of d04-averaged HI_{low} index values for each of the four model experiments.

The results of this study also support the findings of Qian et al. (2013), who investigated the effect of irrigation on land-atmosphere interactions in the United States Great Plains. It is an intuitive comparison, as irrigated land and a shallow active layer saturated by precipitation and spring snowmelt should have similar thermodynamic properties (with parallel linkages between unirrigated land and our discontinuous permafrost cases). In contrast to our experiments, Qian et al. (2013) performed summer-long simulations providing a season-long climatological perspective rather than our process-driven simulation of discrete events. However, the aim of our paper was not to quantify ground and atmospheric variables, but rather to dissect the processes given different synoptic and soil conditions. Future work should expand upon the number of

events analyzed to determine whether modeled climatological means express a quantitative difference based on ground and/or synoptic conditions.

This study is consistent with previous literature from the midlatitudes, however, notable differences are evident for the Arctic. For example, previous literature has shown that moist convection can occur over dry soils from strong sensible heating causing high boundary layers (~3-4 km). Because many of these studies were completed in the midlatitudes, summertime solar energy was sufficient to heat up dry soils and create strong thermal eddies. However, the Arctic does not receive large amounts of solar insolation, even during Northern Hemisphere summer. Because of the Arctic's limited solar input, there is an analogous limit to how much energy can be transferred back into the lower atmosphere and, hence, a limit on how high boundary layers are able to grow in the high latitudes. This is apparent in the results of the quiescent discontinuous experiment. The 72-hour model run saw no large amounts of cloud cover, yet boundary layer heights were only able to reach 2 km for a short period on the morning of day 3. At that time in the simulation, the boundary layer height was near the LCL (~100-200 m difference), but overall, boundary layer heights were 1-1.5 km below the LCL throughout much of the model run. The Arctic is inherently an energy-limited system due to its geometric relationship with the sun. However, as permafrost degradation continues, if soils dry out due to the transition from continuous to discontinuous permafrost, land-atmosphere feedbacks in these regions can also become soil moisture-limited or change the seasonality of any type of transitional regime (Seneviratne et al., 2010).

Permafrost degradation is projected to increase in the future (Slater and Lawrence, 2013, Wang et al., 2019). In the decade since the International Polar Year, Biskaborn et al. (2019) analyzed Global Terrestrial Network for Permafrost observations across the globe and uncovered consistent warming of frozen ground across all continents, latitudes, and elevations. They found that temperatures have increased at continuous permafrost sites faster than at discontinuous, sporadic, or isolated observing stations. In addition, they found an increasing snow depth trend across Arctic continuous and discontinuous permafrost regions, but with snowmelt ending earlier in the summer (continuous: mid-June, discontinuous: early June), which can lead to drier conditions as higher temperatures continue on in the summer months. This promotes a biogeophysical impact on the climate system. However, as reviews and position papers (Oliva and Fritz, 2018) state, most ongoing and calls for future research are geared towards understanding the biogeochemical feedbacks that result from permafrost degradation. While clearly important, as the carbon storage in permafrost regions will play a large and still undetermined part in future warming, land-atmosphere interactions that results from the thawing of these regions must also be included to understand and predict feedbacks on the regional weather and climate in the high-latitudes. Data collected from ongoing projects such as NASA's Arctic-Boreal Vulnerability Experiment, which include field-based measurements of soil moisture and temperature, eddy covariances, and meteorological information in the United States and Canadian Arctic, could be used to help quantify these exchanges.

2.5. Conclusions and Future Work

This WRF modeling study used idealized homogeneous soil characteristics representing summertime continuous and discontinuous permafrost conditions to quantify and describe the impact of transitioning permafrost states on surface, boundary layer, and synoptic-scale weather. An additional experimental factor of ambient synoptic weather conditions was included to examine the impact of large-scale atmospheric forcing on amplifying or reducing the effects of soil conditions. Synoptic forcing associated with the passage of a low-pressure system in the active scenario tends to dominate the impact of the soil condition, though differences exist in precipitation intensity, upper level height patterns, and surface low-pressure intensity and tracks. When there is no ambient synoptic forcing, the injection of low-level moisture due to continuous permafrost (and subsequent removal of moisture when the Arctic transitions to a drier discontinuous permafrost environment) has a large impact on cloud development, which consequently plays a role in precipitation during otherwise fair weather events, as in our quiescent scenario.

While the permafrost characteristics used as initial conditions in our experiments are idealized, the apparent processes at play show that permafrost degradation associated with continued climate change can play a potentially important role on the surface energy balance and associated weather and climate feedbacks. Though biogeochemical feedbacks are an important focus in current permafrost research, exploring how warming of permafrost will directly impact the dynamic and thermodynamic states of the climate system should also be emphasized. As continued permafrost degradation occurs and the

likelihood of drier soils in these regions increases, a positive local- to regional-scale feedback could develop as cloud development is suppressed, increased shortwave radiation is absorbed by the surface, soil temperatures and active layer depths increase, leading to further permafrost degradation. If these feedbacks persist longer into the cold season and over extensive areas, they could contribute to the observed Arctic amplification of climate change. Future work using coupled models is needed to fully determine these feedbacks at the continental and pan-Arctic scales, and their role in current and projected climate change.

2.6. References

ANISIMOV, O., BELOLUTSKAYA, M., GRIGORIEV, M., INSTANES, A., KOKOREV, V., OBERMAN, N., RENEVA, S., STRELCHENKO, Y., STRELETSKIY, D. & SHIKLOMANOV, N. I. 2010. Major natural and social-economic consequences of climate change in the permafrost region: predictions based on observations and modeling. *Moscow: Greenpeace*.

BISKABORN, B. K., SMITH, S. L., NOETZLI, J., MATTHES, H., VIEIRA, G., STRELETSKIY, D. A., SCHOENEICH, P., ROMANOVSKY, V. E., LEWKOWICZ, A. G., ABRAMOV, A., ALLARD, M., BOIKE, J., CABLE, W. L., CHRISTIANSEN, H. H., DELALOYE, R., DIEKMANN, B., DROZDOV, D., ETZELMULLER, B., GROSSE, G., GUGLIELMIN, M., INGEMAN-NIELSEN, T., ISAKSEN, K., ISHIKAWA, M., JOHANSSON, M., JOHANNSSON, H., JOO, A., KAVERIN, D., KHOLODOV, A.,

KONSTANTINOV, P., KROGER, T., LAMBIEL, C., LANCKMAN, J. P., LUO, D., MALKOVA, G., MEIKLEJOHN, I., MOSKALENKO, N., OLIVA, M., PHILLIPS, M., RAMOS, M., SANNEL, A. B. K., SERGEEV, D., SEYBOLD, C., SKRYABIN, P., VASILIEV, A., WU, Q., YOSHIKAWA, K., ZHELEZNYAK, M. & LANTUIT, H. 2019. Permafrost is warming at a global scale. *Nat Commun,* 10**,** 264.

BRYAN, G. H. & FRITSCH, J. M. 2002. A Benchmark Simulation for Moist Nonhydrostatic Numerical Models. *Monthly Weather Review,* 130**,** 2917-2928.

CHEN, F. & DUDHIA, J. 2001. Coupling an Advanced Land Surface–Hydrology Model with the Penn State–NCAR MM5 Modeling System. Part I: Model Implementation and Sensitivity. *Monthly Weather Review,* 129**,** 569-585.

CHEN, H., NAN, Z., ZHAO, L., DING, Y., CHEN, J. & PANG, Q. 2015. Noah Modelling of the Permafrost Distribution and Characteristics in the West Kunlun Area, Qinghai-Tibet Plateau, China. *Permafrost and Periglacial Processes,* 26**,** 160-174.

CHOU, M.-D. & SUAREZ, M. J. 1994. An efficient thermal infrared radiation parameterization for use in general circulation models. *NASA Technical Memorandum 104606,* 3**,** 85.

CULLATHER, R. & LYNCH, A. An analysis of static stability in the Arctic atmosphere. Preprint Volume, Seventh AMS Conference on Polar Meteorology and Oceanography, 2003. 12-16.

DIRMEYER, P. A., CASH, B. A., KINTER, J. L., STAN, C., JUNG, T., MARX, L., TOWERS, P., WEDI, N., ADAMS, J. M., ALTSHULER, E. L., HUANG, B., JIN, E. K. & MANGANELLO, J. 2012. Evidence for Enhanced Land–Atmosphere Feedback in a Warming Climate. *Journal of Hydrometeorology,* 13**,** 981-995.

FEDOROV, A. N., GAVRILIEV, P. P., KONSTANTINOV, P. Y., HIYAMA, T., IIJIMA, Y. & IWAHANA, G. 2014. Estimating the water balance of a thermokarst lake in the middle of the Lena River basin, eastern Siberia. *Ecohydrology,* 7**,** 188-196.

FINDELL, K. L. & ELTAHIR, E. A. B. 2003. Atmospheric Controls on Soil Moisture–Boundary Layer Interactions. Part I: Framework Development. *Journal of Hydrometeorology,* 4**,** 552-569.

FORD, T. W. & FRAUENFELD, O. W. 2016. Surface–Atmosphere Moisture Interactions in the Frozen Ground Regions of Eurasia. *Scientific Reports,* 6**,** 19163.

FRAUENFELD, O. W., ZHANG, T. J., BARRY, R. G. & GILICHINSKY, D. 2004. Interdecadal changes in seasonal freeze and thaw depths in Russia. *Journal of Geophysical Research-Atmospheres,* 109.

GRELL, G. A. & DÉVÉNYI, D. 2002. A generalized approach to parameterizing convection combining ensemble and data assimilation techniques. *Geophysical Research Letters,* 29**,** 38-1-38-4.

GU, L., YAO, J., HU, Z. & ZHAO, L. 2015. Comparison of the surface energy budget between regions of seasonally frozen ground and permafrost on the Tibetan Plateau. *Atmospheric Research,* 153**,** 553-564.

GUO, D., WANG, H. & LI, D. 2012. A projection of permafrost degradation on the Tibetan Plateau during the 21st century. *Journal of Geophysical Research: Atmospheres,* 117.

HAYASHI, M., QUINTON, W. L., PIETRONIRO, A. & GIBSON, J. J. 2004. Hydrologic functions of wetlands in a discontinuous permafrost basin indicated by isotopic and chemical signatures. *Journal of Hydrology,* 296**,** 81-97.

HINES, K. M. & BROMWICH, D. H. 2008. Development and Testing of Polar Weather Research and Forecasting (WRF) Model. Part I: Greenland Ice Sheet Meteorology. *Monthly Weather Review,* 136**,** 1971-1989.

HINES, K. M., BROMWICH, D. H., BAI, L.-S., BARLAGE, M. & SLATER, A. G. 2011. Development and Testing of Polar WRF. Part III: Arctic Land. *Journal of Climate,* 24**,** 26-48.

HIYAMA, T., FUJINAMI, H., KANAMORI, H., ISHIGE, T. & OSHIMA, K. 2016. Recent interdecadal changes in the interannual variability of precipitation and atmospheric circulation over northern Eurasia. *Environmental Research Letters,* 11**,** 065001.

IIJIMA, Y., NAKAMURA, T., PARK, H., TACHIBANA, Y. & FEDOROV, A. N. 2016. Enhancement of Arctic storm activity in relation to permafrost degradation in eastern Siberia. *International Journal of Climatology,* 36**,** 4265-4275.

JAFAROV, E. E., COON, E. T., HARP, D. R., WILSON, C. J., PAINTER, S. L., ATCHLEY, A. L. & ROMANOVSKY, V. E. 2018. Modeling the role of preferential snow accumulation in through talik development and hillslope groundwater flow in a transitional permafrost landscape. *Environmental Research Letters,* 13**,** 105006.

JANJIĆ, Z. I. 1994. The Step-Mountain Eta Coordinate Model: Further Developments of the Convection, Viscous Sublayer, and Turbulence Closure Schemes. *Monthly Weather Review,* 122**,** 927-945.

KOSTER, R. D., DIRMEYER, P. A., GUO, Z., BONAN, G., CHAN, E., COX, P., GORDON, C. T., KANAE, S., KOWALCZYK, E., LAWRENCE, D., LIU, P., LU, C.-H., MALYSHEV, S., MCAVANEY, B., MITCHELL, K., MOCKO, D., OKI, T., OLESON, K., PITMAN, A., SUD, Y. C., TAYLOR, C. M., VERSEGHY, D., VASIC, R., XUE, Y. & YAMADA, T. 2004. Regions of Strong Coupling Between Soil Moisture and Precipitation. *Science,* 305**,** 1138-1140.

KOVEN, C. D., RILEY, W. J. & STERN, A. 2013. Analysis of Permafrost Thermal Dynamics and Response to Climate Change in the CMIP5 Earth System Models. *Journal of Climate,* 26**,** 1877-1900.

KOVEN, C. D., RINGEVAL, B., FRIEDLINGSTEIN, P., CIAIS, P., CADULE, P., KHVOROSTYANOV, D., KRINNER, G. & TARNOCAI, C. 2011. Permafrost carbon-climate feedbacks accelerate global warming. *Proceedings of the National Academy of Sciences,* 108**,** 14769-14774.

LAWRENCE, D. M. & SLATER, A. G. 2005. A projection of severe near-surface permafrost degradation during the 21st century. *Geophysical Research Letters,* 32.

LAWRENCE, D. M., SLATER, A. G. & SWENSON, S. C. 2012. Simulation of present-day and future permafrost and seasonally frozen ground conditions in CCSM4. *Journal of Climate,* 25**,** 2207-2225.

LING, F. & ZHANG, T. 2004. A numerical model for surface energy balance and thermal regime of the active layer and permafrost containing unfrozen water. *Cold Regions Science and Technology,* 38**,** 1-15.

MARGULIS, S. A. & ENTEKHABI, D. 2001. Feedback between the Land Surface Energy Balance and Atmospheric Boundary Layer Diagnosed through a Model and Its Adjoint. *Journal of Hydrometeorology,* 2**,** 599-620.

MATSUMURA, S., YAMAZAKI, K. & TOKIOKA, T. 2010. Summertime land-atmosphere interactions in response to anomalous springtime snow cover in northern Eurasia. *Journal of Geophysical Research: Atmospheres,* 115.

MCGUIRE, A. D., KOVEN, C., LAWRENCE, D. M., CLEIN, J. S., XIA, J., BEER, C., BURKE, E., CHEN, G., CHEN, X., DELIRE, C., JAFAROV, E., MACDOUGALL, A. H., MARCHENKO, S., NICOLSKY, D., PENG, S., RINKE, A., SAITO, K., ZHANG, W., ALKAMA, R., BOHN, T. J., CIAIS, P., DECHARME, B., EKICI, A., GOUTTEVIN, I., HAJIMA, T., HAYES, D. J., JI, D., KRINNER, G., LETTENMAIER, D. P., LUO, Y., MILLER, P. A., MOORE, J. C., ROMANOVSKY, V., SCHÄDEL, C., SCHAEFER, K., SCHUUR, E. A.

G., SMITH, B., SUEYOSHI, T. & ZHUANG, Q. 2016. Variability in the sensitivity among model simulations of permafrost and carbon dynamics in the permafrost region between 1960 and 2009. *Global Biogeochemical Cycles,* 30**,** 1015-1037.

MCGUIRE, A. D., LAWRENCE, D. M., KOVEN, C., CLEIN, J. S., BURKE, E., CHEN, G., JAFAROV, E., MACDOUGALL, A. H., MARCHENKO, S., NICOLSKY, D., PENG, S., RINKE, A., CIAIS, P., GOUTTEVIN, I., HAYES, D. J., JI, D., KRINNER, G., MOORE, J. C., ROMANOVSKY, V., SCHÄDEL, C., SCHAEFER, K., SCHUUR, E. A. G. & ZHUANG, Q. 2018. Dependence of the evolution of carbon dynamics in the northern permafrost region on the trajectory of climate change. *Proceedings of the National Academy of Sciences,* 115**,** 3882-3887.

MICHEL, F. A. & VAN EVERDINGEN, R. O. 1994. Changes in hydrogeologic regimes in permafrost regions due to climatic change. *Permafrost and Periglacial Processes,* 5**,** 191-195.

MLAWER, E. J., TAUBMAN, S. J., BROWN, P. D., IACONO, M. J. & CLOUGH, S. A. 1997. Radiative transfer for inhomogeneous atmospheres: RRTM, a validated correlated-k model for the longwave. *Journal of Geophysical Research: Atmospheres,* 102**,** 16663-16682.

MORRISON, H., CURRY, J. A. & KHVOROSTYANOV, V. I. 2005. A New Double-Moment Microphysics Parameterization for Application in Cloud and Climate Models. Part I: Description. *Journal of the Atmospheric Sciences,* 62**,** 1665-1677.

OLIVA, M. & FRITZ, M. 2018. Permafrost degradation on a warmer Earth: Challenges and perspectives. *Current Opinion in Environmental Science & Health,* 5**,** 14-18.

PAL, J. S. & ELTAHIR, E. A. B. 2003. A feedback mechanism between soil-moisture distribution and storm tracks. *Quarterly Journal of the Royal Meteorological Society,* 129**,** 2279-2297.

PAN, H. L. & MAHRT, L. 1987. Interaction between soil hydrology and boundary-layer development. *Boundary-Layer Meteorology,* 38**,** 185-202.

QIAN, Y., HUANG, M., YANG, B. & BERG, L. K. 2013. A Modeling Study of Irrigation Effects on Surface Fluxes and Land–Air–Cloud Interactions in the Southern Great Plains. *Journal of Hydrometeorology,* 14**,** 700-721.

RISEBOROUGH, D., SHIKLOMANOV, N., ETZELMÜLLER, B., GRUBER, S. & MARCHENKO, S. 2008. Recent advances in permafrost modelling. *Permafrost and Periglacial Processes,* 19**,** 137-156.

ROMANOVSKY, V. E., SAZONOVA, T. S., BALOBAEV, V. T., SHENDER, N. I. & SERGUEEV, D. O. 2007. Past and recent changes in air and permafrost temperatures in eastern Siberia. *Global and Planetary Change,* 56**,** 399-413.

ROMANOVSKY, V. E., SMITH, S. L. & CHRISTIANSEN, H. H. 2010. Permafrost thermal state in the polar Northern Hemisphere during the International Polar Year 2007-2009: a synthesis. *Permafrost and Periglacial Processes,* 21**,** 106-116.

SCHÄR, C., LÜTHI, D., BEYERLE, U. & HEISE, E. 1999. The Soil–Precipitation Feedback: A Process Study with a Regional Climate Model. *Journal of Climate,* 12**,** 722-741.

SCHUUR, E. A. G., ABBOTT, B. W., BOWDEN, W. B., BROVKIN, V., CAMILL, P., CANADELL, J. G., CHANTON, J. P., CHAPIN, F. S., CHRISTENSEN, T. R., CIAIS, P., CROSBY, B. T., CZIMCZIK, C. I., GROSSE, G., HARDEN, J., HAYES, D. J., HUGELIUS, G., JASTROW, J. D., JONES, J. B., KLEINEN, T., KOVEN, C. D., KRINNER, G., KUHRY, P., LAWRENCE, D. M., MCGUIRE, A. D., NATALI, S. M., O'DONNELL, J. A., PING, C. L., RILEY, W. J., RINKE, A., ROMANOVSKY, V. E., SANNEL, A. B. K., SCHÄDEL, C., SCHAEFER, K., SKY, J., SUBIN, Z. M., TARNOCAI, C., TURETSKY, M. R., WALDROP, M. P., WALTER ANTHONY, K. M., WICKLAND, K. P., WILSON, C. J. & ZIMOV, S. A. 2013. Expert assessment of vulnerability of permafrost carbon to climate change. *Climatic Change,* 119**,** 359-374.

SCHUUR, E. A. G., MCGUIRE, A. D., SCHADEL, C., GROSSE, G., HARDEN, J. W., HAYES, D. J., HUGELIUS, G., KOVEN, C. D., KUHRY, P., LAWRENCE, D. M., NATALI, S. M., OLEFELDT, D., ROMANOVSKY, V. E., SCHAEFER, K., TURETSKY, M. R., TREAT, C. C. & VONK, J. E. 2015. Climate change and the permafrost carbon feedback. *Nature,* 520**,** 171-179.

SEGAL, M., PAN, Z., TURNER, R. W. & TAKLE, E. S. 1998. On the Potential Impact of Irrigated Areas in North America on Summer Rainfall Caused by Large-Scale Systems. *Journal of Applied Meteorology,* 37**,** 325-331.

SENEVIRATNE, S. I., CORTI, T., DAVIN, E. L., HIRSCHI, M., JAEGER, E. B., LEHNER, I., ORLOWSKY, B. & TEULING, A. J. 2010. Investigating soil moisture–climate interactions in a changing climate: A review. *Earth-Science Reviews,* 99**,** 125-161.

SERREZE, M. C., BROMWICH, D. H., CLARK, M. P., ETRINGER, A. J., ZHANG, T. & LAMMERS, R. 2002. Large-scale hydro-climatology of the terrestrial Arctic drainage system. *Journal of Geophysical Research: Atmospheres,* 107**,** ALT 1-1-ALT 1-28.

SKAMAROCK, W. C., KLEMP, J. B., DUDHIA, J., GILL, D. O., BARKER, D. M., WANG, W. & POWERS, J. G. 2008. A description of the Advanced Research WRF version 3. NCAR Technical note-475+ STR.

SLATER, A. G. & LAWRENCE, D. M. 2013. Diagnosing present and future permafrost from climate models. *Journal of Climate,* 26**,** 5608-5623.

STRELETSKIY, D. A., SHERSTIUKOV, A. B., FRAUENFELD, O. W. & NELSON, F. E. 2015a. Changes in the 1963-2013 shallow ground thermal regime in Russian permafrost regions. *Environmental Research Letters,* 10.

STRELETSKIY, D. A., SHIKLOMANOV, N. I. & NELSON, F. E. 2012. Permafrost, Infrastructure, and Climate Change: A GIS-Based Landscape Approach to Geotechnical Modeling. *Arctic, Antarctic, and Alpine Research,* 44**,** 368-380.

STRELETSKIY, D. A., TANANAEV, N. I., OPEL, T., SHIKLOMANOV, N. I., NYLAND, K. E., STRELETSKAYA, I. D., TOKAREV, I. & SHIKLOMANOV, A. I. 2015b. Permafrost hydrology in changing climatic conditions: seasonal

variability of stable isotope composition in rivers in discontinuous permafrost. *Environmental Research Letters,* 10**,** 095003.

SUBCOMMITTEE, P. 1988. Glossary of permafrost and related ground-ice terms. *Associate Committee on Geotechnical Research, National Research Council of Canada, Ottawa,* 156.

TEWARI, M., CHEN, F., WANG, W., DUDHIA, J., LEMONE, M., MITCHELL, K., EK, M., GAYNO, G. & WEGIEL, J. Implementation and verification of the unified NOAH land surface model in the WRF model (Formerly Paper Number 17.5). 20th conference on weather analysis and forecasting/16th conference on numerical weather prediction, 2004. 11-15.

WALVOORD, M. A. & KURYLYK, B. L. 2016. Hydrologic Impacts of Thawing Permafrost—A Review. *Vadose Zone Journal,* 15.

WANG, C., WANG, Z., KONG, Y., ZHANG, F., YANG, K. & ZHANG, T. 2019. Most of the Northern Hemisphere Permafrost Remains under Climate Change. *Scientific Reports,* 9**,** 3295.

ZHANG, T., BARRY, R. G., KNOWLES, K., HEGINBOTTOM, J. A. & BROWN, J. 1999. Statistics and characteristics of permafrost and ground-ice distribution in the Northern Hemisphere. *Polar Geography,* 23**,** 132-154.

ZHANG, Y., OHATA, T. & KADOTA, T. 2003. Land-surface hydrological processes in the permafrost region of the eastern Tibetan Plateau. *Journal of Hydrology,* 283**,** 41-56.

3. THE CONTRIBUTION OF CHANGING SURFACE THERMODYNAMICS ON TWENTIETH AND TWENTY-FIRST CENTURY AIR TEMPERATURES OVER EURASIAN PERMAFROST[*]

3.1. Introduction

As a result of anthropogenic climate change, the high latitudes are warming at a faster rate than anywhere else in the world due to a phenomenon known as Arctic amplification (Serreze et al., 2009, Serreze and Barry, 2011). Within the historical record, atmospheric circulation changes in the Arctic cannot be attributed directly to anthropogenic forcing as they cannot be separated from natural climatic variability (Serreze et al., 2000, Screen et al., 2018). However, increases in Arctic surface air temperature, amongst other geophysical variables, can indeed be attributed to greenhouse gas forcing as large-scale patterns such as the Arctic Oscillation play an insignificant role in comparison (Overland et al., 2019). Specifically, observations and historically forced climate model runs have shown significantly increasing temperatures over Eurasia, especially in the high latitudes, and those trends are expected to continue into the future (Peng et al., 2018b). It would be advantageous to decompose these past and future temperature increases to determine the impact of the dynamics associated with the dominant mode of Arctic circulation or whether thermodynamic processes and feedbacks can help to explain the temperature increases of the high latitudes.

---

[*] This section is reprinted with permission from "The contribution of changing surface thermodynamics on twentieth and twenty-first century air temperatures over Eurasian Permafrost" by Vecellio and Frauenfeld, 2021. Climate Dynamics, Copyright [2021] by SpringerNature.

A majority of Russia and much of the Eurasian landmass are underlain by permafrost in various degrees of spatial continuity (Romanovsky et al., 2010a). Permafrost, defined as ground that stays at or below 0°C for at least two consecutive years (Permafrost Subcommittee, 1988), is a control on hydrology, infrastructure, and climate in cold regions (Bense et al., 2012, Streletskiy et al., 2019, Walvoord and Kurylyk, 2016). Permafrost in Eurasia has been on the decline over the past half-century as soil temperatures and active layer thicknesses have increased each warm season and some permafrost has degraded completely (Frauenfeld et al., 2004, Streletskiy et al., 2015, Romanovsky et al., 2010b).Additionally, seasonal freeze depths have significantly decreased over time (Frauenfeld and Zhang, 2011a), requiring less energy in spring to completely thaw these seasonally frozen ground regions. These trends in soil temperature, active layer thickness, and seasonal freeze depth in past observations are expected to continue into the future as the climate continues to warm (Slater and Lawrence, 2013, Peng et al., 2018a, Peng et al., 2020). Additionally, earlier spring snowmelt and ground thaw as well as later fall freeze-up have been noted at Russian permafrost sites (Streletskiy et al., 2015), allowing for increased soil heat storage. As these regions of permafrost degrade and transition, subsequent land-atmosphere interactions are modified as well, which can impact the lower troposphere as well as mid-tropospheric synoptic circulation patterns (Vecellio et al., 2019). Therefore, there are important permafrost-related geophysical feedbacks on climate in addition to the widely reported biogeochemical ones (Schuur et al., 2015). Fully coupled earth system models which combine the biogeophysical and biogeochemical processes that guide the climate system are tools that can provide useful and unique information on these processes.

Climate model output inherently contains uncertainty that arises from external forcing, model physics, and internal variability (Hawkins and Sutton, 2009). Uncertainty due to external forcing centers around, e.g., not being able to account for the evolving state of uncertain future greenhouse gas concentrations, land use changes, aerosol composition, etc. Normally, this is accounted for by keeping these forcings constant within the model, e.g., by choosing one of the representative concentration pathway (RCP) scenarios for consistent radiative forcing from greenhouse gases in the atmosphere. Model physics uncertainty is due to the internal mechanics of the models' code base (i.e., parameterizations, round-off techniques) providing different responses to the same external forcing. This becomes a factor when attempting to compare output between multiple climate models containing different code bases, a limitation in Coupled Model Intercomparison Project (CMIP) evaluation studies. Lastly, uncertainty due to internal variability is climate system-inherent, occurring within each model run which can also subsequently be affected by external climate forcing. In most CMIP studies, a multi-model mean is calculated to extract the externally forced signal of whichever variable is under consideration. However, since that multi-model mean comes from a suite of models with added uncertainty due to the model physics, internal variability of the climate system itself cannot be extricated from the output. The magnitude of climate noise exerted by internal variability can rival the forced signal, especially outside the tropics (Field et al., 2014), and must be considered in attribution detection at regional scales (Deser et al., 2012, Thompson et al., 2015).

The actual, observed weather and climate, by nature, can only provide one realization of the climate system. As above, in attempting to work with a suite of climate

models, the components of internal variability and anthropogenic forcing cannot be analyzed individually in a single realization of a variable like temperature. Similarly, it is not possible to distinguish between local thermodynamic and remote dynamic forcing. Discretizing these effects can provide insight into the multiple different impacts on climate. By separating dynamic and thermodynamic contributions to a variable like surface air temperature (SAT), a common indicator of climate change, we can determine the thermodynamic influence of changing terrestrial conditions such as from permafrost degradation due to a warming climate.

Determining the effects on SAT from biogeochemical processes related to permafrost degradation combined with land and atmosphere components using earth system models allows for estimating the impacts of carbon feedbacks. For example, Schaefer et al. (2014) found as much as a 0.5°C increase in global temperatures due to carbon release via permafrost stocks by 2100. Similarly, MacDougall et al. (2012) examined the effect further into the future, finding a possible 1.69°C carbon-related temperature increase by 2300. In terms of geophysical feedbacks on SAT from permafrost degradation, Eugster et al. (2000) quantified changes to the surface energy budget, but this approach included concurrent feedbacks from vegetation shifts in addition to changes to the ground thermal regime. Quantifying and attributing the geophysical effects of permafrost degradation on a variable like SAT remains a challenge. This study therefore seeks to quantify SAT changes due to geophysical influences. Specifically, we will (1) employ an initial-condition, single-model ensemble—the Community Earth System Model version 1 (CESM1) Large Ensemble (Kay et al., 2015) and a technique known as “dynamical adjustment” (Deser et al., 2016)

to assess the impact of thermodynamics on SAT changes during spring and fall for three different time periods (1976–2005, 2021–2050, 2071–2100) and (2) determine if these impacts vary in different permafrost zones and non-permafrost regions over Eurasia.

3.2. Data and Methods

3.2.1. CESM1 Large Ensemble

Model data for this study comes from the CESM1 Large Ensemble (Kay et al., 2015) which contains 35 ensemble members with gridded output at a 0.9° × 1.25° spatial resolution. These 35 members were completed and provided for public use by the National Center for Atmospheric Research. The CESM-LE is an initial condition ensemble as each ensemble member is initiated from a control model run with a miniscule ($O{\sim}10^{-14}$) perturbation applied to the surface air temperature field. The same model physics and external climate forcings are applied to each of the runs, ensuring that the differences between the ensemble members are only due to the internal variability of the climate system.

To initialize the ensemble, conditions from a randomly selected January 1 of an 1,800-year preindustrial control run were used as a starting point. Because it is forced by preindustrial climate, the control run contains no historical or future anthropogenic climate change. Ensemble member 1 was run from 1850 through 2100. Ensemble members 2–35 were all initialized from ensemble member 1's January 1, 1920 state with the miniscule perturbation described above applied to each of them. These members were then run until 2100 as well. Each model run uses historical natural and anthropogenic climate forcing until 2005 and is then forced using the business-as-usual RCP 8.5

scenario through the end of its run in 2100 which is common practice in CMIP modeling. This CESM-LE output was obtained from the National Center for Atmospheric Research.

3.2.2. Dynamical adjustment

Discretizing the impacts of surface changes on atmospheric variables can be difficult due to the impacts of internal climate variability and changes in atmospheric circulation patterns on the surface. The dynamic and thermodynamic effects on SAT can be separated through a process called "dynamical adjustment" (Deser et al., 2016, Lehner et al., 2017, Merrifield et al., 2017). In essence, this separation of effects allows influences due to atmospheric circulation (dynamical) and the land surface (thermodynamic) to be considered as individual processes. Using dynamical adjustment, Deser et al. (2016) diagnosed the externally forced and internally variable components of winter SAT warming over North America over the past half-century (Deser et al. 2016). Lehner et al. (2017) determined time of emergence of the anthropogenic climate change signal in North American and European temperatures, and Merrifield et al. (2017) confirmed the "hot-spot" of land-atmosphere interactions over the Great Plains region of the south-central United States.

The dynamical adjustment process is summarized here and can be found in greater detail in Deser et al. (2016). Dynamical adjustment provides a way to subtract the influence of the atmospheric flow and the impact of advection on any variable, in this case, SAT, to leave only the thermodynamic effect. For a given ensemble member's (for example, ensemble member 1 or EM1) monthly mean atmospheric circulation pattern over a selected domain, similar patterns are found within the preindustrial control run and, using a Euclidian distance method to determine the level of similarity, the patterns

that most resemble the EM1 monthly pattern of interest are chosen. A sufficient number of these patterns or analogs (Na) are chosen. Both sea-level pressure (SLP) (Deser et al. 2016) and 500-hPa height fields (Merrifield et al. 2017) have been used as the basis for circulation analogs, with very little sensitivity to the choice of analog type. This study uses SLP to represent atmospheric circulation in the computation of analogs.

From the chosen analogs, a random sample (Ns) is picked and the best fit to the target EM1 monthly SLP field is calculated using a linear regression. Weights are applied to the Na members based on the strength of their pattern-match with the target ensemble field. The resulting SAT field which corresponds to this best-fit SLP pattern is the dynamically induced portion of the total SAT field. This subsampling procedure is done a number of times (Nr), and the average of all the Nr is considered the estimate of SAT anomalies brought about by atmospheric circulation (i.e., the dynamical contribution). The Na, Ns, and Nr values chosen for this study are 150, 100, and 50, respectively, as in Deser et al. (2016). This procedure is repeated for all 35 ensemble members. Each of the dynamical contributions is averaged. This average is subtracted from the total SAT field of the ensemble mean and the residual represents the thermodynamic contribution, driven primarily by the land surface, and is referred to as the thermodynamic residual or thermodynamic SAT from hereon.

In Deser et al. (2016), each ensemble member's total thermodynamic residual and dynamically adjusted SAT differ only by the ensemble-mean forced dynamical contribution, a constant added to the thermodynamic residual to produce the dynamically adjusted SAT. Because the differences are a constant, the variability of each of the variables between ensemble members does not change. We skip this final step because

we focus on surface-based (i.e., thermodynamic) influences on SAT and are not interested in the forced dynamical contribution to each ensemble member. We use only the thermodynamic residual and compare it to the total SAT trends.

3.2.3. Permafrost zones

To investigate the impacts of permafrost type on thermodynamic influences on SAT, we classify permafrost regions based on the Permafrost Zonation Index (PZI) (Gruber, 2012). The PZI is a high-resolution, gridded (0.05° × 0.05°) permafrost classification dataset, created from a global model and based on high-resolution air temperatures and elevation. PZI values range between 0.01 and 1.0. The PZI was re-gridded using a center-averaging technique to match the CESM-LE's spatial resolution (Fig. 3.1). We match these PZI values with the International Permafrost Association's permafrost categories as denoted in their Circum-Arctic Map of Permafrost and Ground Ice Conditions (Brown, 1997), describing four terrestrial permafrost categories: continuous (90–100% of an area underlain by frozen ground; PZI: 0.9–1.0), discontinuous (50–90%; PZI: 0.5–0.89), sporadic (10–50%; PZI: 0.1–0.49), and isolated (<10%; PZI: 0.01–0.09) (Permafrost Subcommittee, 1988).

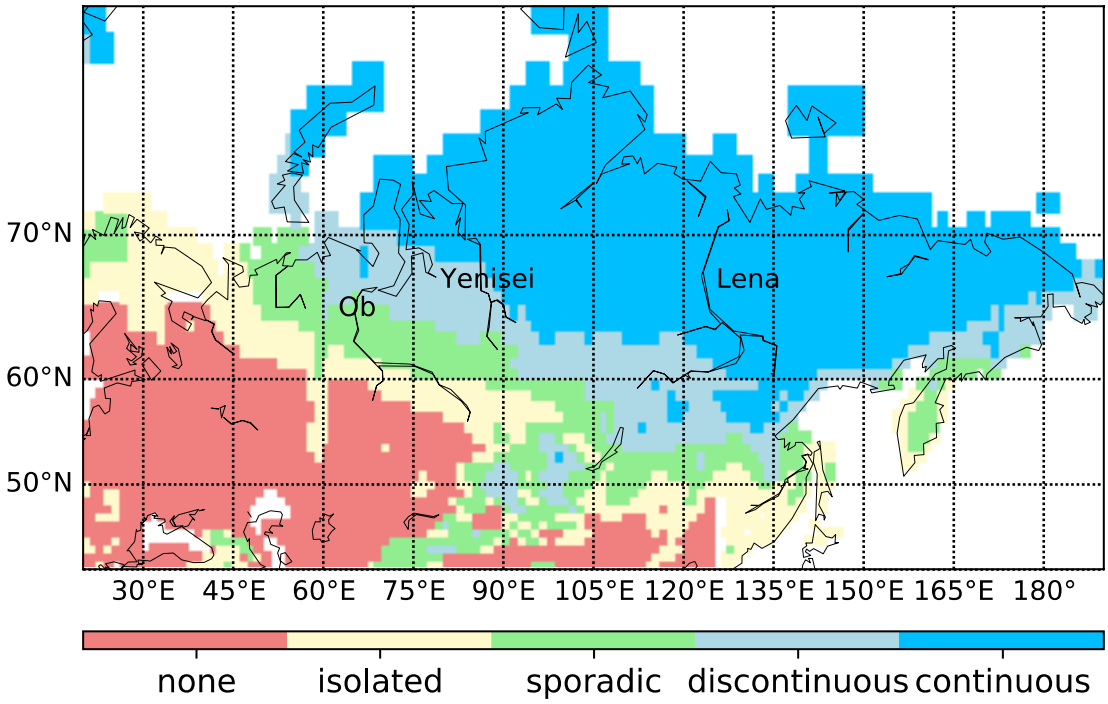

Figure 3.1: Regridded permafrost zones across the study region based on Gruber (2012)'s Permafrost Zonation Index and the definitions by the Permafrost Subcommittee (1988) and Brown et al. (1997). Indicated also are the approximate locations of the Ob, Yenisei, and Lena river basins.

3.2.4. Spatial and temporal domains

This study is focused on Eurasia with two domains used in the dynamical adjustment process. We use the larger domain of 20–90°N, 0–140°W for the SLP analogs and the smaller domain of 40–80°N, 20°E–160°W for the dynamical adjustment of SAT. The SAT domain covers a substantial portion of Russia, including the Central Siberian Plateau. We analyze the spring (March–May) and fall (September–November) seasons for three separate time periods: historical: 1976–2005, near-future: 2021–2050, and end-of-century: 2071–2100. Monthly anomalies are calculated by subtracting the respective 30-year climatology from the corresponding months within the analysis period. Three-

month averages of those anomalies are calculated, and 30-year trends are computed using a least squares regression.

3.3. Results

In using the dynamical adjustment methodology, the impacts of the overlying atmospheric setup are subtracted from the variable under investigation, in this case, SAT. In this study, as in Merrifield et al. (2017), the thermodynamic residual of SAT is tied directly to influence from the land surface on SAT. Going a step further, in the subsequent results, we tie the impact of permafrost zonation (to represent processes such as degradation and deepening of the active layer) to the thermodynamic control on SAT. Internal variability of SAT is represented by the variability of SAT values amongst the 35 CESM-LE members. The ensemble mean SAT is the average of the 35 CESM-LE members and is representative of the externally forced climatic response of SAT.

3.3.1. Thermodynamic impact on Eurasian SAT trends

3.3.1.1. Spring

Historical (1976–2005) spring temperature trends vary widely in both magnitude and spatial pattern amongst the 35 CESM-LE members, highlighting the impact of internal variability on the climate system (Fig. 3.2a). Ensemble members (EMs) such as EMs 1 and 10 show region-wide warming while EM 29 shows a majority cooling trend across Eurasia. Regional variability is also evident, e.g., EM 18's warm-cool-warm west-to-east gradient is flipped from EM 30's cool-warm-cool pattern. Many of the extremes in individual ensemble members are averaged out in the ensemble mean, which represents the externally forced response, and shows a moderate region-wide warming

outside of subtle cooling primarily in the Ob River basin. The median of grid point ensemble mean trends in spring indicates warming of 0.83°C/30 yr (range: −0.47–1.92°C/30 yr) during the historical 1976–2005 period.

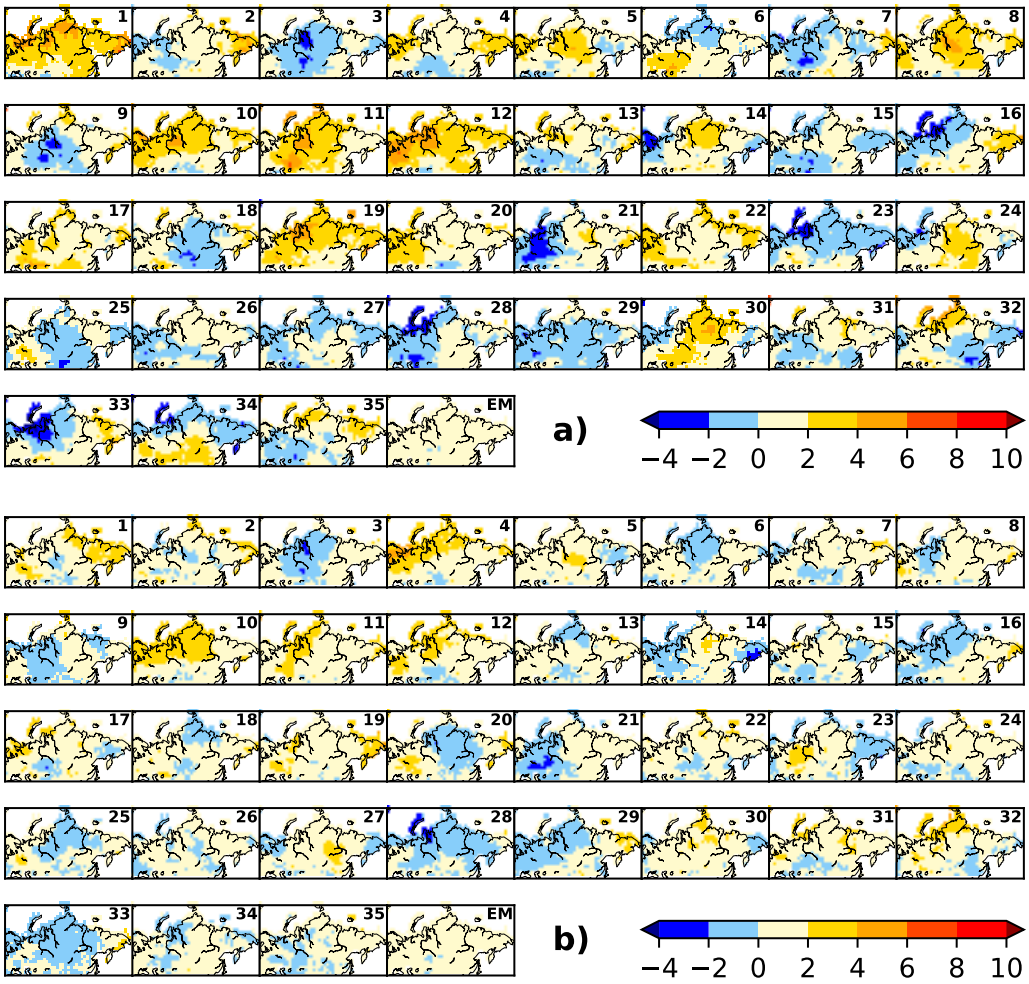

Figure 3.2: (a) Total and (b) thermodynamic surface air temperature (°C/30 yr) trends for each CESM-LE ensemble member (1–35) and the ensemble mean (EM) for the historical 1976–2005 spring period

Dynamically adjusting the total SAT trends highlights the impacts of thermodynamics on SAT in each ensemble member (Fig. 3.2b). Similar regions of warming and cooling among the ensemble members show that thermodynamics does not

necessarily differ from the total trends. For example, EM 3's total and thermodynamic SAT warming and cooling regions are nearly identical, varying only in magnitude. However, the patterns do not match for all EMs. While warming dominates the total SAT trends in EM 1, a thermodynamically induced cool region develops south of the Yenisei River. Conversely, total SAT trends in EM 23 show cooling across the entirety of the Eurasian northern latitudes while thermodynamics produce warming trends across the Ob and Yenisei River Basins as well as the Central Siberian Plateau, though the Russian Far East still shows thermodynamic cooling. Overall, amplitudes of thermodynamic SAT trends are lower in magnitude that the total SAT trends. The median of grid point ensemble mean thermodynamic trends falls to 0.65°C/30 yr from the 0.83°C/30 yr in the total SAT trends while the range also decreased (−0.64 to 1.60°C/30 yr).

To further determine the importance of thermodynamics on the climate system, two measures were calculated comparing the total and thermodynamic SAT trends: thermodynamic variance retention in the total SAT variance and signal-to-noise ratio. The largest variances between the 35 individual ensemble members, representing the internal climate variability produced by the CESM-LE, in the historical spring total SAT trend data is centered over the areas of the Ob and Yenisei Rivers with variances of over 4°C (Fig. 3.3a). Thermodynamic SAT trend variances are highest in the same region, but they are lower in magnitude (~2°C) (Fig. 3.3b). Because the variances differ vastly, thermodynamics explain little of the region's SAT trend variability. However, small variances in both the total and thermodynamic SAT trends in the mountainous region east of the Lena River mean that thermodynamic processes play a large role in SAT variability (~80% variance retention) (Fig. 3.3c). This supports the amplified

temperature-elevation relationships and the thermodynamic mechanisms which are at play (Pepin et al., 2015, Guo et al., 2021).

Signal-to-noise ratios (SNRs) for the total and thermodynamic residual SAT trends (Figs. 3.3d&e) indicate when a climatically forced response has emerged from the internal climate variability in the 35 realizations of the CESM-LE. Except for the area east of the Lena River, the SNRs of total SAT trends are less than one, indicating that a forced (external) response cannot be separated from the background noise of the climate system (internal variability) yet during the 1976–2005 historical spring period across Eurasia (Fig. 3.3d). Localized thermodynamic signatures, however, do emerge as externally forced patterns (Fig. 3.3e). The most notable region of SNRs greater than one in the thermodynamic residual SAT trends is the Lena River Delta, a key region of Eurasian permafrost degradation where higher soil temperatures lead to shifts in surface hydrology of the region (Yang et al., 2002). Other regions with strong thermodynamic signals are the Arctic coast of the Far East region of Russia, south of the Central Siberian Plateau, and western Russia (Fig. 3.3e).

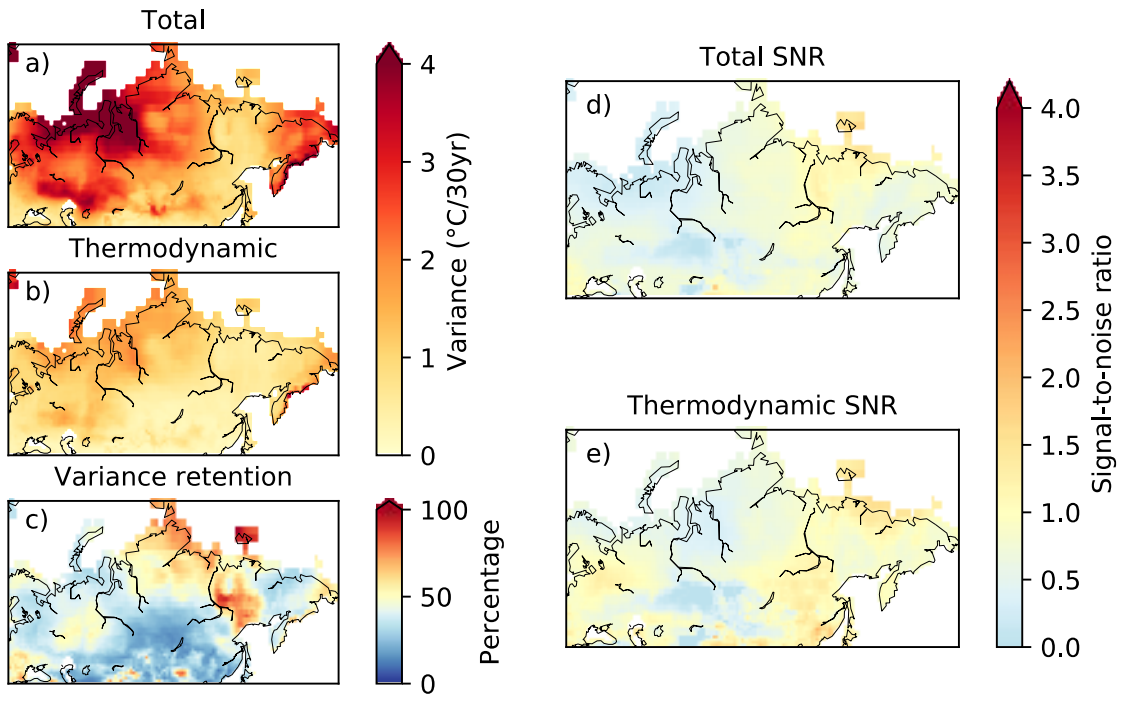

Figure 3.3: Variance across the 35 individual ensemble members in temperature trends for historical spring (a) total and (b) thermodynamic SAT and (c) thermodynamic variance retention in total SAT variance (1 – ((a–b) / a)). Also included are signal-to-noise ratios for (d) total and (e) thermodynamic SAT trends

Spring increases of total SAT are more consistent amongst EM runs in the near future (2021–2050) period (Fig. 3.4a), suggesting decreased internal variability and an emergence of external forcing. Some effects of internal climate variability can still be seen, as cooling is found in a number of EMs, mainly between the Ob and Yenisei River Basins. This provides evidence that external climate forcings play a larger role in Central Siberia and the Russian Far East while internal variability, likely aided by topographic influences, still dominate the region between the Ob and Yenisei, where the Ural Mountains are located. However, once averaged over all EMs, external forcing shows warming across the region with a median of 2.24°C/30 yr (range: 1.15–4.59°C/30 yr). Thermodynamic SAT trends also exhibit consistent warming across Eurasia and cool

spots are once again in the Ob and Yenisei River Basin region, notably in EMs 14, 26, and 28 (Fig. 3.4b). No individual EM median thermodynamic SAT trend is below 0.90°C/30 yr, with ensemble mean grid cells ranging 0.70–4.52°C/30 yr. Some median trends were negative in the total SAT (Fig. 3.4a), again showing the predominant warming effect imparted by thermodynamics on the system. However, additional statistics below show that thermodynamics still only play a small part overall in the near future spring period (Fig. 3.5). Larger variances in the total SAT trends than in the thermodynamic SAT trends lead to thermodynamics explaining less than 40% of the variability in total SAT trends across Eurasia, a decrease from the historical spring run in all regions except for the Russian Far East (Fig. 53.a–c). Signal to noise ratios reinforce that the Ob and Yenisei region is still controlled by natural variability in both total and thermodynamic SAT, though external forcings have emerged as the prevailing control on thermodynamically induced SAT trends during the period (Figs. 3.5d–e).

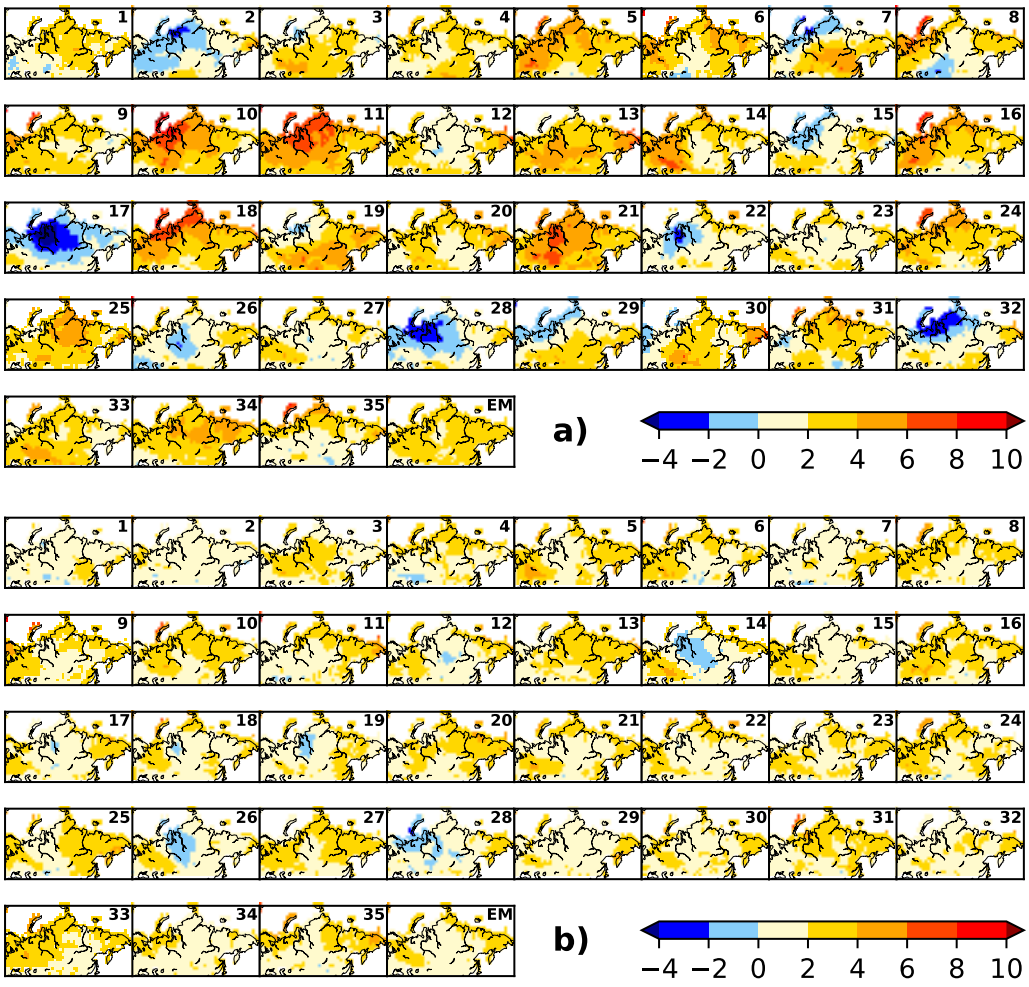

Figure 3.4: As in Figure 2, but for near future spring total and thermodynamic SAT trends

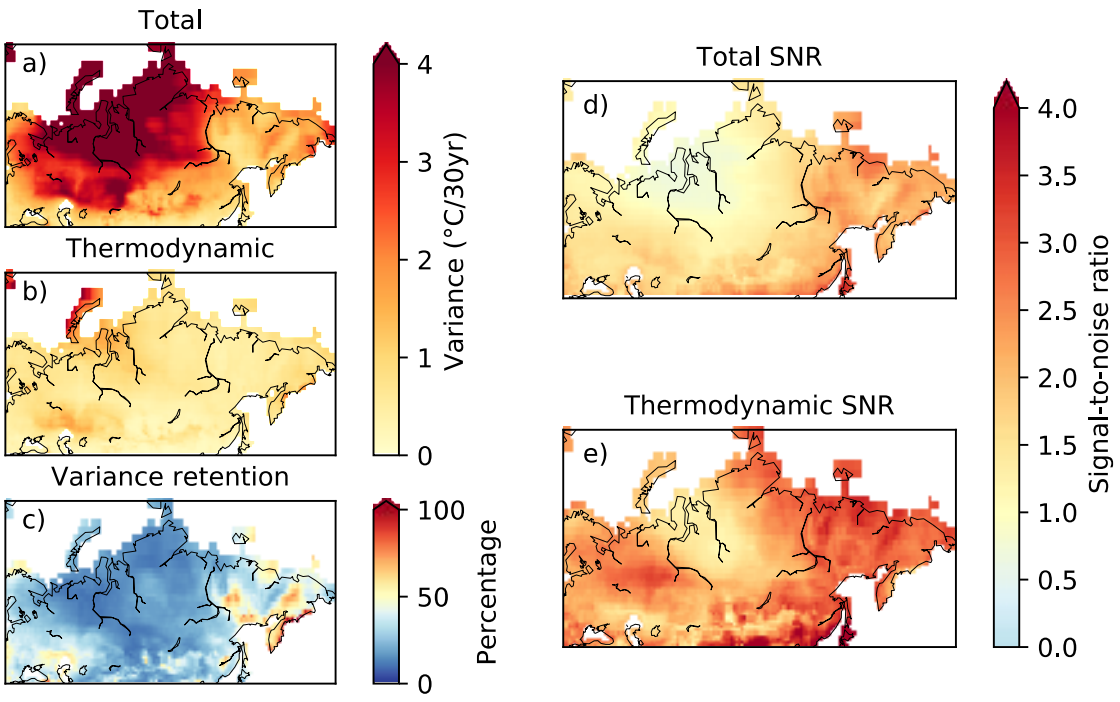

Figure 3.5: As in Figure 3 but for near future spring period

Temperature trends, region-wide and especially in EM regional hotspots (e.g., values exceeding 15°C/30 yr in the Russian Far East in EM 10) continue to rise in the end-of-century (2071–2100) run while cool patches occur sparingly (e.g., Ob and Yenisei River Basins again in EMs 2, 3, and 6 and southern Siberia in EM 22) (Fig. 3.6a). The median externally forced trend as represented by the ensemble mean decreases to 2.08°C/30 yr in the 2071–2100 period, but the range across the region widens from a minimum of 0.82°C/30 yr west of the Ob River to a maximum of 8.12°C/30 yr in the Russian Far East. The warming gradient to the north and east is also evident in the ensemble mean of the thermodynamic SAT (Fig. 3.6b). Much like the historical and near future periods, total SAT trend variance (Fig. 3.7a) far exceeds that of the thermodynamic SAT trends (Fig. 3.7b), leading to small variance retention values across most of Eurasia

(Figs. 3.7c). Conversely, SNRs are higher for thermodynamic SAT trends when compared to total SAT trends, especially in the Russian Far East (Figs. 3.7d–e).

In summary, while the CESM-LE shows increased spring warming on average in total SAT and due to thermodynamics, variability across ensemble members shows a large amount of internal variability throughout the three time periods, especially in the western half of the study domain near the Ob and Yenisei River basins. Positive and negative total SAT trends are found amongst the individual EMs in each time period in the area surrounding the Ob and Yenisei Rivers, leading to large variances, while variance in thermodynamic SAT trends is subdued. This effect is also evident over the Central Siberian Plateau and on the Russian Far East coast. SNRs in total SAT trends also lag behind those of thermodynamic SAT trends, indicating that forced climate changes are more apparent in thermodynamic influences on SAT, but other factors help to control the total SAT. These results show that thermodynamic surface changes potentially related to permafrost degradation, do not have a large impact on SAT trends in the spring over the three thirty-year time periods in this study.

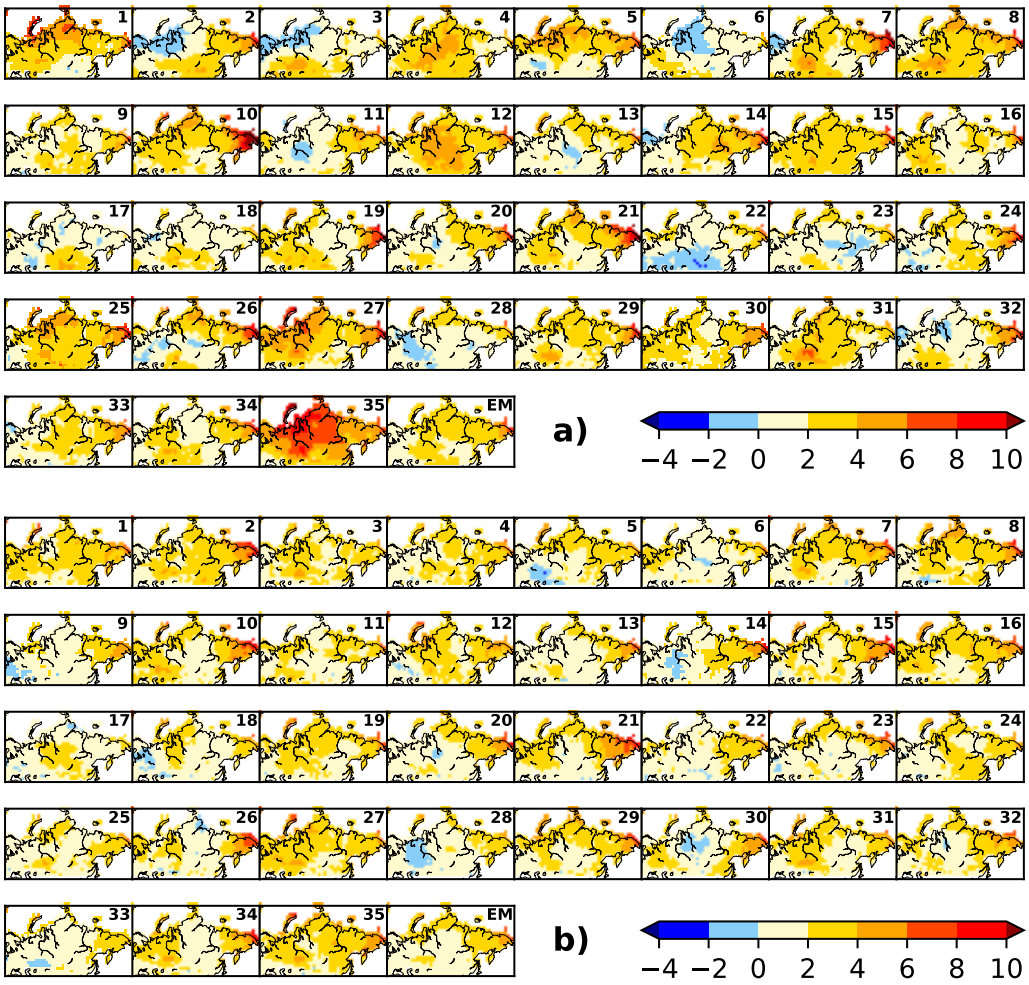

Figure 3.6: As in Figure 2, but for end-of-century spring trends

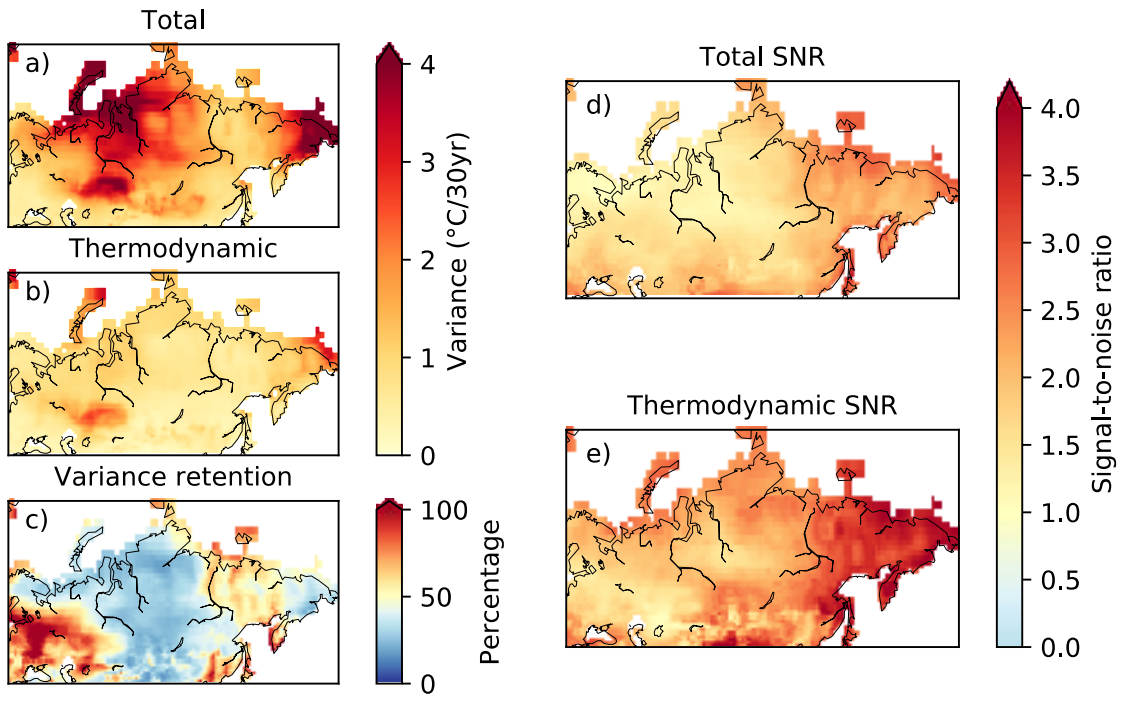

Figure 3.7: As in Figure 3, but for end-of-century spring period

3.3.1.2. Fall

Historical (1976–2005) total SAT trends across the Eurasian continent exhibit both warming and cooling trends in all ensemble members (Fig. 3.8a). While cooling trends in the spring were primarily found in the Ob and Yenisei River Basins, they are focused in the eastern two-thirds of the study area in fall, though, there are exceptions (EMs 2, 25, and 33, for example). While warming between 0–2°C/30 yr occurs predominantly in the interior of Eurasia, exceptionally high trends are primarily on the northern coastlines with some EMs having warming only along the coastline while others extend inland (EM 19 vs. EM 8). In the ensemble mean, warming across the interior ranges 0–2°C/30 yr, exceeding 2°C/30 yr along the northern coastline with cooling near

the coast of the Sea of Okhotsk. The median grid cell mean value is 0.84°C/30 yr with a range of −0.69–2.90°C/30 yr.

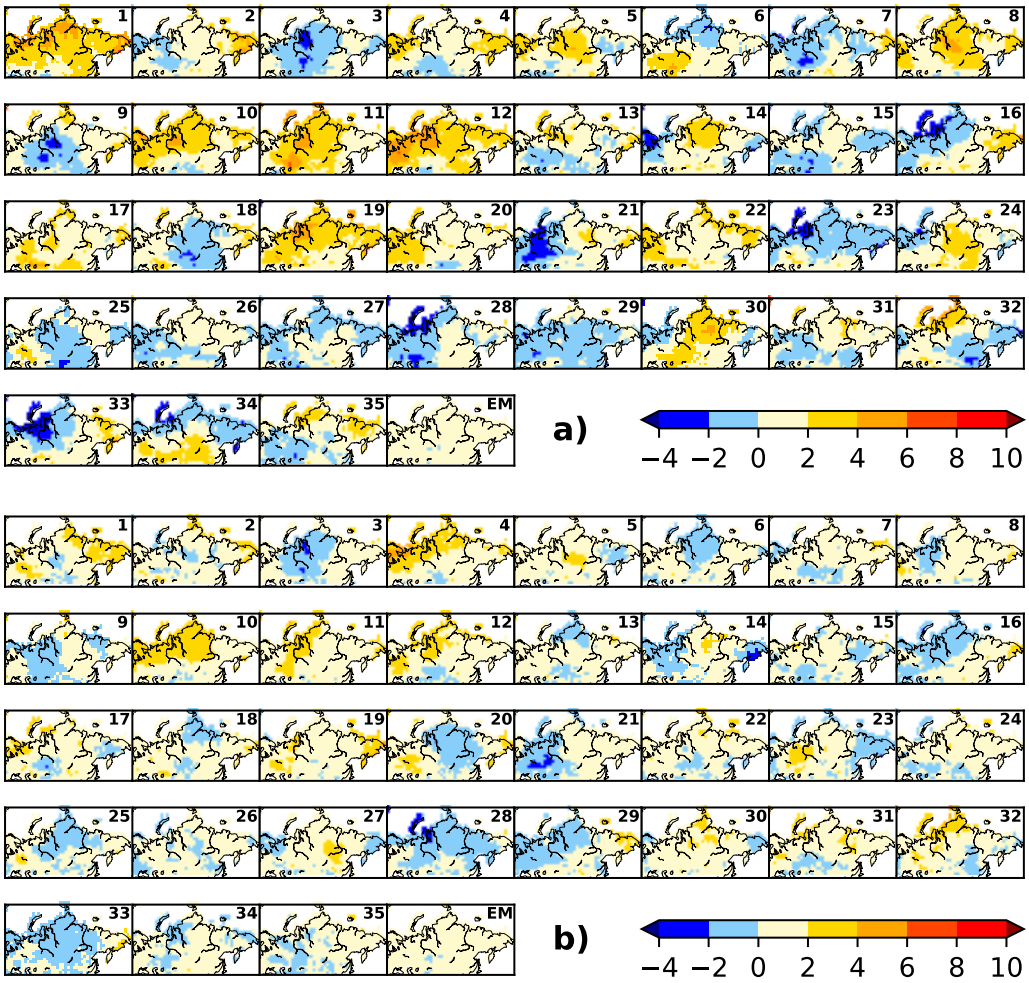

Figure 3.8: a) Total and (b) thermodynamic surface air temperature (°C/30 yr) for each CESM-LE ensemble member and the ensemble mean for the historical fall period

Fall thermodynamic SAT trends are noticeably lower among most EMs during the historical period in comparison to total SAT trends (Fig. 3.8b), also indicated by the quartiles of the grid cell thermodynamic SAT trends relative to total SAT trends across EMs (first quartile: −0.60 vs. −0.36°C/30 yr; median: −0.01 vs. 0.14°C/30 yr; third

quartile: 0.36 vs. 0.55°C/30 yr). This represents a downward shift of the lowest thermodynamic SAT trends (i.e., the lowest thermodynamic SAT trends are smaller than the lowest total SAT trends). The opposite occurred in spring, with the lowest thermodynamic SAT trends being higher than the lowest total SAT trends. Cooling occurs mainly in central Siberia and the Russian Far East in most EMs, though this is not consistent across all members (e.g., differences between EMs 2, 14, and 30). Most thermodynamic warming is slight (between 0–2°C/30 yr) among EMs, with warming over 2°C/30 yr along the northern coastlines and on the northern part of the Central Siberian Plateau. The median grid cell ensemble mean value is less than that of the total SAT, at 0.62°C/30 yr, but the range is very comparable to the total SAT trends at −0.64–2.83°C/30 yr.

Variance in both total and thermodynamic SAT trends increases to the north with the large variances in each occurring along the Arctic coastline (Fig. 3.9a–b). The biggest thermodynamic influence on the variance of total SAT temperature trends has the same northward gradient across the western half of the study region, however, variance is thermodynamically induced along the extent of the Lena River (Fig. 3.9c), a region dominated by continuous permafrost. SNRs for both total and thermodynamic SAT decrease west to east (disregarding the northern coastline) and the cooling along the Sea of Okhotsk in both SATs coincides with SNRs substantially below 1.0 (Figs. 3.9d–e). This indicates a progression of the emergence of an externally forced climate signal in the west to the strength of internal variability in the east.

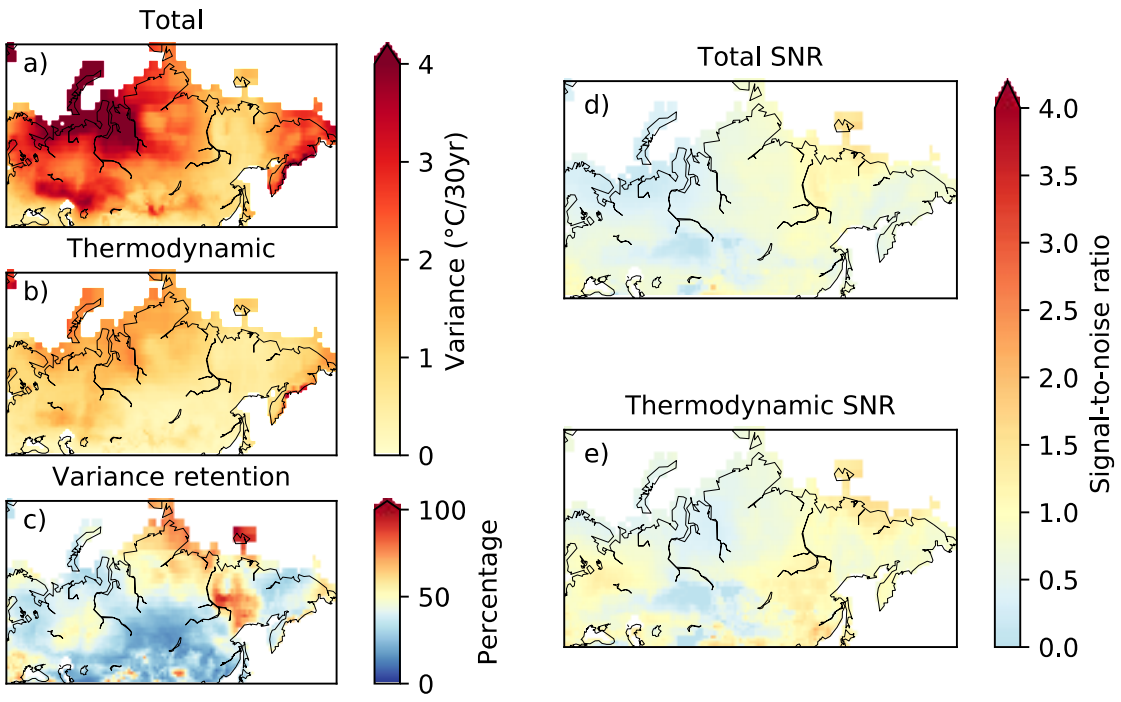

Figure 3.9: Variance across the 35 individual ensemble members in historical fall temperature trends for (a) total and (b) thermodynamic SAT and (c) thermodynamic variance retention by the total SAT variance. Also included are signal-to-noise ratios for (d) total and (e) thermodynamic SAT trends

In the near future period (2021–2050), increasing trends in total SAT are nearly consistent across the study area with few exceptions, such as EMs 15 and 28 (Fig. 3.10a). However, there is still some spatial variability in warming trends, as moderate (2–4°C/30 yr) warming occurs across the landmass (EM 1), or restricted to a smaller region (EM 27). Only a few EMs exhibit warming of more than 4°C/30 yr in areas other than the northern coastline, such as in the Central Siberian Plateau in EMs 9 and 19 and the Russian Far East in EM 13. The ensemble mean indicates moderate warming over the entire region west of the Western Russian Plain (median: 2.15°C/30 yr; range: 1.50–4.32°C/30 yr).

There are no notably large regions of decreasing trends in thermodynamic SAT in the near future period (Fig. 3.10b). More EMs have regions of thermodynamic SAT trends >4°C/30 yr compared to total SAT, but they encompass a smaller area with EM 9 showing the largest continuous pattern. The thermodynamic SAT trend ensemble mean pattern looks similar to that of the total SAT trend, though there is a northward expansion of trends between 0–2°C/30 yr over Central Siberia. The ensemble mean median thermodynamic SAT trend is 2.03°C/30 yr (range: 1.24–4.41°C/30 yr), only 0.12°C/30 yr less than the median from the ensemble mean total SAT trend. This value is much smaller than the 0.49°C/30 yr that separated total and thermodynamic ensemble mean median SAT trends in the spring, suggesting that surface forcing through thermodynamics will play a much larger role in SAT in the near-future fall seasons.

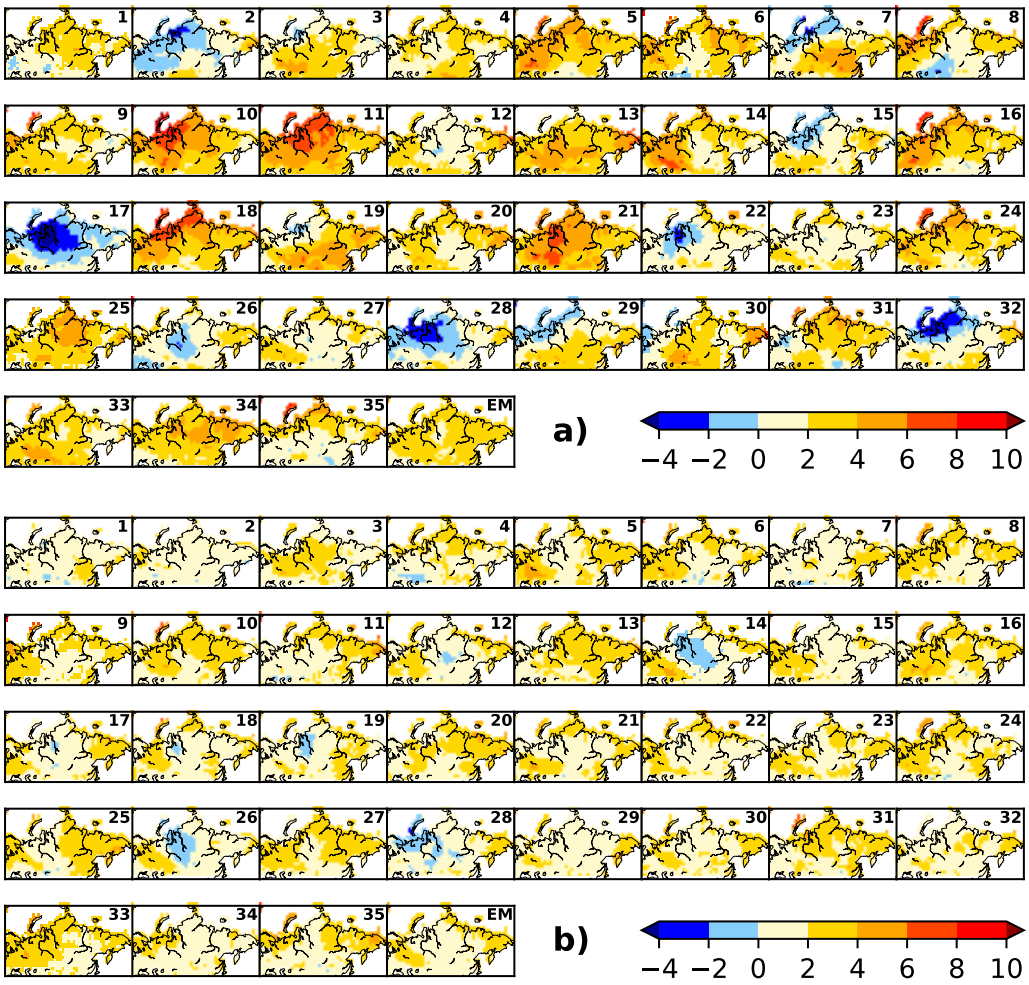

Figure 3.10: As in Figure 8, but for near future fall SAT trends

The variance patterns of total and thermodynamic SAT trends in the near future look fairly similar to the historical period with the same northward gradient and coastal maxima (Fig. 3.11a–b). Thermodynamic explained variance of total SAT trends is once again high around the Lena River, but also in the area between the Ob and Yenisei Rivers (Fig. 3.11c) underlain by discontinuous permafrost, indicating a positive relationship between permafrost coverage and thermodynamic influence on SAT. Both total and thermodynamic SAT trend SNRs are above 2.0 over the entire landmass, signifying the

forced climate signal has emerged from internal variability for both SAT measures (Fig. 3.11d–e).

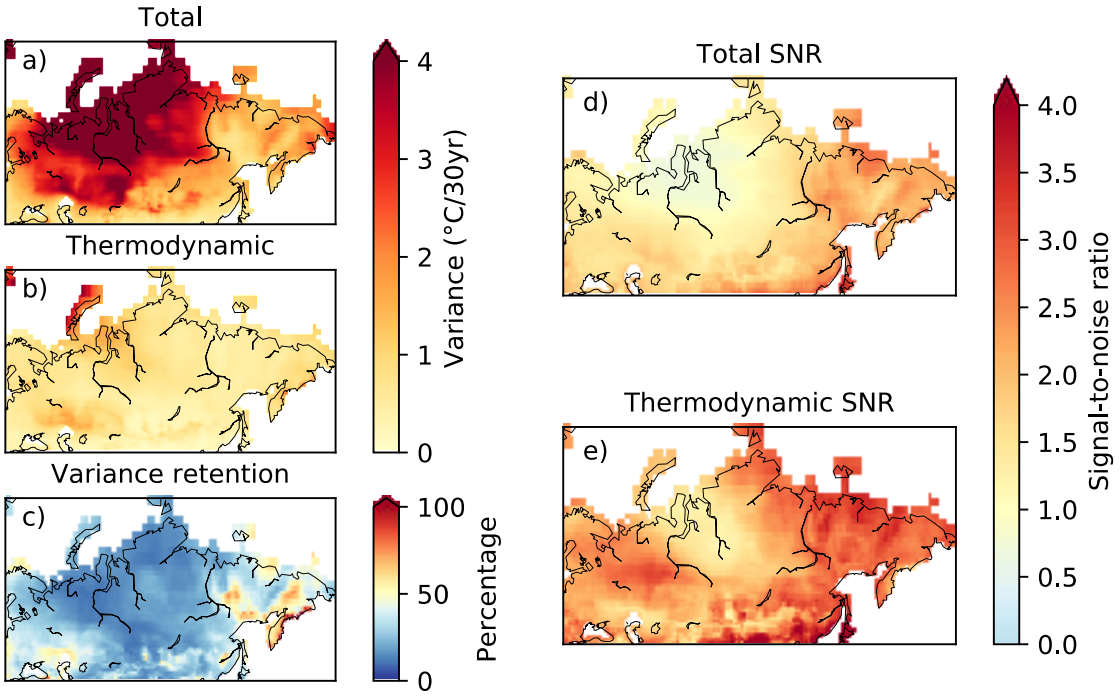

Figure 3.11: As in Figure 9, but for the near future fall period

Total SAT warming is still evident across the Eurasian continent at the end of the century (2071–2100; Figure 3.12a), though it will be of lower magnitude than in 2021–2050. Moderate warming between 2–4°C/30 yr is evident across all EMs, though its location varies and occurs, e.g., along the northern coastline in EM 25, in the Russian Far East in EM 13, or widespread as in EM 35. The ensemble mean indicates moderate warming from the Ob River to the Russian Far East, with the southern boundary of these positive trends being the source regions of the Ob and Lena Rivers. Both the ensemble mean grid cell median (1.99°C/30 yr) and range (1.28–3.00°C/30 yr) decrease relative to the 2021–2050 maxima. Thermodynamic SAT trends are also lower in the end-of-century in comparison to the near future (Fig. 3.12b). Decreasing trends are found in a few of the

EMs, most notably in the region of the Ob and Yenisei Rivers in EM 3. Similar to total SAT, EM 35 exhibits the largest warming trends along the northern coastline in the region of the Lena River. Moderate ensemble mean thermodynamic SAT trends (2–4°C/30 yr) resemble those of the total SAT trends, though there are differences at the western boundary (east of the Yenisei River) and extending to southeastern Russia. The ensemble mean grid cell median is comparable to that of the total SAT (1.87°C/30 yr; range: 1.21–2.63°C/30 yr). All of this indicates the continued importance of thermodynamics, hypothesized through heat transfer from the ground to near-surface atmosphere, on total SAT trends, especially over central Siberia and extending into the Russian Far East.

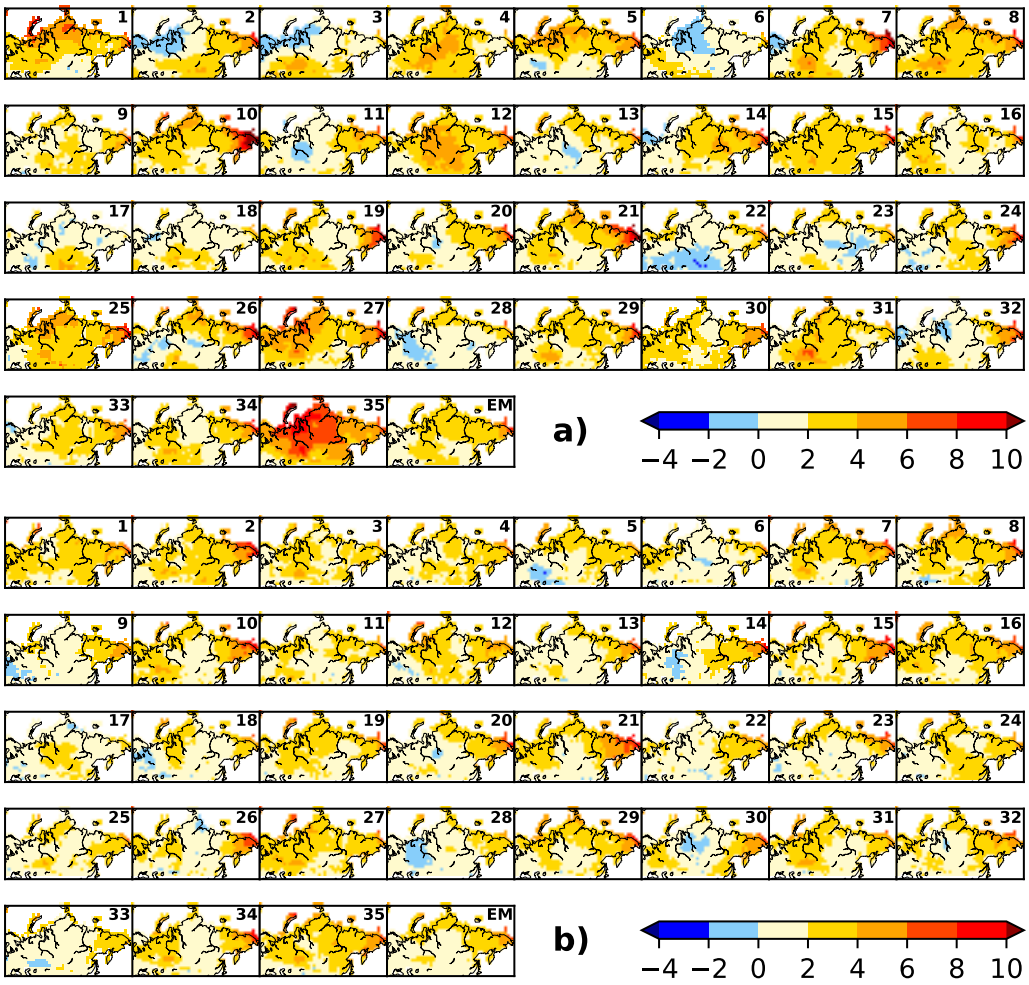

Figure 3.12: As in Figure 8, but for end-of-century fall SAT trends

Variance in both total and thermodynamic SAT trends again increases to the north in the end-of-century period, with a local maximum on the Central Siberian Plateau rather than the northern coastline for the total SAT trend (Fig. 3.13a–b). Higher variance is explained by thermodynamics in the far western part of Russia, in the Ob and Yenisei River basins, across northern Central Siberia, and over most of the Russian Far East (Fig. 3.13c). SNR values for both total and thermodynamic SAT trends are well above 1.0 (Fig. 3.13d–e) as in the near future period, so even though the magnitude of trends decreased, they still have emerged from the internal variability of the system.

Overall, the changes in total SAT during the fall are more closely tied to thermodynamic influence than they were in the spring. In addition, the coupling between the total and thermodynamic SAT trends appears to strengthen over the three time periods, as ensemble variability decreases across EMs in both total and thermodynamic SAT and covariance between the two temperature measures strengthens, especially across the northern half of the domain as well as in the major Eurasian river basins. These findings suggest that there are surface-based influences on SAT and they will become stronger as time passes. Based on the spatial patterns of the SAT trend measures and variance retention, permafrost distribution could be a controlling factor on the strength of surface-atmosphere energy transfer. Therefore, we look at permafrost next to determine whether the projected changes in that cryospheric variable factor into the changing thermodynamic surface forcing on total SAT trends.

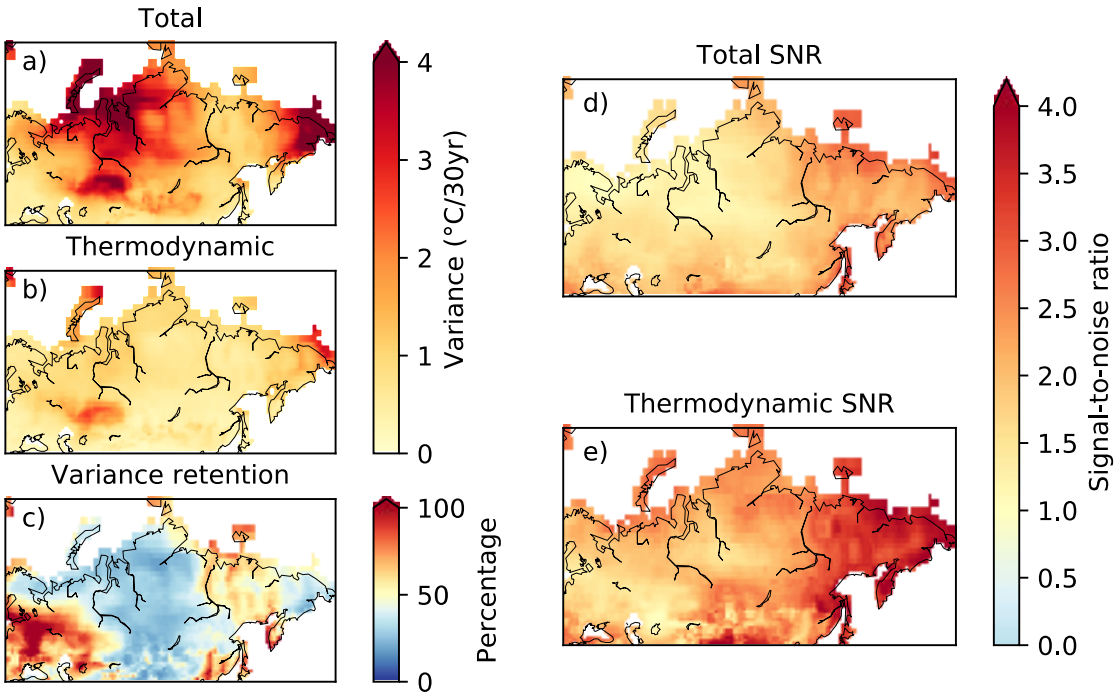

Figure 3.13: As in Figure 9, but for end-of-century fall period

3.3.2. Effects of Permafrost on SAT trends

Given the difference in warming rates in soil temperatures across different permafrost zones (Biskaborn et al., 2019) and expected future permafrost degradation across Eurasia (Lawrence et al., 2012), there will likely be a shift in the magnitude of energy exchange between the surface and atmosphere across these zones. Hence, to quantify the impact of this degradation on SAT trends through thermodynamics, we quantify the ensemble mean trend (Table 3.1) of total and thermodynamic SAT, thermodynamic variance retention, and SNRs in the continuous, discontinuous, sporadic, and isolated permafrost zones. Additionally, we analyze permafrost-free regions, as another check to determine if air temperature changes are dependent on frozen ground and its future degradation. A Welch's t-test is used to compare the means between the permafrost regions to determine if there are statistical differences between different ground thermal regimes. The t-tests are applied to the means of the continuous permafrost zone relative to all other zones (i.e., discontinuous, sporadic, isolated, and non-permafrost) as well as the discontinuous permafrost zone to all zones. The sporadic and isolated permafrost zones were only compared to the non-permafrost region.

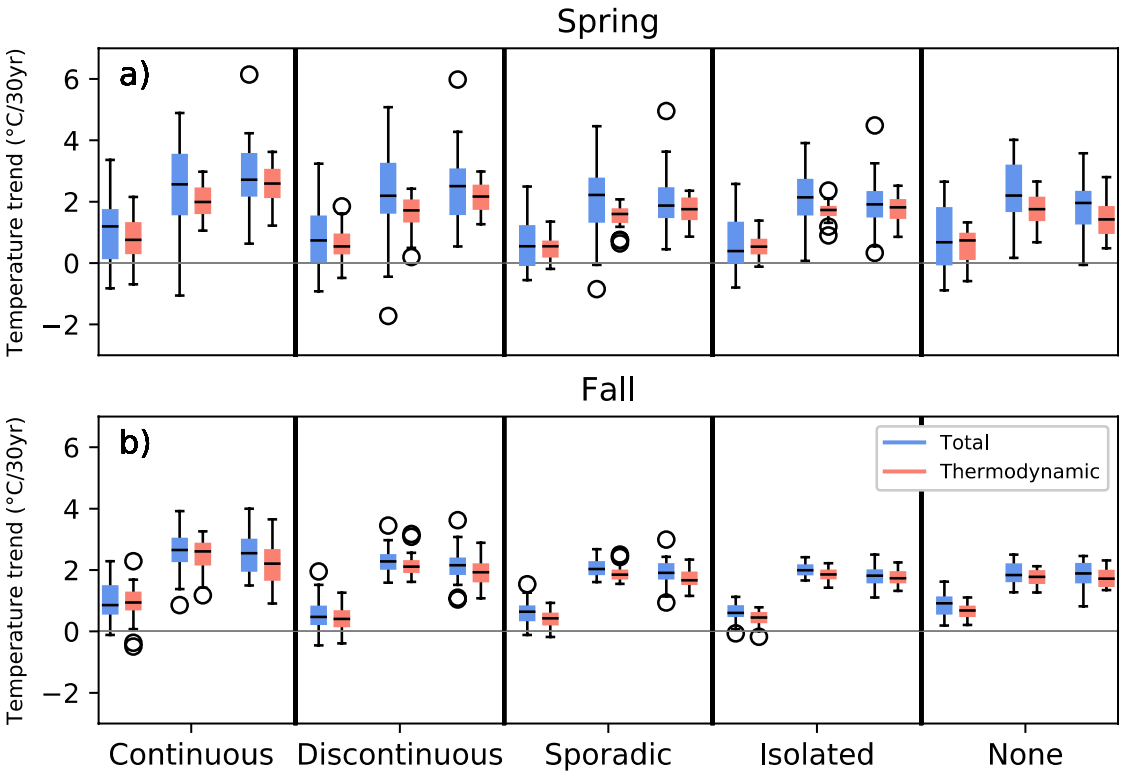

Figure 3.14: Distribution of total (blue) and thermodynamic (pink) SAT trends across frozen ground regions for historical (left), near future (center), and end-of-century (right) periods for (a) spring and (b) fall season

Table 3.1 Spring and fall ensemble mean total and thermodynamic (in parentheses) SAT trends (°C/30 yr) for the five frozen ground regions in the 1976–2005 (historical), 2021–2050 (near-future), and 2071–2100 (end-of-century) periods

	Spring	Fall
	Continuous Permafrost	
1976–2005	1.07 (0.78)	0.98 (0.92)
2021–2050	2.50 (2.01)	2.63 (2.52)
2071–2100	2.77 (2.59)	2.53 (2.22)
	Discontinuous Permafrost	
1976–2005	0.89 (0.63)	0.55 (0.37)
2021–2050	2.28 (1.67)	2.27 (2.14)
2071–2100	2.42 (2.13)	2.15 (1.93)
	Sporadic Permafrost	
1976–2005	0.67 (0.50)	0.62 (0.39)
2021–2050	2.11 (1.53)	2.08 (1.87)
2071–2100	2.04 (1.76)	1.92 (1.72)
	Isolated Permafrost	
1976–2005	0.67 (0.55)	0.63 (0.43)
2021–2050	2.16 (1.70)	2.00 (1.86)
2071–2100	1.97 (1.77)	1.81 (1.75)
	Non-Permafrost Regions	
1976–2005	0.76 (0.62)	0.89 (0.66)
2021–2050	2.27 (1.74)	1.90 (1.78)
2071–2100	1.83 (1.44)	1.85 (1.75)

Table 3.2: Statistically significant differences (✓) between individual permafrost zones for total (*Tot*) and thermodynamic (*TD*) SAT trend ensemble means based on Welch's t-test (95% significance level)

	Spring						Fall					
	1976–2005		2021–2050		2071–2100		1976–2005		2021–2050		2071–2100	
	Tot	*TD*	*Tot*	*TD*	*Tot*	*TD*	*Tot*	*TD*	*Tot*	*TD*	*Tot*	*TD*
Continuous												
vs. none				✓	✓	✓		✓	✓	✓	✓	✓
vs. isolated				✓	✓	✓	✓	✓	✓	✓	✓	✓
vs. sporadic		✓		✓	✓	✓	✓	✓	✓	✓	✓	✓
vs. discontinuous				✓		✓	✓	✓	✓	✓	✓	✓
Discontinuous												
vs. none					✓	✓	✓	✓	✓	✓	✓	✓
vs. isolated						✓			✓	✓	✓	✓
vs. sporadic						✓			✓	✓	✓	✓
Sporadic												
vs. none						✓	✓	✓	✓			
Isolated												
vs. none						✓	✓	✓				

3.3.2.1. Spring

The largest variability in both total and thermodynamic SAT trends across the frozen ground regions in all of the time periods is in spring, with variability largest in total SAT trends (Fig. 3.14). The magnitude of total ensemble mean SAT trends increases for the historical and near future periods across all permafrost regions, but at the end of the century it only increases over the continuous (2.50 to 2.77°C/30 yr) and discontinuous (2.28 to 2.42 C/30 yr) zones, while decreasing by 0.07, 0.19, and 0.42°C/30 yr in the sporadic, isolated, and non-permafrost zones, respectively (Table 3.1). It is not until the end-of-century period when the total mean SAT trends over continuous permafrost are

significantly different from other studied regions, specifically the non-permafrost, isolated, and sporadic zones. However, it remains statistically indistinguishable from the discontinuous permafrost zone (Table 3.2). The end-of-century total mean SAT trend in the discontinuous zone is only statistically different from the non-permafrost zone.

In regard to thermodynamic SAT, all regions with permafrost experience an increase in the magnitude of thermodynamic ensemble-mean SAT trends across all time periods. This signifies the increasing influence of surface and external climate forcing on the overall spring SAT signal in permafrost regions (Table 3.1). Thermodynamically, the continuous permafrost zone is distinct in terms of SAT trend from all other zones beginning in the near future period, while no differences are found between any of the lower-concentration permafrost zones. By the end-of-century, however, the continuous and discontinuous permafrost zones have statistically different means in spring, as do the sporadic and isolated zones in comparison with the non-permafrost zone (Table 3.2). This highlights how the ground thermal regime has an increasing influence on spring SATs by 2100.

Table 3.3: Spring and fall ensemble mean thermodynamic variance retention for the five frozen ground regions in the 1976–2005 (historical), 2021–2050 (near-future), and 2071–2100 (end-of-century) periods

	Spring	Fall
	Continuous Permafrost	
1976–2005	51.9%	74.7%
2021–2050	28.2%	89.7%
2071–2100	43.7%	110.1%
	Discontinuous Permafrost	
1976–2005	34.9%	58.7%
2021–2050	24.4%	90.9%
2071–2100	33.3%	76.3%
	Sporadic Permafrost	
1976–2005	32.8%	54.2%
2021–2050	24.7%	76.3%
2071–2100	31.6%	64.5%
	Isolated Permafrost	
1976–2005	33.4%	61.5%
2021–2050	29.7%	71.2%
2071–2100	47.7%	66.4%
	Non-Permafrost Regions	
1976–2005	36.4%	51.2%
2021–2050	30.8%	65.6%
2071–2100	65.2%	67.6%

Thermodynamic influence on the variance of SAT is distinctly higher in the continuous permafrost zone, especially in the historical and end-of-century periods while there is not much difference in the discontinuous, sporadic, and isolated zones (Table 3.3). However, it still only accounts for about half of the total SAT trend variance during those periods. The largest spring thermodynamically induced variance is in the non-permafrost zone at the end-of-century (65.2%), likely influenced by its decrease in trend

magnitude which is not the case for any of the other permafrost zones during that period. Thermodynamic SAT trend SNRs are higher than the total in all permafrost zones across all time periods in spring, again showing the impact that dynamics have on total SAT trends (Table 3.4). While SNRs for both total and thermodynamic SAT trends are less than 1.0 during the historical period, an externally forced climate signal begins to emerge from the noise in both the total and thermodynamic SAT trends in the near future period, with the signal being much stronger in the thermodynamic component. This continues in the end-of-century period. As with the explained variance, there is a gap between the continuous permafrost zone and the other four zones, especially in the non-permafrost zone, in SNRs, notably tied to the thermodynamics (Table 3.4).

Table 3.4: Spring and fall ensemble mean total and thermodynamic (in parentheses) SNRs for the five frozen ground regions in the 1976–2005 (historical), 2021–2050 (near-future), and 2071–2100 (end-of-century) periods

	Spring	Fall
	Continuous Permafrost	
1976–2005	0.81 (0.84)	0.81 (0.87)
2021–2050	1.69 (2.53)	3.02 (3.89)
2071–2100	1.95 (2.79)	2.87 (2.55)
	Discontinuous Permafrost	
1976–2005	0.64 (0.79)	0.64 (0.55)
2021–2050	1.43 (2.12)	3.60 (3.60)
2071–2100	1.64 (2.48)	3.01 (3.24)
	Sporadic Permafrost	
1976–2005	0.53 (0.68)	0.92 (0.80)
2021–2050	1.51 (2.26)	3.93 (4.18)
2071–2100	1.69 (2.41)	3.16 (3.65)
	Isolated Permafrost	
1976–2005	0.56 (0.79)	1.00 (0.87)
2021–2050	1.73 (2.57)	4.02 (4.38)
2071–2100	1.83 (2.42)	3.24 (3.93)
	Non-Permafrost Regions	
1976–2005	0.62 (0.82)	1.39 (1.49)
2021–2050	1.68 (2.37)	3.21 (3.80)
2071–2100	1.78 (1.86)	2.96 (3.51)

3.3.2.2. Fall

Total fall SAT temperature trends are very similar in magnitude to spring's, with the exception of the historical period in the continuous and discontinuous permafrost zones; however, the within-zone variability in the fall trends is much less when compared to spring. Fall thermodynamic SAT trends are comparably higher than those in spring, especially in the near future period, and make up a larger proportion of the total SAT

trend across all permafrost zones (Fig. 3.14). In the ensemble mean, across all time periods, both total and thermodynamic SAT trends are statistically distinct from all other zones, except when comparing the total SAT trend with the non-permafrost zone during the historical period (Tables 3.1 and 3.2). The distinction between the other permafrost zones evolves over time as total and thermodynamic SAT trends within the permafrost zones become significantly different from the non-permafrost zone in the historical period. This separation from the sporadic and isolated permafrost zones is delayed until the near future period, indicating a lag in the significance of permafrost degradation's impact on temperature compared with continuous permafrost. Similarly, the sporadic and isolated permafrost zones are statistically different in terms of thermodynamic SAT trends in the historical period but become indistinguishable from the non-permafrost zone in the near future. This does not occur for both the sporadic and isolated permafrost zones in terms of total SAT trends until the end-of-century period. These results indicate that the geophysical impacts of sporadic and isolated permafrost will either become indistinguishable from permafrost-free areas or that the regions may become permafrost-free themselves.

Similar to the influences in the ensemble means, retention of variance due to thermodynamics in total SAT trends is highest in the fall with the strongest relationships in continuous permafrost and, to a lesser extent, discontinuous permafrost (Table 3.3). This means that variance in thermodynamics is driving the variance in total temperature trends in continuous and discontinuous permafrost regions, suggesting an influence due to differences in ground thermal regime. The only zones where the proportion of variance due to thermodynamics increases across all three time periods are in continuous and non-

permafrost zones. The effect is much larger within the continuous permafrost zone where thermodynamic SAT trend variance even exceeds that of the total SAT (110.1%) at the end-of-century. Notably, thermodynamically induced variance in the other three zones increases between the historical and near-future periods (with a high in the discontinuous zone of 90.9% induced variance). Variance due to thermodynamics again decreases at the end-of-century, perhaps due to lesser permafrost remaining, and its thermodynamic impacts weakening. Still, these analyses show that thermodynamics play the largest role on total SAT trends in the fall, most notably in continuous permafrost and, to a lesser extent, discontinuous permafrost. This influence increases over time, especially in the continuous permafrost zone where the largest warming occurs.

While there are modest SNRs for both total and thermodynamic fall SAT trends in the historical period, in the near-future and end-of-century both SNRs are much higher than they were during the spring (Table 3.4). While the mean SAT trends are similar or even less than in spring, the lower noise (variability) amongst ensemble members results in consistent SNRs above 3.0, especially in the zones other that continuous permafrost. We find that thermodynamics play a much larger role on total SAT trends in fall, at the end of the warm season, compared to spring. Thermodynamics impact more of the mean response and cause more of the variability exhibited by the ensemble members. This signifies that ground conditions play a much larger role in the near-surface climate across Eurasia in fall, and that it is most important in continuous and discontinuous permafrost zones where a ground thermal regime transition will likely be still in progress through the end of the century.

3.4. Discussion and Conclusion

Using the 35-member CESM Large Ensemble and the technique of dynamical adjustment, we investigate the role that thermodynamics play on surface air temperatures in Eurasia in spring and fall for three different periods. In combination, these techniques allow for a physical interpretation of the simulated SAT trends. This technique has previously been used to discretize dynamical impacts on surface quantities (Smoliak et al., 2015, Wallace et al., 2012) and separate forced changes from those imparted by internal variability (Deser et al. 2016). Here, we used the thermodynamic residual (Merrifield et al. 2017) to investigate the ground-based influence on total SAT trends which are tied to changing soil thermal regimes due to permafrost degradation. Additionally, the effect of the ground thermal regime is examined by analyzing SAT trends, variance retention, and signal-to-noise ratios between permafrost zones and non-permafrost regions. Although spring and fall are both getting longer and frozen ground is thawing earlier and freezing later, the climate system's influences on SAT differ between the two seasons and over time. Internal variability and dynamics play a larger role in SAT trends in the spring and its effects are noticed through the end of the century. Meanwhile, the effects of anthropogenic climate forcing are more apparent in the fall. Additionally, the thermodynamic impact of the ground thermal regime on SAT, notably in the continuous and discontinuous permafrost zones, is stronger in the fall and is shown to increase through the 21st century. Taken in concert, we conclude that permafrost degradation in tandem with changing annual freeze/thaw cycles in frozen ground does indeed have an influence on the overlying atmosphere and that there are disparate seasonal ramifications on how it will feed back onto the climate system. We note here

that our permafrost zone definitions are static over the three time periods in our study, although continued climate change and permafrost warming will surely alter them. As Guo and Wang (2016) note, the largest impacts will first occur at the southern edges of permafrost and progress north over time. Because our significant changes are primarily located in the northern portion of the continuous and discontinuous permafrost regions, we believe this will not substantially impact our findings. Nonetheless, we acknowledge the non-stationarity of the permafrost zonation as a limitation.

Variability in historical spring SAT trends is linked to dynamics and shifts in circulation patterns linked to internal climate factors. This is consistent with previous findings from Chen et al. (2016), Chen et al. (2019) which link Eurasian SAT variations to Arctic Oscillation-based changed using both atmospheric reanalysis coupled with gridded observations and the historical runs from the CMIP5 suite of models, respectively. One hypothesis is that the strength of dynamic influence on variability in spring SAT trends can be linked to winter precipitation. The largest amount of internal variability amongst ensemble members is focused primarily in the Ob and Yenisei River Basins as some members show slight positive trends while a number exhibit negative SAT trends. That area where internal variability seems to dominate is co-located with local maxima of observed spring snowfall. Ye and Lau (2019) note how this snowfall and resulting snowmelt can impact soil moisture and fuel subsequent circulation anomalies, especially in concurrent months. If spring snowfall and subsequent soil moisture anomalies are less, higher temperature extremes may occur across the entirety of Siberia as happened in 2020 when a warmer than average winter and early spring led to some

Siberian weather stations being 10°C above average in the month of May due to an anomalous ridging pattern (Copernicus Climate Change Service, 2020).

This is in contrast with the fall when SAT trends have a stronger link to thermodynamics in the historical period and that connection increases in strength as time progresses. This is especially evident in continuous permafrost regions and, to a lesser extent, discontinuous permafrost. Spring snow cover extent has decreased over the past few decades linked to earlier snowmelt (Yeo et al., 2017). Consequently, soil water is either directed into river channels as runoff (Tan et al., 2011) or evaporated into the overlying air (Chen et al. 2016) earlier in the spring or early summer. This leads to drier soils which begin storing energy in the top layers earlier in the year, rather than being used in evaporation or being conducted to deeper layers via soil water. Chen et al. (2019) have shown this will lead to increasing springtime temperatures in the future with the largest increases in northern Eurasia, areas underlain by continuous and discontinuous permafrost. With extra weeks in the early season to absorb energy coupled with increasing air temperatures, the active layer has (Frauenfeld et al. 2004) and is projected to deepen over the rest of this century (Slater and Lawrence 2013) with soil temperatures projected to increase most in regions of continuous and discontinuous permafrost (Biskaborn et al. 2019). Future projections show a northward progression of degradation, as isolated and sporadic permafrost regions fully degrade and disappear first, with significant degradation also occurring in discontinuous and continuous permafrost regions by 2100 (Guo and Wang, 2016). All of this leads to net heat storage in soil lasting through the transition into the cold season (Frauenfeld and Zhang, 2011b), providing a source of sensible heat to keep SATs higher into the fall. This is aided by trends towards

later snow onset and coverage during October (Brown and Derksen, 2013, Peng et al., 2013, Estilow et al., 2015) which are likely to persist with continued autumnal warming.

Given the differing responses between spring and fall, there are separate effects on the surface energy budget in each season. Specifically, the fall terrestrial-based, thermodynamic warming signal underscores the need to continue to examine geophysical impacts on near-surface climate in permafrost regions (Vecellio et al. 2019). While this study was conducted in the high latitudes, we note that the use of large ensembles to quantify uncertainties in other 'hotspots' of land-atmosphere interactions would also be advantageous. A deeper understanding is required of the role of how the local energy transfers over these larger swaths of thawed land could have non-local consequences, perhaps providing a deeper understanding of the nature of Arctic amplification and the connecting link between the Arctic and the mid-latitudes.

3.5. References

BENSE, V. F., KOOI, H., FERGUSON, G. & READ, T. 2012. Permafrost degradation as a control on hydrogeological regime shifts in a warming climate. *Journal of Geophysical Research-Earth Surface*, 117.

BISKABORN, B. K., SMITH, S. L., NOETZLI, J., MATTHES, H., VIEIRA, G., STRELETSKIY, D. A., SCHOENEICH, P., ROMANOVSKY, V. E., LEWKOWICZ, A. G., ABRAMOV, A., ALLARD, M., BOIKE, J., CABLE, W. L., CHRISTIANSEN, H. H., DELALOYE, R., DIEKMANN, B., DROZDOV, D., ETZELMULLER, B., GROSSE, G., GUGLIELMIN, M., INGEMAN-NIELSEN, T., ISAKSEN, K., ISHIKAWA, M., JOHANSSON, M., JOHANNSSON, H., JOO, A., KAVERIN, D., KHOLODOV, A., KONSTANTINOV, P., KROGER,

T., LAMBIEL, C., LANCKMAN, J. P., LUO, D., MALKOVA, G., MEIKLEJOHN, I., MOSKALENKO, N., OLIVA, M., PHILLIPS, M., RAMOS, M., SANNEL, A. B. K., SERGEEV, D., SEYBOLD, C., SKRYABIN, P., VASILIEV, A., WU, Q., YOSHIKAWA, K., ZHELEZNYAK, M. & LANTUIT, H. 2019. Permafrost is warming at a global scale. *Nat Commun,* 10**,** 264.

BROWN, J. 1997. *International Permafrost Association Circum-Arctic map of permafrost and ground ice conditions*, 1:10,000,000 ;. Reston, Va.: U.S. Geological Survey.

BROWN, R. D. & DERKSEN, C. 2013. Is Eurasian October snow cover extent increasing? *Environmental Research Letters,* 8.

CHEN, S. F., WU, R. G. & LIU, Y. 2016. Dominant modes of interannual variability in Eurasian surface air remperature during boreal spring. *Journal of Climate,* 29**,** 1109-1125.

CHEN, S. F., WU, R. G., SONG, L. Y. & CHEN, W. 2019. Present-day status and future projection of spring Eurasian surface air temperature in CMIP5 model simulations. *Climate Dynamics,* 52**,** 5431-5449.

COPERNICUS CLIMATE CHANGE SERVICE. 2020. *Investigating an unusually mild winter and spring in Siberia* [Online]. Copernicus Climate Change Service. Available: https://climate.copernicus.eu/investigating-unusually-mild-winter-and-spring-siberia [Accessed June 20 2020].

DESER, C., PHILLIPS, A., BOURDETTE, V. & TENG, H. Y. 2012. Uncertainty in climate change projections: the role of internal variability. *Climate Dynamics,* 38**,** 527-546.

DESER, C., TERRAY, L. & PHILLIPS, A. S. 2016. Forced and internal components of winter air temperature trends over North America during the past 50 years: Mechanisms and implications. *Journal of Climate,* 29**,** 2237-2258.

ESTILOW, T. W., YOUNG, A. H. & ROBINSON, D. A. 2015. A long-term Northern Hemisphere snow cover extent data record for climate studies and monitoring. *Earth System Science Data,* 7**,** 137-142.

EUGSTER, W., ROUSE, W. R., PIELKE, R. A., MCFADDEN, J. P., BALDOCCHI, D. D., KITTEL, T. G. F., CHAPIN, F. S., LISTON, G. E., VIDALE, P. L., VAGANOV, E. & CHAMBERS, S. 2000. Land-atmosphere energy exchange in Arctic tundra and boreal forest: available data and feedbacks to climate. *Global Change Biology,* 6**,** 84-115.

FIELD, C. B., BARROS, V. R., MASTRANDREA, M. D., MACH, K. J., ABDRABO, M.-K., ADGER, N., ANOKHIN, Y. A., ANISIMOV, O. A., ARENT, D. J. & BARNETT, J. 2014. Summary for policymakers. *Climate change 2014: impacts, adaptation, and vulnerability. Part A: global and sectoral aspects. Contribution of Working Group II to the Fifth Assessment Report of the Intergovernmental Panel on Climate Change.* Cambridge University Press.

FRAUENFELD, O. W. & ZHANG, T. J. 2011a. An observational 71-year history of seasonally frozen ground changes in the Eurasian high latitudes. *Environmental Research Letters,* 6.

FRAUENFELD, O. W. & ZHANG, T. J. 2011b. Observed station-based 1956-2000 soil heat flux anomalies at 423 sites across the Eurasian high latitudes. *AGUFM,* 2011**,** C41B-0409.

FRAUENFELD, O. W., ZHANG, T. J., BARRY, R. G. & GILICHINSKY, D. 2004. Interdecadal changes in seasonal freeze and thaw depths in Russia. *Journal of Geophysical Research-Atmospheres,* 109.

GRUBER, S. 2012. Derivation and analysis of a high-resolution estimate of global permafrost zonation. *Cryosphere,* 6**,** 221-233.

GUO, D., PEPIN, N., YANG, K., SUN, J. & LI, D. 2021. Local changes in snow depth dominate the evolving pattern of elevation-dependent warming on the Tibetan Plateau. *Science Bulletin*.

GUO, D. L. & WANG, H. J. 2016. CMIP5 permafrost degradation projection: A comparison among different regions. *Journal of Geophysical Research-Atmospheres,* 121**,** 4499-4517.

HAWKINS, E. & SUTTON, R. 2009. The potential to narrow uncertainty in regional climate predictions. *Bulletin of the American Meteorological Society,* 90**,** 1095.

KAY, J. E., DESER, C., PHILLIPS, A., MAI, A., HANNAY, C., STRAND, G., ARBLASTER, J. M., BATES, S. C., DANABASOGLU, G., EDWARDS, J., HOLLAND, M., KUSHNER, P., LAMARQUE, J. F., LAWRENCE, D., LINDSAY, K., MIDDLETON, A., MUNOZ, E., NEALE, R., OLESON, K., POLVANI, L. & VERTENSTEIN, M. 2015. The Community Earth System Model (CESM) Large Ensemble Project: A community resource for studying climate change in the presence of internal climate variability. *Bulletin of the American Meteorological Society,* 96**,** 1333-1349.

LAWRENCE, D. M., SLATER, A. G. & SWENSON, S. C. 2012. Simulation of present-day and future permafrost and seasonally frozen ground conditions in CCSM4. *Journal of Climate,* 25**,** 2207-2225.

LEHNER, F., DESER, C. & TERRAY, L. 2017. Toward a new estimate of "time of emergence" of anthropogenic warming: Insights from dynamical adjustment and a large initial-condition model ensemble. *Journal of Climate,* 30**,** 7739-7756.

MACDOUGALL, A. H., AVIS, C. A. & WEAVER, A. J. 2012. Significant contribution to climate warming from the permafrost carbon feedback. *Nature Geoscience,* 5**,** 719-721.

MERRIFIELD, A., LEHNER, F., XIE, S. P. & DESER, C. 2017. Removing circulation effects to assess central US land-atmosphere interactions in the CESM Large Ensemble. *Geophysical Research Letters,* 44**,** 9938-9946.

OVERLAND, J. E., WANG, M. Y. & BOX, J. E. 2019. An integrated index of recent pan-Arctic climate change. *Environmental Research Letters,* 14.

PENG, S. S., PIAO, S. L., CIAIS, P., FRIEDLINGSTEIN, P., ZHOU, L. M. & WANG, T. 2013. Change in snow phenology and its potential feedback to temperature in the Northern Hemisphere over the last three decades. *Environmental Research Letters,* 8.

PENG, X. Q., ZHANG, T. J., FRAUENFELD, O. W., DU, R., WE, Q. & LIANG, B. B. 2020. Soil freeze depth variability across Eurasia during 1850-2100. *Climatic Change,* 158**,** 531-549.

PENG, X. Q., ZHANG, T. J., FRAUENFELD, O. W., WANG, K., LUO, D. L., CAO, B., SU, H., JIN, H. J. & WU, Q. B. 2018a. Spatiotemporal changes in active layer

thickness under contemporary and projected climate in the Northern Hemisphere. *Journal of Climate,* 31**,** 251-266.

PENG, X. Q., ZHANG, T. J., FRAUENFELD, O. W., WANG, K., SUN, W. & LUO, J. 2018b. Evaluation and quantification of surface air temperature over Eurasia based on CMIP5 models. *Climate Research,* 77**,** 167-180.

PEPIN, N., BRADLEY, R. S., DIAZ, H. F., BARAER, M., CACERES, E. B., FORSYTHE, N., FOWLER, H., GREENWOOD, G., HASHMI, M. Z., LIU, X. D., MILLER, J. R., NING, L., OHMURA, A., PALAZZI, E., RANGWALA, I., SCHONER, W., SEVERSKIY, I., SHAHGEDANOVA, M., WANG, M. B., WILLIAMSON, S. N., YANG, D. Q. & GRP, M. R. I. E. W. 2015. Elevation-dependent warming in mountain regions of the world. *Nature Climate Change,* 5**,** 424-430.

PERMAFROST SUBCOMMITTEE 1988. Glossary of permafrost and related ground-ice terms. *Associate Committee on Geotechnical Research, National Research Council of Canada, Ottawa,* 156.

ROMANOVSKY, V. E., DROZDOV, D. S., OBERMAN, N. G., MALKOVA, G. V., KHOLODOV, A. L., MARCHENKO, S. S., MOSKALENKO, N. G., SERGEEV, D. O., UKRAINTSEVA, N. G., ABRAMOV, A. A., GILICHINSKY, D. A. & VASILIEV, A. A. 2010a. Thermal state of permafrost in Russia. *Permafrost and Periglacial Processes,* 21**,** 136-155.

ROMANOVSKY, V. E., SMITH, S. L. & CHRISTIANSEN, H. H. 2010b. Permafrost thermal state in the polar Northern Hemisphere during the International Polar Year 2007-2009: a synthesis. *Permafrost and Periglacial Processes,* 21**,** 106-116.

SCHAEFER, K., LANTUIT, H., ROMANOVSKY, V. E., SCHUUR, E. A. G. & WITT, R. 2014. The impact of the permafrost carbon feedback on global climate. *Environmental Research Letters,* 9.

SCHUUR, E. A. G., MCGUIRE, A. D., SCHADEL, C., GROSSE, G., HARDEN, J. W., HAYES, D. J., HUGELIUS, G., KOVEN, C. D., KUHRY, P., LAWRENCE, D. M., NATALI, S. M., OLEFELDT, D., ROMANOVSKY, V. E., SCHAEFER, K., TURETSKY, M. R., TREAT, C. C. & VONK, J. E. 2015. Climate change and the permafrost carbon feedback. *Nature,* 520**,** 171-179.

SCREEN, J. A., BRACEGIRDLE, T. J. & SIMMONDS, I. 2018. Polar climate change as manifest in atmospheric circulation. *Current Climate Change Reports,* 4**,** 383-395.

SERREZE, M. C., BARRETT, A. P., STROEVE, J. C., KINDIG, D. N. & HOLLAND, M. M. 2009. The emergence of surface-based Arctic amplification. *Cryosphere,* 3**,** 11-19.

SERREZE, M. C. & BARRY, R. G. 2011. Processes and impacts of Arctic amplification: A research synthesis. *Global and Planetary Change,* 77**,** 85-96.

SERREZE, M. C., WALSH, J. E., CHAPIN, F. S., OSTERKAMP, T., DYURGEROV, M., ROMANOVSKY, V., OECHEL, W. C., MORISON, J., ZHANG, T. & BARRY, R. G. 2000. Observational evidence of recent change in the northern high-latitude environment. *Climatic Change,* 46**,** 159-207.

SLATER, A. G. & LAWRENCE, D. M. 2013. Diagnosing present and future permafrost from climate models. *Journal of Climate,* 26**,** 5608-5623.

SMOLIAK, B. V., WALLACE, J. M., LIN, P. & FU, Q. 2015. Dynamical adjustment of the Northern Hemisphere surface air temperature field: Methodology and application to observations. *Journal of Climate,* 28**,** 1613-1629.

STRELETSKIY, D. A., SHERSTIUKOV, A. B., FRAUENFELD, O. W. & NELSON, F. E. 2015. Changes in the 1963-2013 shallow ground thermal regime in Russian permafrost regions. *Environmental Research Letters,* 10.

STRELETSKIY, D. A., SUTER, L. J., SHIKLOMANOV, N. I., PORFIRIEV, B. N. & ELISEEV, D. O. 2019. Assessment of climate change impacts on buildings, structures and infrastructure in the Russian regions on permafrost. *Environmental Research Letters,* 14.

TAN, A., ADAM, J. C. & LETTENMAIER, D. P. 2011. Change in spring snowmelt timing in Eurasian Arctic rivers. *Journal of Geophysical Research-Atmospheres,* 116.

THOMPSON, D. W. J., BARNES, E. A., DESER, C., FOUST, W. E. & PHILLIPS, A. S. 2015. Quantifying the role of internal climate variability in future climate trends. *Journal of Climate,* 28**,** 6443-6456.

VECELLIO, D. J., NOWOTARSKI, C. J. & FRAUENFELD, O. W. 2019. The role of permafrost in Eurasian land-atmosphere interactions. *Journal of Geophysical Research-Atmospheres,* 124**,** 11644-11660.

WALLACE, J. M., FU, Q., SMOLIAK, B. V., LIN, P. & JOHANSON, C. M. 2012. Simulated versus observed patterns of warming over the extratropical Northern Hemisphere continents during the cold season. *Proceedings of the National Academy of Sciences of the United States of America,* 109**,** 14337-14342.

WALVOORD, M. A. & KURYLYK, B. L. 2016. Hydrologic impacts of thawing permafrost - A review. *Vadose Zone Journal,* 15.

YANG, D. Q., KANE, D. L., HINZMAN, L. D., ZHANG, X. B., ZHANG, T. J. & YE, H. C. 2002. Siberian Lena River hydrologic regime and recent change. *Journal of Geophysical Research-Atmospheres,* 107.

YE, K. H. & LAU, N. C. 2019. Characteristics of Eurasian snowmelt and its impacts on the land surface and surface climate. *Climate Dynamics,* 52**,** 1115-1138.

YEO, S. R., KIM, W. & KIM, K. Y. 2017. Eurasian snow cover variability in relation to warming trend and Arctic Oscillation. *Climate Dynamics,* 48**,** 499-511.

4. SURFACE AND SUB-SURFACE DRIVERS OF AUTUMN TEMPERATURE INCREASE OVER EURASIAN PERMAFROST

4.1. Introduction

The Arctic is a region experiencing amplified climate change in comparison to the mid-latitudes and the tropics (IPCC 2013) and is expected to continue to exhibit this temperature disparity over the course of the 21st century (Barnes and Polvani 2015). Consequences have manifested in the northern cryosphere with focus mostly on reductions in sea ice due to its positive feedback back resulting in Arctic amplification (Dai et al. 2019; Holland and Bitz 2003; Polyakov et al. 2012). A warmer Arctic has also led to permafrost degradation (Biskaborn et al. 2019), but the literature has focused mainly on feedbacks relating to carbon released from thawing soils and the subsequent biogeochemical cycles (Schuur et al. 2015; Turetsky et al. 2020). A recent bibliographic analysis of the permafrost literature showed that while climate change has become the prevailing focus of permafrost science, its main emphasis is on carbon-related research (Sjöberg et al. 2020). Very little work has been done on the geophysical influences of warming soils on the overlying atmosphere in cryospheric regions. In a review of literature from the early 2010s, Grosse et al. (2016) highlighted vegetation shifts, hydrologic, and biologic impacts which affect the surface energy balance, though the surface energy balance and impacts on the overlying atmosphere and climate were not analyzed in any detail. Eugster et al. (2000) initially established the basic concepts of how the surface energy balance changes due to permafrost degradation and vegetation succession. Now, the suite of earth system models that have been developed in recent

decades can be used to determine the effects and impacts of permafrost degradation on longer scales and in terms of accelerated climate change on the near-surface climate.

An increase in permafrost temperatures and associated active layer deepening for nearly a century have been shown across Eurasia (Frauenfeld et al. 2004; Streletskiy et al. 2015). Near-surface soils (down to 3.2 m) in permafrost regions of Russia have shown significant recent warming, most notably in continuous permafrost regions where trends in minimum soil temperature have outpaced those in maximum soil temperature (Chen et al. 2021a), which can exacerbate permafrost instability. Chen et al. (2021a) also discovered less warming of shallow soils in discontinuous permafrost where, likely due to latent heat effects when soils are closer to 0ºC, phase changes may play a role (Kane et al. 2001). The soil warming trends are projected to continue and accelerate in the 21st century (Soong et al. 2020). Permafrost degradation not only leads to morphological changes to the landscape (e.g., thaw slumps, thermokarst development), but alters the ground thermal regime and the surface energy budget via changing below-surface temperature and moisture gradients.

The partitioning of the surface energy budget and its turbulent fluxes impact the amount of energy either retained in the soil or transferred to the near-surface atmosphere, which can alter land-atmosphere interactions. Based on a historical analysis, Ford and Frauenfeld (2016) found a strong correlation between increased evaporative fraction and precipitation over permafrost in Eurasia, due to a shifting partitioning from sensible to latent heat fluxes. That same region is projected to be a future hotspot for land-atmosphere interactions (Dirmeyer et al. 2013) and permafrost type has been shown to alter the surface energy budget to modify energy transfer between the ground and near-

surface atmosphere (Vecellio et al. 2019). Teufel and Sushama (2019) notes a rapid transition between wet and dry soil regimes once permafrost degrades, which will alter not only the surface energy budget, but also atmospheric variables such as stability and convective parameters.

Vecellio and Frauenfeld (2021) found that the drivers of observed and projected surface air temperature (SAT) increases in the Eurasian high latitudes differ between the expanding shoulder seasons of spring and autumn over Eurasia. In spring, dynamical influences like atmospheric circulation variability dominate the temperature response, while temperature increases in autumn are driven by the land surface via thermodynamic influences. Because the autumn surface forcing is strongest in continuous and discontinuous permafrost regions and increases over time, we hypothesize that permafrost degradation plays an important role. In this study, therefore, we determine which specific surface and sub-surface variables control that thermodynamic influence on autumn SAT. We first assess trends in the surface energy budget to determine if seasonal shifts are occurring and use an information flow methodology to determine whether these shifts can account for the larger magnitude of thermodynamic influence during autumn. We then examine other variables including soil moisture and snow depth across different months to determine where and when surface-based changes play the largest role in autumn's thermodynamic influence on SAT. Similar to Merrifield et al. (2017), we develop a descriptive thermodynamic narrative that seeks to account for the covarying sub-, near-, and above-surface variables and how they will influence the ground-based forcing of autumn SAT over Eurasian permafrost throughout the 21st century.

4.2. Data and Methods

We investigate the role of surface variables on autumn SAT variability over three 30-year periods, historical (1976 – 2005), near future (2021 – 2050), and end-of-century (2071 – 2100) using the National Center for Atmospheric Research's Community Earth System Model's Large Ensemble (CESM-LE). CESM is a fully coupled earth system model, run at a horizontal resolution of 1°. The CESM-LE is a 35-member, initial condition ensemble (Kay et al. 2015) where members are identically forced per the CMIP5 standard with historical forcing until 2005, and RCP 8.5 from 2006 – 2100. Internal variability is created between ensemble members by adding a different order of $\sim 10^{-14}$ °C perturbation to the SAT field of the January 1, 1920 output of the first ensemble member, which then serves as the initial condition for the other 34 ensemble member runs. Each member can be thought of as a possible climate trajectory due to forces inherent within the Earth system while the ensemble mean of all 35 members represents the externally forced response. Analysis is focused on this forced response. Trends for ensemble mean variables were calculated using a linear least squares regression and were considered significant at the 95% confidence level.

We use the Permafrost Zonation Index (PZI) developed by Gruber (2012) to classify the region by permafrost type and determine the thermodynamic differences between these types. The PZI, which has values ranging from 0.01 – 1.0, is used with the Permafrost Subcommittee (1988)'s definition of area percentage of frozen ground to define the different permafrost classes: continuous (0.90 – 1.0); discontinuous (0.50 – 0.89), sporadic (0.10 – 0.49), and isolated (0.01 – 0.09). Land areas where there is no PZI value is considered to be a non-permafrost region. Based on results from Vecellio and

Frauenfeld (2021), we combine the continuous and discontinuous (ContDis) and the sporadic and isolated (SporIso) permafrost zones given their similar thermodynamic impacts on SAT variability, and also consider the non-permafrost region (NonPF; Figure 4.1).

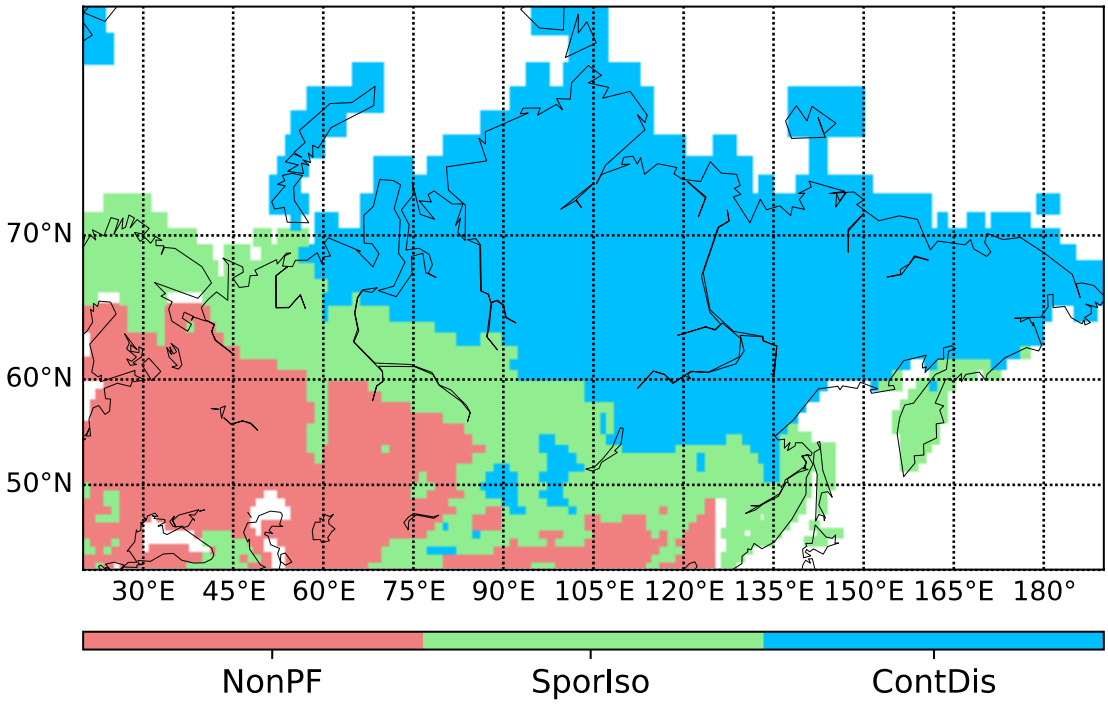

Figure 4.1: Study domain containing permafrost region boundaries

To determine the causality of the major driving forces on autumn SAT in each ensemble member as well as the forced response, variable time series are analyzed using Liang-Kleeman Information Flow (hereafter, IF). Detailed derivations and descriptions can be found in Liang (2014) and Liang (2016). IF combines elements of Granger causality (Granger 1969) and transfer entropy (Schreiber 2000) to determine the magnitude and direction of variable influence based on two single-realization time series. IF has been proven to work with both linear and nonlinear systems, as nonlinear systems are most commonly represented by a linear one (Liang 2014). It represents a true physical

cause-and-effect association between the two variables rather than a statistical one such as, e.g., lagged correlation, making the results easier to interpret.

The rate of information flowing from one variable time series (X_2) to another (X_1), here denoted as $T_{2\to1}$, is calculated via a statistical estimation of the interaction between the variances of X_2 and X_1 and their differentials and is produced in an easily computable formula:

$$T_{2\to1} = \frac{C_{11}C_{12}C_{2,d1} - C^2{}_{12}C_{1,d1}}{C^2{}_{11}C_{22} - C_{11}C^2{}_{12}} \quad (1)$$

where C_{ij} is the sample covariance between X_i and X_j and $C_{i,dj}$ is the covariance between X_i and the differential of the time series $X_j = \frac{X_{j,n+1} - X_j}{\Delta t}$ where Δt is the time step, which in our case is 1 (one year). $T_{2\to1}$ has the units of nats/unit time, where a nat is a unit of information or entropy. If $T_{2\to1}$ is zero, it means that X_2 has no role in the evolution of X_1. However, if it is non-zero, X_2 is considered causal to X_1. As Liang (2014) notes, a positive $T_{2\to1}$ means that X_2 makes X_1 more uncertain, while a negative $T_{2\to1}$ indicates stability. In an updated derivation using multidimensional variables, Liang (2018) notes the inclusion of a negative in Eq. (1) which indicates predictability (i.e., positive $T_{2\to1}$ makes processes more unpredictable and vice versa). In addition, Liang (2018) showed that the IF between any two variables does not change when other system variables are present. In other words, as an example in this study, IF between latent heat flux and autumn SAT does not change even though we do not consider the role of other variables (i.e., monthly sensible heat flux, snow depth, etc.) in that computation.

Liang (2014) also provides the equation for the calculation of IF confidence intervals (90% confidence level shown):

$$T_{2\to1} - 1.645\left(\frac{C_{12}}{C_{11}}\right)^2 \hat{\theta}^2_{a_{12}} \, , T_{2\to1} + 1.645\left(\frac{C_{12}}{C_{11}}\right)^2 \hat{\theta}^2_{a_{12}} \qquad (2)$$

where $\hat{\theta}^2_{a_{12}}$ is retrieved from a Fisher information matrix (see Liang (2014) and references therein for more). As in other studies (Stips et al. 2016; Xiao et al. 2020), we deem small IFs (absolute values < 0.1 nat/unit time) and IFs with absolute values > 0.1 nat/unit time whose confidence interval includes 0.0 nat/unit time as insignificant. To ensure that the true variance in $T_{2\to1}$ is not under-represented, we use the 90% confidence interval to test for significance (Xiao et al. 2020).

We apply the information flow methodology to surface flux variables for the months March – November (i.e., the spring, summer, and autumn seasons). We do not include the winter given the insulating effect of snow on the coupling between the surface and sub-surface with the overlying atmosphere. While snow is still present during the spring and fall, the seasons are not characterized by snow's dampening effect on land-atmosphere interactions. However, in performing the information flow analysis on the effects of snow depth on SATs, the winter season is included as that is when snow is most prevalent in the study area.

4.3. Results

Across all the regions of interest, temperature trends increase between the historical period and near future before experiencing a decrease in the magnitude of warming by the end of the century (Table 4.1). In each time period, the ContDis region exhibits the largest warming trends, peaking at 0.112°C/yr during the near future period. SporIso and NonPF temperature increases in all three periods are much more comparable than either are to the ContDis region.

Table 4.1 Autumn surface air temperature trends (°C/yr) averaged over the ContDis, SporIso, and NonPF regions for the three time periods of interest. All trends were significant at the 95% confidence level.

	Historical	*Near future*	*End of century*
ContDis	0.044	0.112	0.087
SporIso	0.026	0.071	0.062
NonPF	0.029	0.061	0.057

To verify that permafrost soils are accumulating heat to drive the thermodynamic responses to surface air temperature, we analyze soil heat content across each region. Increases in soil heat content are nearly identical across the spring, summer, and autumn seasons for each region (Figure 4.2a–c). Of note, by 2100, ContDis soils contain as much heat as soils in the SporIso region did at the start of the analysis, lending credence to the hypothesis that ContDis permafrost will experience significant degradation by the end of the century. Setting the ContDis region apart, though, is the rate at which it accumulates heat. By 2100, soil heat content in the ContDis region is nearly 800 mJ/m^2 more than its 1976 – 2005 average in all seasons, about double the accumulation found in SporIso and NonPF soils (Figure 4.2d–f).

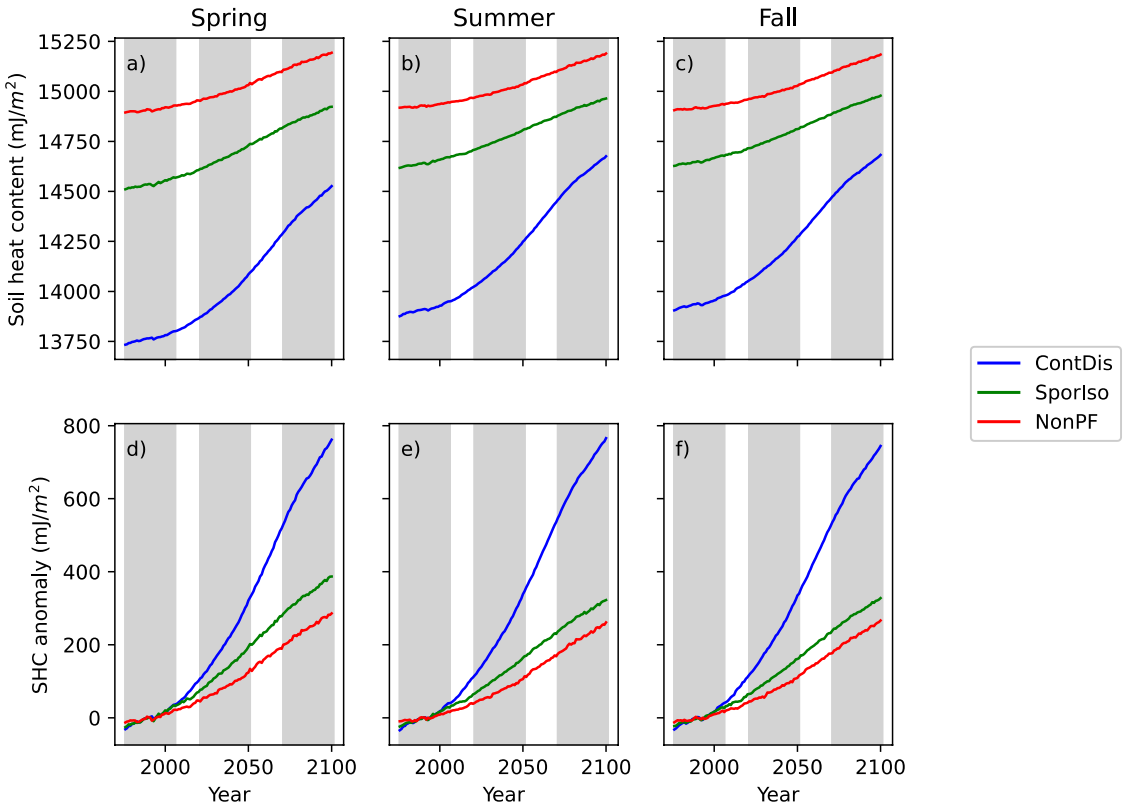

Figure 4.2: (a–c) Soil heat content in mJ/m^2 and (d–f) its anomalies based on the 1976 – 2005 average for the ContDis, SporIso, and NonPF regions

4.3.1. Surface turbulent fluxes

Using the IF method, we establish the causality between surface fluxes on autumn SATs. Results reveal a shift in how the warm season surface energy balance drives autumn SAT over the ContDis region as time progresses. In the historical period, there is a significant impact from the changes in sensible heat flux in both summer (0.106 nat/ut) and autumn (0.216 nat/ut) on autumn SAT in the region. On a monthly time scale, July through October all show significant IF values for the sensible heat flux – autumn SAT relationship (Table 4.2). Non-significant IF values are found across all seasons in the

latent heat flux analysis, while spring ground heat flux is found to significantly drive autumn SATs in the region during the historical period (0.214 nat/ut).

Table 4.2: Ensemble mean information flow factors from sensible heat flux to autumn SAT temperatures across the ContDis, SporIso, and NonPF regions for the historical, near future, and end-of century time periods. Bolded numbers represent significance at the 90% CI. IFs less than 0.1 cannot be considered significant.

	ContDis			**SporIso**			**NonPF**		
	Hist	*NF*	*EOC*	*Hist*	*NF*	*EOC*	*Hist*	*NF*	*EOC*
March	-0.054	0.032	0.015	-0.008	0.000	0.011	-0.007	0.010	0.117
April	-0.072	0.007	0.058	-0.030	0.046	0.025	**0.183**	0.098	0.042
May	0.000	-0.020	-0.014	0.045	0.037	0.037	**0.205**	-0.044	0.013
June	-0.087	0.101	0.124	0.090	-0.008	-0.115	**0.215**	0.027	0.080
July	**0.128**	0.036	0.037	0.060	-0.009	0.058	**0.430**	**0.122**	-0.011
August	**0.249**	0.003	-0.067	0.069	0.008	0.091	**0.281**	**0.125**	0.064
September	**0.278**	-0.043	-0.012	0.001	0.000	0.051	**0.371**	0.055	**0.179**
October	**0.137**	0.025	0.058	0.115	-0.044	0.024	**0.132**	0.035	0.067
November	0.011	0.005	0.013	-0.041	-0.028	-0.021	-0.010	-0.016	-0.042
Spring	-0.075	0.044	0.060	0.016	**0.127**	0.150	**0.283**	0.056	0.019
Summer	**0.106**	0.090	0.070	0.114	-0.012	0.056	**0.410**	**0.138**	0.083
Autumn	**0.216**	-0.004	0.026	0.000	-0.063	0.034	**0.324**	0.081	**0.198**

The increased warming seen in autumn SATs in the near future and end-of-century periods is coincident with a switch of influence from summer and autumn sensible heat flux to a combination of latent and ground heat flux during those seasons (Tables 4.3 and 4.4). Near-future latent heat fluxes in the summer (0.272 nat/ut) and autumn (0.398 nat/ut) are the predominant drivers of autumn SAT change, though ground heat flux IF values are comparable albeit slightly lower in magnitude for those seasons (0.207 and -0.201 nat/ut, respectively). The negative IF value in the autumn ground heat flux signifies that it acts as a stabilizing driver of autumn SAT rather than making it more uncertain (Liang 2014). The end-of-century autumn SATs are again driven by summer and autumn latent and ground heat fluxes. Summer ground heat flux plays a larger role in autumn SAT change than latent heat flux (0.244 vs. 0.161 nat/ut), though that relationship is reversed in autumn as the latent heat flux produces larger IF values in the concurrent season than ground heat flux (0.264 vs. 0.161 nat/ut).

While the shift in seasonal drivers is clear in the ContDis region, no comparable transition is found in the SporIso or NonPF regions. Turbulent fluxes are not significant drivers of autumn SAT in the SporIso region until the near-future period when summer and autumn latent fluxes have a large influence (0.448 and 0.386 nat/ut, respectively) before becoming non-significant at the end of the century. Sensible heat flux significantly influences autumn SATs in all seasons during the historical period as well as in the summer in the near future and autumn at the end of century in the NonPF region. Concurrent autumn latent heat flux is also important in the historical period, though that relationship does not carry through the rest of the period of study.

Table 4.3: Ensemble mean information flow factors from latent heat flux to autumn SAT temperatures across the ContDis, SporIso, and NonPF regions for the historical, near future, and end-of century time periods. Bolded numbers represent significance at the 90% CI. IFs less than 0.1 cannot be considered significant.

	ContDis			**SporIso**			**NonPF**		
	Hist	*NF*	*EOC*	***Hist***	*NF*	*EOC*	*Hist*	*NF*	*EOC*
March	-0.038	-0.026	0.015	-0.020	**-0.176**	-0.032	0.193	0.036	**0.136**
April	-0.023	**0.157**	-0.017	-0.078	0.100	0.032	0.091	0.163	0.017
May	0.016	-0.044	0.009	-0.024	-0.008	0.006	0.189	**0.108**	-0.012
June	-0.020	**0.245**	**0.193**	**-0.161**	**0.252**	-0.014	**0.312**	0.024	0.006
July	0.099	0.121	0.019	-0.019	**0.284**	0.003	-0.122	-0.006	-0.032
August	**0.146**	0.112	0.049	-0.011	**0.227**	0.033	-0.011	-0.013	-0.011
September	0.001	0.228	0.102	**-0.177**	**0.195**	-0.036	0.107	0.047	0.011
October	-0.110	0.133	0.145	-0.010	0.215	-0.036	**0.339**	0.115	0.001
November	**0.197**	**0.270**	**0.165**	0.087	0.130	0.097	**0.324**	0.088	0.044
Spring	-0.006	-0.040	0.012	-0.057	-0.033	0.019	0.206	**0.197**	0.092
Summer	0.048	**0.272**	**0.161**	-0.085	**0.448**	0.023	0.024	-0.009	-0.027
Autumn	-0.060	**0.398**	**0.264**	-0.112	**0.386**	-0.057	**0.484**	0.164	0.064

Table 4.4: Ensemble mean information flow factors from ground heat flux to autumn SAT temperatures across the ContDis, SporIso, and NonPF regions for the historical, near future, and end-of century time periods. Bolded numbers represent significance at the 90% CI. IFs less than 0.1 cannot be considered significant.

	ContDis			**SporIso**			**NonPF**		
	Hist	*NF*	*EOC*	***Hist***	*NF*	*EOC*	*Hist*	*NF*	*EOC*
March	-0.005	-0.027	0.003	-0.001	-0.031	0.003	0.003	-0.001	0.096
April	0.020	-0.020	0.014	0.017	-0.010	-0.003	**0.120**	0.089	-0.005
May	**0.384**	**0.159**	0.111	0.018	0.004	0.103	-0.009	0.006	-0.042
June	-0.073	0.000	**0.151**	0.055	0.038	-0.030	-0.014	-0.015	0.002
July	**0.276**	**0.222**	0.098	0.058	-0.030	0.066	-0.073	0.033	-0.001
August	0.111	**0.227**	0.042	-0.001	-0.013	-0.024	0.037	0.019	0.091
September	0.018	-0.078	**0.178**	-0.020	0.056	-0.030	-0.025	0.015	-0.476
October	0.020	-0.019	0.026	0.047	-0.003	0.048	-0.001	0.002	0.026
November	-0.074	0.021	0.059	-0.028	0.038	0.010	0.001	0.003	0.012
Spring	**0.214**	0.017	0.095	0.066	-0.043	**0.165**	0.014	0.086	0.071
Summer	0.087	**0.207**	**0.244**	0.063	-0.017	0.009	0.021	0.029	0.097
Autumn	-0.079	**-0.201**	**0.161**	0.069	0.073	0.048	-0.013	0.020	0.017

The change in partitioning of energy between the turbulent fluxes provides insight as to why a temporal evolution in surface drivers on autumn SAT occurs only in the ContDis region (Figure 4.2). Sensible heat flux in the NonPF region increases over time in all three seasons, with larger increases compared to the ContDis and SporIso regions whose time series nearly mirror each other for each season. As the NonPF region has the warmest soils, it makes sense that the magnitude of its sensible heat flux is greater than either of the permafrost regions, but of note also is a lack of divergence in

the evolution between ContDis and SporIso (Figure 4.3a–c). A similar relationship is seen in latent heat flux anomalies, especially in the summer and autumn, as the ContDis and SporIso trends once again are nearly identical (Figure 4.3d–f). Noticeable differences in the distribution of the surface energy budget across permafrost regions develop in terms of ground heat flux, however. In the spring, there are large increases in ground heat flux in ContDis over the period of record while little change from the mean period occurs in the SporIso region and small decreases in the NonPF region. The opposite is evident in summer as larger decreases in ground heat flux occur in the ContDis region (i.e., more energy transferred to the surface) compared to smaller decreases in the SporIso region and increases in the NonPF region. In autumn, SporIso and NonPF follow similar patterns while the ground heat flux in the ContDis region increases from the historical period through the near future before declining at the end of the 21st century (Figure 4.3g–i).

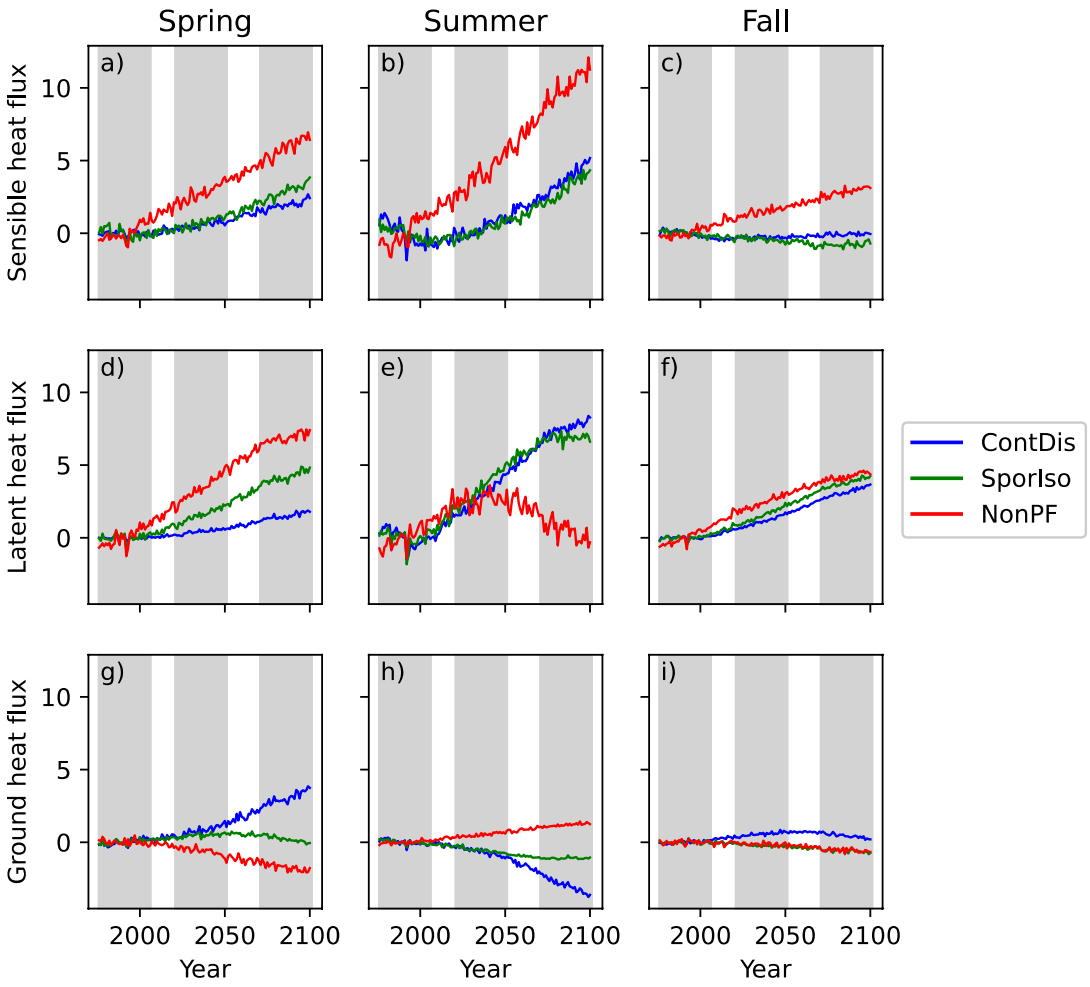

Figure 4.3: Monthly time series of sensible (top row), latent (middle row), and ground (bottom row) heat flux anomalies (W m^{-2}) for spring (left), summer (center), and autumn (right) for the ContDis, SporIso, and NonPF regions over the period 1976 – 2100. Anomalies calculated are departures from the 1976 – 2005 mean

The SporIso and NonPF regions have noticeably different ground thermal regimes than the ContDis region, which is undergoing degradation over the entire 20th

and 21st century. It therefore follows that the same transitional relationship is not observed. This difference is most clearly exhibited in ground heat flux changes between the three regions. It furthermore helps confirm the conclusions of Vecellio and Frauenfeld (2021) that thermodynamics are playing a larger role in SAT change in the ContDis region over the twentieth and twenty-first centuries in these northern permafrost zones, in comparison to the more southern zones or regions where there is no permafrost. We therefore focus subsequent analyses on the ContDis region only.

4.3.2. Role of snow and snowmelt

To clarify the cause for the shift in the surface energy balance's influence on autumn SATs in Eurasia's permafrost regions, we further investigate other surface or atmospheric impacts on the summer and autumn components of the surface energy balance. Specifically, monthly mean snow depth water equivalent is examined due to its impacts in high latitudes and snow's seasonally varying role in influencing the surface heat budget (Jan and Painter 2020).

In the historical period, ContDis snow depth water equivalent decreases in every month and each season, with the largest decreases during summer and autumn. The largest decrease is in June with a statistically significant trend of -0.045 cm/yr (Figure 4.4). Seasonally, summers experience the largest decreases with a trend of -0.033 cm/yr, followed by autumn with a -0.023 cm/yr trend, both statistically significant. However, seasonal differences in snow depth water equivalent begin to emerge in the near future with sharp increases in the winter and spring months, dominated by the monthly trends

from January – April (Figure 4.4). It should be noted that snow depth water equivalent in winter and spring in the near future period experienced large decreases in the SporIso and NonPF regions, again showing a divergence in land surface characteristics between zones (not shown). The summer and autumn periods are once again characterized by statistically significant decreasing amounts of snow in the ContDis region (-0.020 and -0.010 cm/yr, respectively) with the bulk of the decrease occurring in June (-0.046 cm/yr). End-of-century February–April increases in snow depth water equivalent are again significant, albeit lower than in the near future. Seasonally, there are no trends. Conversely, large decreases in snow depth water equivalent occur in May and June during the period. The months of July – September are virtually snow-free by the end of the century. Late autumn (October and November) snow trends also decrease at the end of the century. Overall, the ContDis region is characterized by increased snow from January – April in the future while snow decreases the rest of the months throughout the year, leading to a shift in the seasonal snow cycle.

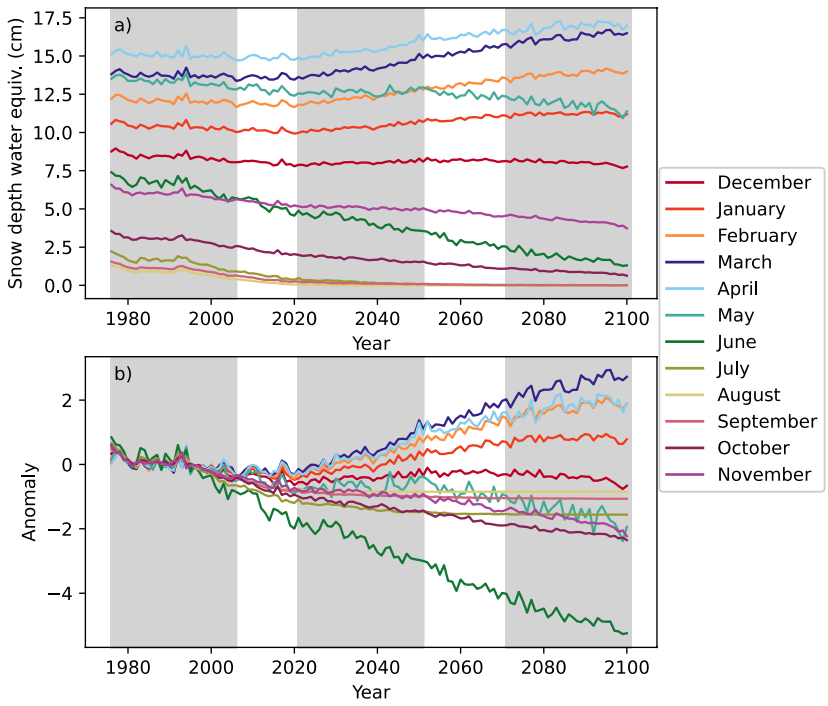

Figure 4.4: (a) Monthly snow depth water equivalent and (b) its anomalies in the ContDis region over the period 1976 – 2100. Anomalies calculated are departures from the 1976 – 2005 mean.

Using IF analysis to specifically establish the cause-and effect of snow depth water equivalent on autumn SATs, we find similarities between significant IFs and the significant trends in snow depth water equivalent described above over the historical and near future periods (Table 4.5). The large decreases in snow in the summer and autumn in the historical period correspond to IFs of 0.572 nat/ut for each season. Monthly IF values peak in September with a maximum of 0.623 nat/ut, though IFs are significant from June through November. There is a shift in the seasonal timing of significant snow to autumn SAT IF values in the near future period, as snow in the months of January – July is a dominant influence on autumn SATs. May snow does not significantly

influence autumn SAT, which corresponds to the transition between significantly increasing (months before May) and decreasing snow depth water equivalent (months after May) in the near future (Figure 4.4). While all seasons have IF values over 0.1 nat/ut, only winter (0.249 nat/ut) and summer (0.186 nat/ut) are significant. Increases in winter and spring snow depth water equivalent begin to level off and are no longer statistically significant in the end-of-century period, though the anomalies remain well above their 1976 – 2005 mean (Figure 4.4b). Continued late-season decreases in snow (Figure 4.4) lead to only November being a significant driver (0.247 nat/ut), with both summer and autumn seasonal values 0.116 and 0.202 nat/ut, respectively, but insignificant.

Table 4.5: Ensemble mean IFs for average snow depth water equivalent to autumn SAT for the ContDis region in the historical, near future, and end-of century time periods. Bolded numbers represent significance at the 90% CI.

	Historical	*Near Future*	*End of Century*
December	0.146	0.082	0.084
January	0.022	**0.223**	0.003
February	-0.041	**0.321**	0.055
March	-0.038	**0.273**	0.074
April	-0.037	**0.242**	-0.002
May	0.123	0.006	0.029
June	**0.497**	**0.144**	0.118
July	**0.500**	**0.247**	-0.014
August	**0.550**	0.078	0.052
September	**0.623**	0.079	-0.068
October	**0.566**	0.117	0.009
November	**0.443**	0.053	**0.247**
Winter	0.021	**0.249**	0.002
Spring	-0.009	0.128	0.001
Summer	**0.572**	**0.186**	0.116
Autumn	**0.572**	0.115	0.202

As snowmelt infiltrates the soil column, it can modify the soil thermal regime by transporting heat downward, and by increasing soil moisture in the upper layers for

increased thermal conductivity into the soil and potential subsequent evaporation. To verify this mechanism, we calculate soil moisture trends and find differences in the upper soil column as time progresses (Figure 4.5). In May, soil moisture in the layers closest to the surface (0.1 – 0.4 m) consistently increases throughout the entire period of record, though the magnitudes of those trends decrease as soil depth increases. The autumn months of October and November also exhibit soil moisture increases at the surface levels, though not until the near-future period. The summer months of July and August stand out with largest decreases in soil moisture in the upper layers. At 0.8 m, soil moisture increases only in May and June, while values are below their 1976 – 2005 mean in all other months. At 1.6 m, the largest increases occur in June, while May and, to an extent through the mid-21st century, July soil moisture values again are above their historical mean value. However, the early spring and autumn months see decreases which accelerate after 2050. At 3.2 m, soil moisture increases in all months, leveling off by the end of the 21st century. Overall, substantial soil moisture increases occur in the months following snowmelt, delayed from May to June deeper in the soil column. These increases correspond to the increases also evident in the amount of snow in the region in the near future and end-of-century periods. Also noteworthy are the increases in near-surface soil moisture in the later autumn months of October and November over time. As snow trends are decreasing in those months, there may be more rainfall over high-latitude terrestrial Eurasia increasing soil moisture in the active layer, which remains unfrozen longer into the cold season. The increased soil moisture may contribute to a

positive feedback whereby the soil stays warmer relative to drier autumn soils in the past.

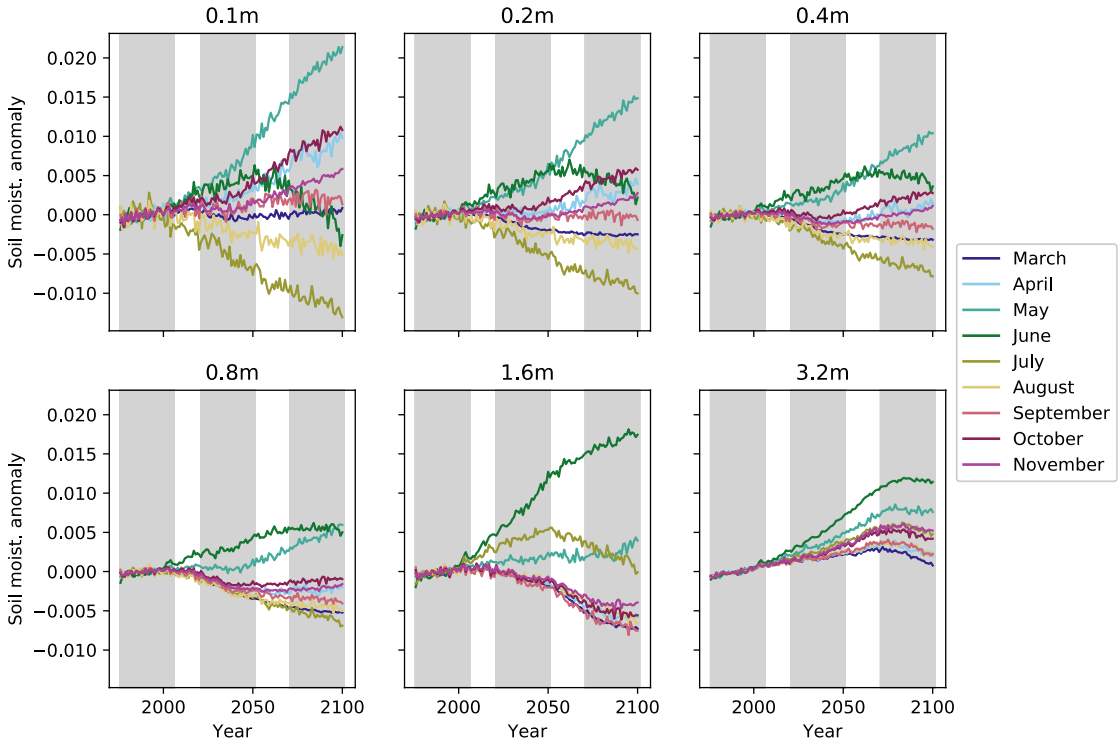

Figure 4.5: Monthly soil moisture anomaly time series (in m^3/m^3) for six soil levels in the ContDis region over 1976 – 2100. Anomalies calculated are departures from the 1976 – 2005 mean.

4.4. Constructing a thermodynamic narrative

The results of this study show that the increasing influence of thermodynamic changes at the land surface associated with permafrost degradation in Eurasia, especially in regions of continuous and discontinuous permafrost, are closely linked to changes in

seasonal snow cover. Large changes in permafrost characteristics in these regions compared to regions of less permafrost have already been documented in the Russian Arctic drainage basin (Wang et al. 2021). Changes in snow subsequently contribute to a surface energy budget switch in the driving factors of autumn SATs, transitioning from a predominately sensible heat regime during the historical period, when snow totals decreased throughout the year, to a regime driven by a changing latent and ground heat flux, tied to winter and spring increases in snow.

The increase in snow depth and its water equivalent in winter and spring over continuous and discontinuous permafrost in the 21st century results in altered moisture pathways for energy transport and exchange in and out of the soil throughout the year. Increased snow in winter and spring allows for increased insulation of the soil late into spring, with less heat flux to the atmosphere. This causes increased (or less decreased) spring ground heat flux which allows soils to stay warmer. The relationship between snow and permafrost warming has been well established in the past (Goodrich 1982; Stieglitz et al. 2003). While not a direct comparison, the simulations by Jan and Painter (2020) indicate more gradual or later-season snowfall could actually cool permafrost soils, confirming previous conclusions (Goodrich 1982; Zhang 2005). The results presented here contest our general understanding of the impact of the timing of seasonal snow cover on the ground thermal regime. The impacts of climate change and a lengthening warm season on increasingly warmer soils may decrease the importance of

the timing of snow cover on ground temperatures and should be investigated more thoroughly.

Snowmelt, starting around May/June in the near future period, also has an impact on the ground thermal regime. The increase in summertime moisture in the northern high-latitudes is also expected to lead to convective available potential energy (Chen et al. 2021b) and precipitation increases (Ford and Frauenfeld, 2016) which can become a positive feedback to increasing soil moisture, latent heat, and impacts on air temperature later into autumn. This multi-step process may explain how increased latent heat used for evaporation at the surface could have a warming effect instead of a cooling effect. Substantial future summer (June, July, and August) increases in convective precipitation are still evident in September. (Figure 4.6). This also supports our results showing increased near-surface soil moisture during the autumn, specifically October and November even though snowfall is decreasing during those months (Figure 4.4a). Localized deep convection replenishes evaporated moisture with rainfall which has been shown to transfer its sensible heat into the soil and aid in continued warming via subsurface convective heat flow (Kollet et al. 2009; Mekonnen et al. 2021).

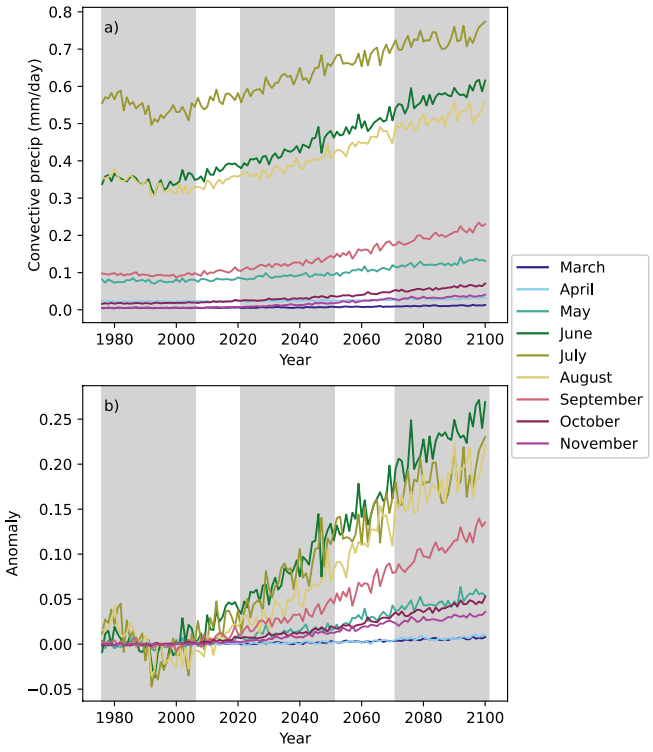

Figure 4.6: (a) Monthly convective precipitation and (b) its anomalies in the ContDis region over the period 1976 – 2100. Anomalies calculated are departures from the 1976 – 2005 mean.

While ground heat flux in the ContDis region remains positive during the summer throughout the period of study, its departure from the historical average becomes more negative as time goes on (Figure 4.3h) with smaller effects at the end of the century as well (Figure 4.3i). We can attribute that to the increase in latent heat flux and how soil continues to gain heat and increase surface temperature when conductive heat flux into the soil is decreased. Increased snowmelt still causes soil heat gain through the thermal conductivity of soil moisture, transported to deeper layers as the meltwater infiltrates the column, even as energy is used in evaporation and subsequent convective

precipitation as described above. Kane et al. (2001) noted the importance of snowmelt infiltration as a means of non-conductive heat transfer in frozen soils. Mekonnen et al. (2021) modeled the impact of heat from precipitation and general soil water conductivity to verify that hydrothermal effects can provide similar magnitude impacts on permafrost degradation as air temperature. Increased soil moisture from snowmelt and increased summer as well as autumn rainfall causes increased soil heat content and provides subsequent energy to increase air temperatures in the extended warm season. Again, the effect is shown to be more largely apparent in the ContDis region in comparison to the SporIso and NonPF regions discussed earlier through increased emitted longwave radiation (Figure 4.7). Longwave radiative influences on surface temperatures in the high latitudes have been thoroughly documented in the context of Arctic Ocean sea ice decline (Pithan and Mauritsen 2014). A more thorough study of implications of changing radiative drivers and feedbacks over Arctic terrestrial areas would be a pertinent avenue for future work.

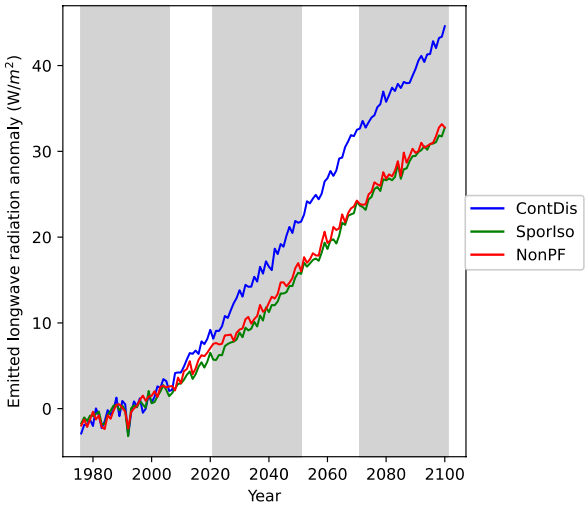

Figure 4.7: Emitted longwave radiation anomalies over the ContDis, SporIso, and NonPF regions for the period 1976 – 2100. Anomalies calculated are departures from the 1976 – 2005 mean.

4.5. Conclusions

We used information flow (Liang 2014; Liang 2016; Liang 2018), or information transfer, based on the concepts of Granger causality, to establish the cause and effect of land surface drivers of autumn SAT temperature increases over regions underlain by permafrost, previously shown to be thermodynamically induced (Vecellio and Frauenfeld 2021). Here, we document a change in the partitioning of turbulent heat fluxes on autumn SATs after the historical period, when summer and autumn sensible heat fluxes were the dominant drivers of autumn SAT change. In the near-future and end-of-century periods, latent and ground heat fluxes will be the dominant drivers of autumn SAT. This corresponds to the increase in thermodynamic influence on autumn SATs found in Vecellio and Frauenfeld (2021). Changes in latent and ground heat fluxes

may thus be larger controlling factors of land-atmosphere coupling than sensible heat flux. This is predicated upon a changing seasonal snow cycle in the future, with winter and spring increases projected to occur in continuous and discontinuous permafrost areas. Subsequent soil warming and resulting local subsurface moisture modifications due to both increased convective precipitation and infiltration will play a role through the end of the century. This leads to further questions of how land-atmosphere interactions may shape the future weather and climate of the high latitudes in Eurasia, as soils warm and more energy is transferred between soil and atmosphere. The region was previously shown to be a future hotspot for land-atmosphere interactions, similar to the central Great Plains of the United States or the Sahel. Future research might consider how increased feedbacks will affect local-scale convection or larger-scale synoptic circulation in climate scenarios over these large areas of thawing permafrost, based on the documented relationships in the current surface-atmosphere hotspots.

4.6. References

BARNES, E. A. & POLVANI, L. M. 2015. CMIP5 projections of Arctic amplification, of the North American/North Atlantic circulation, and of their relationship. *Journal of Climate,* 28**,** 5254-5271.

BISKABORN, B. K., SMITH, S. L., NOETZLI, J., MATTHES, H., VIEIRA, G., STRELETSKIY, D. A., SCHOENEICH, P., ROMANOVSKY, V. E., LEWKOWICZ, A. G., ABRAMOV, A., ALLARD, M., BOIKE, J., CABLE, W. L., CHRISTIANSEN, H. H., DELALOYE, R., DIEKMANN, B., DROZDOV,

D., ETZELMULLER, B., GROSSE, G., GUGLIELMIN, M., INGEMAN-NIELSEN, T., ISAKSEN, K., ISHIKAWA, M., JOHANSSON, M., JOHANNSSON, H., JOO, A., KAVERIN, D., KHOLODOV, A., KONSTANTINOV, P., KROGER, T., LAMBIEL, C., LANCKMAN, J. P., LUO, D., MALKOVA, G., MEIKLEJOHN, I., MOSKALENKO, N., OLIVA, M., PHILLIPS, M., RAMOS, M., SANNEL, A. B. K., SERGEEV, D., SEYBOLD, C., SKRYABIN, P., VASILIEV, A., WU, Q., YOSHIKAWA, K., ZHELEZNYAK, M. & LANTUIT, H. 2019. Permafrost is warming at a global scale. *Nat Commun,* 10**,** 264.

CHEN, L., AALTO, J. & LUOTO, M. 2021a. Significant shallow–depth soil warming over Russia during the past 40 years. *Global and Planetary Change,* 197**,** 103394.

CHEN, Y., ROMPS, D. M., SEELEY, J. T., VERAVERBEKE, S., RILEY, W. J., MEKONNEN, Z. A. & RANDERSON, J. T. 2021b. Future increases in Arctic lightning and fire risk for permafrost carbon. *Nature Climate Change*.

DAI, A., LUO, D., SONG, M. & LIU, J. 2019. Arctic amplification is caused by sea-ice loss under increasing CO 2. *Nature communications,* 10**,** 1-13.

DIRMEYER, P. A., JIN, Y., SINGH, B. & YAN, X. 2013. Trends in Land–Atmosphere Interactions from CMIP5 Simulations. *Journal of Hydrometeorology,* 14**,** 829-849.

EUGSTER, W., ROUSE, W. R., PIELKE, R. A., MCFADDEN, J. P., BALDOCCHI, D. D., KITTEL, T. G. F., CHAPIN, F. S., LISTON, G. E., VIDALE, P. L., VAGANOV, E. & CHAMBERS, S. 2000. Land-atmosphere energy exchange in Arctic tundra and boreal forest: available data and feedbacks to climate. *Global Change Biology,* 6**,** 84-115.

FORD, T. W. & FRAUENFELD, O. W. 2016. Surface–Atmosphere Moisture Interactions in the Frozen Ground Regions of Eurasia. *Scientific Reports,* 6**,** 19163.

FRAUENFELD, O. W., ZHANG, T. J., BARRY, R. G. & GILICHINSKY, D. 2004. Interdecadal changes in seasonal freeze and thaw depths in Russia. *Journal of Geophysical Research-Atmospheres,* 109.

GOODRICH, L. E. 1982. The influence of snow cover on the ground thermal regime. *Canadian geotechnical journal,* 19**,** 421-432.

GRANGER, C. W. 1969. Investigating causal relations by econometric models and cross-spectral methods. *Econometrica: journal of the Econometric Society***,** 424-438.

GROSSE, G., GOETZ, S., MCGUIRE, A. D., ROMANOVSKY, V. E. & SCHUUR, E. A. 2016. Changing permafrost in a warming world and feedbacks to the Earth system. *Environmental Research Letters,* 11**,** 040201.

GRUBER, S. 2012. Derivation and analysis of a high-resolution estimate of global permafrost zonation. *Cryosphere,* 6**,** 221-233.

HOLLAND, M. M. & BITZ, C. M. 2003. Polar amplification of climate change in coupled models. *Climate Dynamics,* 21**,** 221-232.

IPCC 2013. Climate Change 2013: The Physical Science Basis. Contribution of Working Group I to the Fifth Assessment Report of the Intergovernmental Panel on Climate Change. *In:* STOCKER, T. F., D. QIN, G.-K. PLATTNER, M. TIGNOR, S.K. ALLEN, J. BOSCHUNG, A. NAUELS, Y. XIA, V. BEX AND P.M. MIDGLEY (ed.). Cambridge, United Kingdom and New York, NY, USA.

JAN, A. & PAINTER, S. L. 2020. Permafrost thermal conditions are sensitive to shifts in snow timing. *Environmental Research Letters,* 15**,** 084026.

KANE, D. L., HINKEL, K. M., GOERING, D. J., HINZMAN, L. D. & OUTCALT, S. I. 2001. Non-conductive heat transfer associated with frozen soils. *Global and Planetary Change,* 29**,** 275-292.

KAY, J. E., DESER, C., PHILLIPS, A., MAI, A., HANNAY, C., STRAND, G., ARBLASTER, J. M., BATES, S. C., DANABASOGLU, G., EDWARDS, J., HOLLAND, M., KUSHNER, P., LAMARQUE, J. F., LAWRENCE, D., LINDSAY, K., MIDDLETON, A., MUNOZ, E., NEALE, R., OLESON, K., POLVANI, L. & VERTENSTEIN, M. 2015. The Community Earth System Model (CESM) Large Ensemble Project: A community resource for studying climate change in the presence of internal climate variability. *Bulletin of the American Meteorological Society,* 96**,** 1333-1349.

KOLLET, S. J., CVIJANOVIC, I., SCHÜTTEMEYER, D., MAXWELL, R. M., MOENE, A. F. & BAYER, P. 2009. The Influence of Rain Sensible Heat and Subsurface Energy Transport on the Energy Balance at the Land Surface. *Vadose Zone Journal,* 8**,** 846-857.

LIANG, X. S. 2014. Unraveling the cause-effect relation between time series. *Physical Review E,* 90**,** 052150.

LIANG, X. S. 2016. Information flow and causality as rigorous notions ab initio. *Physical Review E,* 94**,** 052201.

LIANG, X. S. 2018. Causation and information flow with respect to relative entropy. *Chaos: An Interdisciplinary Journal of Nonlinear Science,* 28**,** 075311.

MEKONNEN, Z. A., RILEY, W. J., GRANT, R. F. & ROMANOVSKY, V. E. 2021. Changes in precipitation and air temperature contribute comparably to permafrost degradation in a warmer climate. *Environmental Research Letters,* 16**,** 024008.

MERRIFIELD, A., LEHNER, F., XIE, S. P. & DESER, C. 2017. Removing circulation effects to assess central US land-atmosphere interactions in the CESM Large Ensemble. *Geophysical Research Letters,* 44**,** 9938-9946.

PITHAN, F. & MAURITSEN, T. 2014. Arctic amplification dominated by temperature feedbacks in contemporary climate models. *Nature Geoscience,* 7**,** 181-184.

POLYAKOV, I. V., WALSH, J. E. & KWOK, R. 2012. Recent changes of Arctic multiyear sea ice coverage and the likely causes. *Bulletin of the American Meteorological Society,* 93**,** 145-151.

SCHREIBER, T. 2000. Measuring Information Transfer. *Physical Review Letters,* 85**,** 461-464.

SCHUUR, E. A. G., MCGUIRE, A. D., SCHADEL, C., GROSSE, G., HARDEN, J. W., HAYES, D. J., HUGELIUS, G., KOVEN, C. D., KUHRY, P., LAWRENCE, D. M., NATALI, S. M., OLEFELDT, D., ROMANOVSKY, V. E., SCHAEFER, K., TURETSKY, M. R., TREAT, C. C. & VONK, J. E. 2015. Climate change and the permafrost carbon feedback. *Nature,* 520**,** 171-179.

SJÖBERG, Y., SIEWERT, M. B., RUDY, A. C., PAQUETTE, M., BOUCHARD, F., MALENFANT-LEPAGE, J. & FRITZ, M. 2020. Hot trends and impact in permafrost science. *Permafrost and Periglacial Processes,* 31**,** 461-471.

SOONG, J. L., PHILLIPS, C. L., LEDNA, C., KOVEN, C. D. & TORN, M. S. 2020. CMIP5 Models Predict Rapid and Deep Soil Warming Over the 21st Century. *Journal of Geophysical Research: Biogeosciences,* 125**,** e2019JG005266.

STIEGLITZ, M., DÉRY, S., ROMANOVSKY, V. & OSTERKAMP, T. 2003. The role of snow cover in the warming of arctic permafrost. *Geophysical Research Letters,* 30.

STIPS, A., MACIAS, D., COUGHLAN, C., GARCIA-GORRIZ, E. & LIANG, X. S. 2016. On the causal structure between CO2 and global temperature. *Scientific Reports,* 6**,** 21691.

STRELETSKIY, D. A., SHERSTIUKOV, A. B., FRAUENFELD, O. W. & NELSON, F. E. 2015. Changes in the 1963-2013 shallow ground thermal regime in Russian permafrost regions. *Environmental Research Letters,* 10.

SUBCOMMITTEE, P. 1988. Glossary of permafrost and related ground-ice terms. *Associate Committee on Geotechnical Research, National Research Council of Canada, Ottawa,* 156.

TEUFEL, B. & SUSHAMA, L. 2019. Abrupt changes across the Arctic permafrost region endanger northern development. *Nature Climate Change,* 9**,** 858-862.

TURETSKY, M. R., ABBOTT, B. W., JONES, M. C., ANTHONY, K. W., OLEFELDT, D., SCHUUR, E. A., GROSSE, G., KUHRY, P., HUGELIUS, G. & KOVEN, C. 2020. Carbon release through abrupt permafrost thaw. *Nature Geoscience,* 13**,** 138-143.

VECELLIO, D. J. & FRAUENFELD, O. W. 2021. The contribution of changing surface thermodynamics on twentieth and twenty-first century air temperatures over Eurasian permafrost. *Climate Dynamics***,** 1-20.

VECELLIO, D. J., NOWOTARSKI, C. J. & FRAUENFELD, O. W. 2019. The role of permafrost in Eurasian land-atmosphere interactions. *Journal of Geophysical Research-Atmospheres,* 124**,** 11644-11660.

WANG, K., ZHANG, T. & YANG, D. 2021. Permafrost dynamics and their hydrologic impacts over the Russian Arctic drainage basin. *Advances in Climate Change Research*.

XIAO, H., ZHANG, F., MIAO, L., SAN LIANG, X., WU, K. & LIU, R. 2020. Long-term trends in Arctic surface temperature and potential causality over the last 100 years. *Climate Dynamics*, 55**,** 1443-1456.

ZHANG, T. 2005. Influence of the seasonal snow cover on the ground thermal regime: An overview. *Reviews of Geophysics,* 43.

5. CONCLUSIONS

This dissertation provided the first study to examine the geophysical impact of permafrost degradation on the near-surface climate. First, I confirmed that degrading permafrost would have an impact on surface-atmosphere energy exchanges using idealized WRF simulations. Based on these results, I used the CESM-LE to determine the specific impact of permafrost degradation on SATs over different permafrost zones in Eurasia over historical and future time periods. Once determining that surface-based influence (i.e., permafrost-related) on SATs was seasonally dependent, I examined the specific land-surface and sub-surface drivers of the thermodynamic influence on SATs over permafrost in the fall over Eurasia. Altogether, this dissertation finds that the geophysical impacts on permafrost degradation influence the local climate system, not only at the near surface, but in the upper atmosphere as well. These results show that energy exchanges between the surface and atmosphere in permafrost regions must be considered in addition to the exchange of terrestrially stored greenhouse gases (i.e., CO_2 and CH_4) which has been the focus of most climate-related permafrost degradation studies over the last decade.

5.1. Permafrost regime impact on land-atmosphere interactions

Four idealized WRF experiments were conducted to investigate the impact of differing ground thermal regimes on the surface energy budget, boundary layer, and synoptic circulation patterns given both active and quiescent weather conditions. Larger sensible heat fluxes were generally found over discontinuous permafrost in comparison to continuous permafrost while latent heat fluxes generally had the opposite relationship,

though, increased turbulence due to wind and presence of precipitation made differences in the active experiment less drastic. Increased moisture flux into the near surface atmosphere over continuous permafrost soils inundated with snowmelt and/or precipitation lowers lifting condensation levels below boundary layer heights, allowing for formation of low clouds and increasing the likelihood for precipitation, even when there is no large synoptic forcing present. This highlights the importance of wet soil regimes on local climates and how permafrost degradation could alter those local climates. Surface changes also altered atmospheric circulation patterns in the synoptically active case. The surface low in the discontinuous run was ~3 hPa lower than in the continuous run while minimum heights at 500 hPa in the continuous run was ~4 dam lesser, centered further south by ~3° of latitude, and exhibited a wider swath of stronger winds associated with it as compared to its discontinuous counterpart. While only run in an idealized state for 72 hours, these model runs provided a proof of concept that changing ground conditions do have a geophysical influence throughout the atmosphere. Over time, this influence could induce larger scale climatic changes.

5.2. Influence of permafrost degradation on regional surface air temperature

The degradation on permafrost, specifically within the Eurasian domain, does exhibit an influence on SAT changes through modification of the surface energy budget. Chapter 3 showed that the influence of the surface on SATs will become stronger in the future as the climate continues to warm and permafrost thaws at a faster rate. However, when examining the lengthening shoulder seasons, the thermodynamic, ground-based influence on SAT is only present in the fall. Spring warming increases are more variable

and tied to synoptic circulation features. Ground control on SATs was primarily focused in the continuous permafrost zone and, to a lesser but still significant extent, the discontinuous permafrost zone.

In discretizing the surface and sub-surface drivers of the thermodynamically driven SAT increase over continuous and discontinuous permafrost, a transition in the importance of turbulent fluxes on surface air temperature over time was found in Chapter 4. In the historical period, fall SATs were driven by summer and fall sensible heat flux. However, in the twenty-first century, summer and fall latent and ground heat fluxes became the primary influence on fall SAT. Increases in winter and spring snow water equivalent in the future and subsequent increases in late spring and summer soil moisture are the impetus for this transition and larger influence. No other permafrost zone (or non-permafrost region) experiences this future increase in snow. This lagged yet carried over seasonal effect seems to be the representative factor controlling the thermodynamic influence found in the continuous and discontinuous permafrost zones. Prolonged snow cover keeps soils warmer in spring and increased meltwater infiltration allows for increased heat transfer into the soil due to higher heat conductivity. The melting of ground ice likely also plays a role. Increased soil moisture also allows for increased evaporation and latent heat release into the near surface atmosphere throughout summer and fall. A longer snow-free fall aide in this process as well.

5.3. Overall contribution and future work

This dissertation provides a novel study of the geophysical impacts of permafrost degradation on the climate system. Previous literature has focused on the impact of

carbon release from frozen soils on future surface air temperature change (Schuur et al., 2015, MacDougall et al., 2012, Schaefer et al., 2014). This study used both numerical weather prediction and coupled earth system models to confirm and quantify this geophysical, thermodynamic forcing on the local, mesoscale, and synoptic-scale climate. The exchange of heat and moisture via turbulent fluxes is essential in the understanding of how the climate over transitioning permafrost regions has and will continue to evolve in the future. The knowledge produced in this dissertation provides a proof of concept to build upon for future studies investigating the changing surface-atmosphere interactions in permafrost regions as we progress through the twenty-first century.

Increased surface and atmospheric observations, especially over the large, isolated regions of Siberia, will be needed to confirm the results of the simulations used in this study. Near surface measurements of turbulent fluxes and surface air temperature will be important to correlate with the already extensive soil temperature observation network to verify the impact of permafrost degradation on surface-atmosphere energy exchange. Additionally, boundary layer and upper-air measurements, which are far sparser within the region, should be increased to determine the mesoscale and synoptic implications of the evolving climatic relationship. Recent studies have shown increases in observed lightning strikes in the Arctic (Holzworth et al., 2021) with expected increases in CAPE and convective precipitation over Arctic terrestrial regions to continue in the future (Chen et al., 2021). With the results of Chapter 2 showing how shifting ground thermal regimes can modify heat and moisture transfer into the near-surface atmosphere and subsequent height parameters associated with convective uplift,

finding a quantifiable and observable link between ground conditions and atmospheric convection would help to confirm the thermodynamic influence this dissertation has ascertained.

In the same vein, this research provides reason to re-examine the nature of Arctic and mid-latitude connections. The linkages between Arctic warming, specifically over the Arctic Ocean, and weather extremes in the mid-latitudes was first proposed by Francis and Vavrus (2012) where they provided evidence for a slowing of eastward propagation of Rossby waves due to the warming of the high latitudes. While focusing on sea ice, they did note that warming and drying of terrestrial lands in the Arctic also might have effects on the poleward temperature and 500 hPa height gradient driving this linkage during the summer. However, by critiquing and modifying the Francis and Vavrus (2012) methodology, Barnes (2013) found that wave phase speeds and elongation of 500 hPa heights did not present the significant trends the original hypothesis and subsequent evidence were founded upon. A back-and-forth has played out in the literature over the past decade, though evidence confirming the Arctic and mid-latitude link has become less convincing with more observational data (Blackport and Screen, 2020, Riboldi et al., 2020).

Shepherd (2014) notes the importance of thermodynamics on the externally forced changes in surface air temperature as well as how it works in tandem with large-scale dynamics on changes in precipitation. The recent abrupt warming over central Eurasia (Blackport and Screen, 2020) and projected thermodynamically induced warming via permafrost degradation over the region that acts at the terrestrial bridge

between the Arctic Ocean and mid-latitudes could be a primary factor in the slowing down of this linkage. Future work should examine the sensitivity of the connection between the Arctic and mid-latitudes to terrestrial warming and increased land-atmosphere interactions, specifically over the Eurasian landmass.

Lastly, this dissertation did not consider the biophysical impacts that would accompany new vegetation growth in northern regions that will have the capacity to harbor plant life in the future. Historical observations have shown a greening of Northern Hemisphere permafrost regions correlated with deeper active layers and higher soil temperatures (Peng et al., 2020). Vegetation encroachment is accompanied by changes to surface albedo, hydrology, and turbulent fluxes, all of which can also have impacts on land-atmosphere interactions. Studies have long suggested a relationship between vegetation boundaries and the position of the Arctic frontal zone which plays a substantial role in high-latitude climate (Krebs and Barry, 1970, Liess et al., 2012, Snyder and Liess, 2014). Again, sensitivity studies exploring the impact of thawed ground versus the impact of vegetation sprouting from that newly thawed ground would continue to enhance the knowledge of surface-based influence on the climate system in transitioning permafrost zones.

5.4. References

BARNES, E. A. 2013. Revisiting the evidence linking Arctic amplification to extreme weather in midlatitudes. *Geophysical Research Letters,* 40**,** 4734-4739.

BLACKPORT, R. & SCREEN, J. A. 2020. Weakened evidence for mid-latitude impacts of Arctic warming. *Nature Climate Change,* 10**,** 1065-1066.

CHEN, Y., ROMPS, D. M., SEELEY, J. T., VERAVERBEKE, S., RILEY, W. J., MEKONNEN, Z. A. & RANDERSON, J. T. 2021. Future increases in Arctic lightning and fire risk for permafrost carbon. *Nature Climate Change*.

FRANCIS, J. A. & VAVRUS, S. J. 2012. Evidence linking Arctic amplification to extreme weather in mid-latitudes. *Geophysical Research Letters,* 39.

HOLZWORTH, R. H., BRUNDELL, J. B., MCCARTHY, M. P., JACOBSON, A. R., RODGER, C. J. & ANDERSON, T. S. 2021. Lightning in the Arctic. *Geophysical Research Letters,* 48**,** e2020GL091366.

KREBS, J. S. & BARRY, R. G. 1970. The Arctic Front and the Tundra-Taiga Boundary in Eurasia. *Geographical Review,* 60**,** 548-554.

LIESS, S., SNYDER, P. K. & HARDING, K. J. 2012. The effects of boreal forest expansion on the summer Arctic frontal zone. *Climate Dynamics,* 38**,** 1805-1827.

MACDOUGALL, A. H., AVIS, C. A. & WEAVER, A. J. 2012. Significant contribution to climate warming from the permafrost carbon feedback. *Nature Geoscience,* 5**,** 719-721.

PENG, X., ZHANG, T., FRAUENFELD, O. W., WANG, S., QIAO, L., DU, R. & MU, C. 2020. Northern Hemisphere Greening in Association With Warming Permafrost. *Journal of Geophysical Research: Biogeosciences,* 125**,** e2019JG005086.

RIBOLDI, J., LOTT, F., D'ANDREA, F. & RIVIÈRE, G. 2020. On the Linkage Between Rossby Wave Phase Speed, Atmospheric Blocking, and Arctic Amplification. *Geophysical Research Letters,* 47**,** e2020GL087796.

SCHAEFER, K., LANTUIT, H., ROMANOVSKY, V. E., SCHUUR, E. A. G. & WITT, R. 2014. The impact of the permafrost carbon feedback on global climate. *Environmental Research Letters,* 9.

SCHUUR, E. A. G., MCGUIRE, A. D., SCHADEL, C., GROSSE, G., HARDEN, J. W., HAYES, D. J., HUGELIUS, G., KOVEN, C. D., KUHRY, P., LAWRENCE, D. M., NATALI, S. M., OLEFELDT, D., ROMANOVSKY, V. E., SCHAEFER, K., TURETSKY, M. R., TREAT, C. C. & VONK, J. E. 2015. Climate change and the permafrost carbon feedback. *Nature,* 520**,** 171-179.

SHEPHERD, T. G. 2014. Atmospheric circulation as a source of uncertainty in climate change projections. *Nature Geoscience,* 7**,** 703-708.

SNYDER, P. K. & LIESS, S. 2014. The simulated atmospheric response to expansion of the Arctic boreal forest biome. *Climate Dynamics,* 42**,** 487-503.